ANALYTICAL DETERMINATION OF UAV WING STIFFNESS REQUIREMENTS FOR A STRUCTURALLY INTEGRATED CONFORMAL ANTENNA ARRAY

By

SCOTT GALLAWAY

Bachelor of Arts/Science in Mechanical Engineering

Oklahoma State University

Stillwater, Oklahoma

2015

Submitted to the Faculty of the
Graduate College of the
Oklahoma State University
in partial fulfillment of
the requirements for
the Degree of
MASTER OF SCIENCE
May, 2017

ANALYTICAL DETERMINATION OF UAV WING

STIFFNESS REQUIREMENTS FOR A

STRUCTURALLY INTEGRATED

CONFORMAL ANTENNA ARRAY

Thesis Approved:

Dr. James A. Kidd

Thesis Adviser

Dr. Joseph P. Conner

Dr. Shuodao Wang

Dr. James C. West

ACKNOWLEDGEMENTS

Thanks to everyone who helped me through the last 2 years in general and to the following individuals in particular:

My Family for their support through this process

Leon Keck and Guy Gallaway for sparking my interest in engineering

John Ragsdale for pushing me to get a M.S.

Dr. Kidd for mentoring and advising me through this process

Dr. West for his advice on the Radar portion of this work

Dr. Conner and Dr. Wang for serving on my committee

Dr. Weckler and Dr. Wilber for their EWB Expertise

Michael Bartley, Janina Graves and the OSU Wesley for their support these last 6 years

And the OSU Faculty for teaching all the classes I've taken along the way

Name: SCOTT GALLAWAY

Date of Degree: MAY 2017

Title of Study: EXAMINATION OF UAV WING STIFFNESS REQUIREMENTS FOR A STRUCTURALLY INTEGRATED CONFORMAL ANTENNA ARRAY

Major Field: MECHANICAL & AEROSPACE ENGINEERING

Abstract: A need for airborne ground mapping through foliage is identified for a project in Guatemala. After an examination of current systems, technologies and methods related to this task, a low frequency cruciform conformal array mounted to the underside of a small, vehicle portable UAV is proposed to meet the need. Wing deflections due to small changes in wing loading are expected to result in changes to antenna performance. A method utilizing computer modeling and antenna theory is developed to quantify this effect and determine the relationships between wing construction and stiffness, frequency selection, wing loading and antenna performance. Losses in the expected flight envelope is found to be small and general relationships between the wing construction and stiffness, frequency selection, wing loading and antenna performance are developed.

TABLE OF CONTENTS

Chapter Page

LIST OF TABLES

Table Page

LIST OF FIGURES

Figure Page

CHAPTER I

INTRODUCTION

This research examines the behavior of a structurally integrated conformal antenna array on typical small unmanned aerial vehicle (sUAV) wings to determine effects on radar performance and develop structural design guidelines. The primary focus was determining the effect that small changes in loading or wing stiffness would have on antenna gain and beamwidth when not properly corrected for with phasing. The goal of the conformal array was to allow a small to medium size UAV to carry a low frequency radar. The long wavelengths of these systems dictate correspondingly large antennas, which are difficult to accommodate on small UAV's.

Motivations

The original motivation for this research stems from a need for ground elevation survey to support remote area water distribution system design. The Oklahoma State University (OSU) chapter of Engineers Without Borders (EWB) was examining the feasibility of a project centered on a water piping and distribution network in a remote portion of rural Guatemala. The piping network design

requires that the elevation profile along the route be known in order to determine the pressure head at each location. This information is then used to position components such as pumps and pressure relief.

There is minimal survey data available for this area, so EWB would need to perform a survey to develop the elevation profile. This can be done from the ground using traditional optical systems, or a series of GPS readings. Since the local terrain is primarily hills with a forest canopy and there are few roads, this process would need to be done on foot. This results in the survey being tedious and inefficient.

Figure 1 Example of terrain in Guatemala

The survey process could potentially be expedited by performing it from the air. Experiments such as [22] have shown that aircraft can provide a very accurate elevation model using a ranging device such as a radar or LIDAR. These systems transmit electromagnetic signals and use the

time required for the signals to return to determine range. The difference between the two is the frequency used, with LIDAR operating in the near-infrared and visible spectrums and radar using radio waves. The difficulty with using an airborne LIDAR and most radars to map the location in Guatemala is the heavy forest canopy. The sensor will detect the canopy but will be unable to penetrate to the ground below. This difficulty can be addressed by selecting a radar frequency that penetrates foliage. These systems are known as foliage penetrating or FOPEN radar. These radars typically operate in the ultra-high frequency (UHF) band.

Discussion with members of the OSU School of Civil and Environmental Engineering (CIVE) advisers to EWB-OSU indicated that an area resolution between 3 and 6 meters is desirable, along with an altitude resolution of 0.3 to 1 meter [27]. The requirement for area resolution would require a relatively narrow beam at a close range. For example, an 11° beam at 30 meters above ground level (AGL) will provide 6-meter area resolution, while a 5.5° beam will provide 3-meter area resolution from the same height. The elevation resolution is not a function of the antenna, but rather the processing equipment that is determining range and the pulse repetition frequency. Additionally, the hilly terrain also dictates that side lobe levels be kept down, especially near the main lobe in order to eliminate clutter from terrain not being mapped.

These requirements for the beam pattern, combined with the relationships between frequency and beamwidth discussed in chapter 2, suggest that a large nadir pointing array is necessary if such a survey is to be done from the air. The local terrain in Guatemala, as well as lack of available airstrips and cost concerns make it desirable that the antenna be paired with an aircraft that can be launched and recovered without a runway and that is small enough to be transported by a light truck. The obvious location for such an array on a sUAV is the lower surface of the wing and fuselage. A similar arrangement is proposed in [3] but no analysis is performed. It was decided to perform research into the feasibility of integrating such a radar system into a sUAV as a means of developing a small airborne survey system.

CHAPTER II

LITERATURE REVIEW

The objectives of the literature review were to examine the methods of airborne radar ground mapping, identify existing ground mapping radar systems, develop an understanding of radar antenna operation in general and radiation patterns specifically, review research already done to support conformal arrays, and identify the current gaps in research and capabilities relevant to the mounting of a low frequency conformal antenna for a sUAV.

Methods for Ground Mapping

There are 2 primary methods of mapping the ground with regards to elevation: synthetic aperture (SAR) and radar altimetry. SAR is able to map a larger area, but radar altimetry is likely to provide much better resolution of the elevation. A SAR can quickly provide a map of a large area, but altimetry may be faster and more accurate over a chosen route.

Synthetic aperture mode refers to the use of the antenna's motion to artificially elongate the antenna. By having a longer antenna, the resolution of a ground map can be increased. In order to do this, the beam is steered to a side looking orientation, and the radar transmits a series of pulses

as it travels. The returns from these pulses are sorted into range bins that are then integrated to produce an image that can be similar to a photograph. The resolution of each pixel is determined by the beamwidth of the antenna, and the pulse repetition frequency of the radar, which is independent of the antenna and will not be discussed here. SAR can provide a very detailed image of a large area, but the elevation data is limited, and objects such as hills can cast shadows that hide smaller features from view [20].

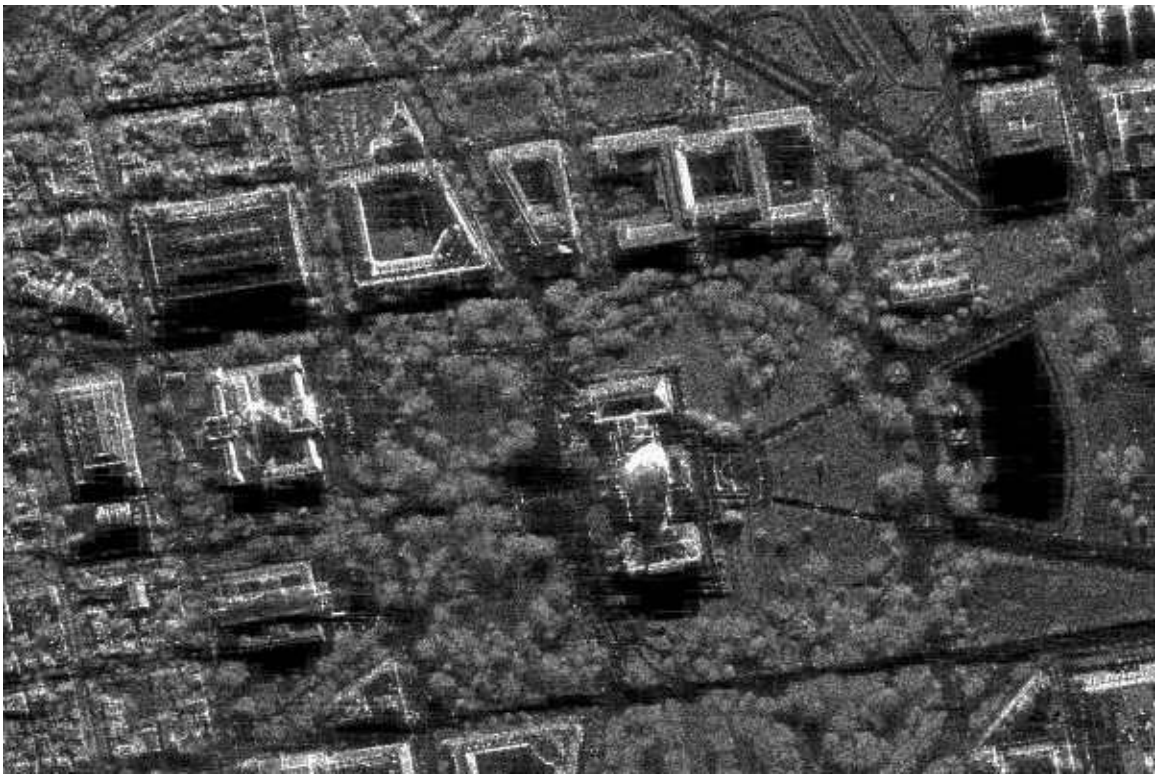

Figure 2 A SAR image. Source: Purdue Univ.

Radar altimeters are common to most commercial aircraft and are used to determine the true height above ground. Many operate as frequency modulated continuous wave radars, or FM-CW. In these systems, the radar continuously transmits and receives. The frequency is changed according to a saw tooth function, and the return signal is combined with the transmission. This result is put through a Fourier transform and the difference of the 2 signals is used to determine the range. Typical radar altimeters have very wide beams, in order to detect possible hazards

ahead and to the side of the aircraft. For a ground mapping application this is unacceptable, as the patch of ground mapped would be too large. Also, the aircraft must overfly every point of interest to develop a full map [20].

An ideal antenna is one that can perform both roles. The SAR mode can be used to map large areas in order to identify possible candidate routes for a pipeline. Following missions can overfly these routes and use radar altimetry to develop a digital elevation model of the proposed route. Fortunately, the requirements for the antennas are similar, as they would both operate at UHF frequencies in order to provide FOPEN capability and would require a narrow beam. This antenna would then be paired to a sUAV that can be easily transported by truck and operated in austere conditions.

Current Systems

There are several radar systems currently in use aboard UAVs for SAR and other ground mapping tasks, including some with foliage penetrating capabilities. These include the Lynx system used aboard the Predator family and the FORESTER system developed by DARPA for rotary wing aircraft [23] [15].

The LYNX radar uses a parabolic reflector antenna mounted in a radome occupying the nose of a UAV, in the location usually used for EO-IR sensor payloads. The system is capable of operating as both a SAR as well as being able to detect moving targets through Doppler shift, which is referred to as ground moving target indicator (GMTI). When functioning as a SAR, the LYNX system is able to provide resolution of 3 m from ranges up to 30 km. The LYNX operates between 15.3 and 18.2 GHz, so it has no foliage penetrating capability. Additionally, the higher frequency allows for the antenna to be much smaller than a FOPEN system. The reflector is 17.5 inches across [23].

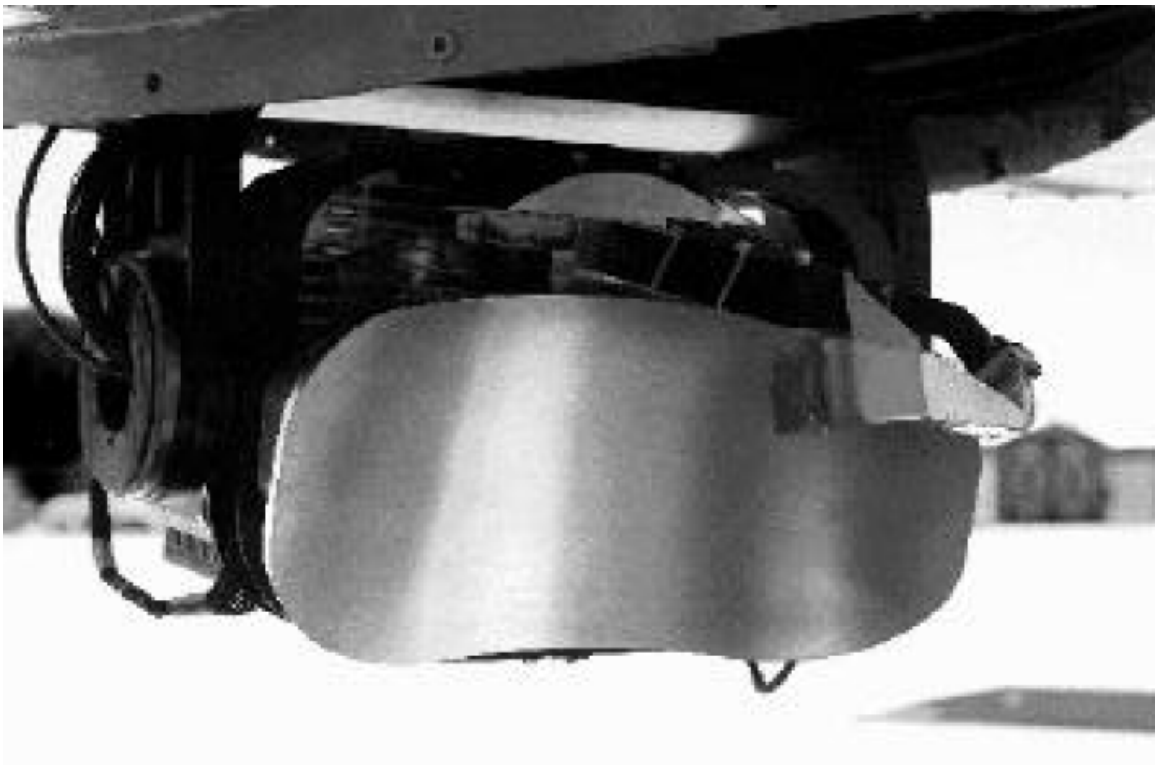

Figure 3 The LYNX radar antenna [23]

The LYNX is able to provide the desired resolution required for the terrain mapping mission and may be small enough to be mounted on a sUAV, but it's high frequency prevents it from operating as a foliage penetrating radar. In order to add a FOPEN capability to the system, the frequency would need to be lowered below 1 GHz. This means cutting the frequency by a factor of 15, and increasing the wavelength by the same. According to correlations discussed later in the chapter, this also means that the antenna dimensions would be increased by a factor of 15, to over 260 inches. This would prevent it from being used on any but the largest manned aircraft. This would suggest that a reflector type antenna is an unacceptable choice for terrain mapping through foliage from a sUAV.

The FORESTER radar developed by DARPA is a FOPEN system designed primarily for the detection of moving objects under foliage through the use of GMTI operation with a secondary SAR operation. The radar is a stand-alone system meant to be deployed on helicopters, as their

lower ground velocity in hover allows slower moving objects to be detected. The antenna is contained in a 21 ft. long pod mounted below the aircraft and allowed to rotate to scan through 360°. When operating as a SAR, the system has an area resolution of 6m. The elevation resolution is not discussed, but will be independent of the antenna [15].

Figure 4 The FORESTER mounted on a Boeing A-160. [15]

The FORESTER is a more suitable system for the ground mapping mission required in Guatemala, as it provides FOPEN capability as well as the desired resolution. However, the antenna is still very large and not suitable for a vehicle portable UAV. The antenna is housed in a pod that is meant to be aerodynamic and resembles an airfoil, suggesting that the design could possibly be adapted to a fixed wing s UAV. Moving from a rotary wing to a fixed wing platform should have minimal effect on the radar's effectiveness, as the selection of the rotary wing

platform was made for the GMTI mission, which can be omitted for the purposed of ground mapping.

Antenna Operation Overview

Radar systems operate by transmitting, receiving and interpreting electromagnetic signals in the radio spectrum, 3 kHz to 300 GHz. The portion of the system that transmits and receives the signals is the antenna.

The relationship between frequency and antenna size is determined by wavelength and the expression

$$C = f\,\lambda \tag{2.1}$$

With C being the speed of light. Therefore, frequency and wavelength are inversely related, and a lower frequency will result in a longer wavelength. This longer wavelength will demand a correspondingly larger antenna. The correlation between wavelength and antenna size means that RF antennas, especially those that function at lower frequencies in the UHF range can be quite large. UHF covers frequencies ranging from 300 to 1000 MHz, with corresponding wavelengths of 30 to 100 cm [20]. Each element of an antenna will be sized proportionally to the wavelength as shown in [20], and array antennas will combine many individual elements to create a larger antenna array by spacing elements at some separation such as ½ λ. These size constraints prevent a sUAV from carrying a large antenna in conventional arrangements as the antenna becomes too large to be mounted or results in an unacceptable drag penalty.

Gain and Beamwidth

The basic criteria of antenna performance for this paper, gain and beamwidth, are defined in [5].

The gain of an antenna refers to the ratio of power transmitted in a certain direction to the power radiated in the same direction by some reference antenna. The reference antenna is taken to be an ideal isotropic antenna by convention. Therefore, an isotropic antenna would have a gain of 1. Gain is often expressed in decibels for convenience according to

$$G = 10\log\left(\frac{P}{P_{isotropic}}\right) dBi \qquad 2.2$$

Where dBi, refers to decibels relative to isotropic. The gain of an isotropic antenna would therefore be 0 dBi. Other forms can use a dipole as a reference, with units of dBd, but this paper will use the isotropic reference and dBi exclusively, and abbreviate to dB in most cases. If a single value is given for gain, it refers to the maximum gain across all directions.

The beamwidth can be measured in several ways, but a measurement at 3 dBi below the peak is common, (the "half power" point). The beamwidth is often measured in each of the principal planes of the antenna. Beamwidth is correlated with gain in that a high gain antenna will have a narrow beam and a low gain antenna will have a wide beam.

The relationships between frequency selection and the antenna gain and beamwidth are defined in [20]. The beamwidth of an antenna array, whether measured to a 3 dB drop from peak or to the null angles of the beam, will depend on the ratio of wavelength to array length. This ratio also corresponds to the inverse of the number of elements in the array in a single direction for a set spacing. Therefore, to narrow the beamwidth, more elements have to be added in the corresponding direction.

Gain is also dependent on the ratio of physical aperture area over wavelength squared. This ratio corresponds to the total number of elements in the array. As more elements are added to the array, the gain will increase. This would suggest that in order to install a high gain, narrow beam

antenna on an aircraft, it should be long in both the longitudinal and the lateral directions, and have as many elements as practical.

The most common way to increase gain and narrow beamwidth for an array antenna is the use of phasing. Phasing is the introduction of a time delay to the transmission of each element relative to its neighbors. Because the transmitted signal travels as a wave, the time delay phase shifts the signals from each element to account for small differences in range to the target. By correcting for these differences, the signals from each element will arrive in phase and interfere constructively, increasing the power radiated in the chosen direction. Phasing has the additional advantage of allowing the beam to be steered, but it is still not a substitute for the requirements of increasing antenna size and the number of elements.

This requirement for an antenna that is very long in both the lateral and longitudinal directions with many elements, as well as the low frequency required for a FOPEN system and the correspondingly large wavelength will require that an antenna designed to provide a tight beam through a forest canopy may become very large relative to the aircraft. As an example 1 GHz system that is 10 elements wide will require 1.5 m of available space.

Conformal Antennas

One means of installing a large antenna on a small aircraft is a conformal antenna. A conformal antenna matches or nearly matches the aircrafts outer surface, allowing it to have a large area without affecting the aerodynamic performance of the aircraft. Such antennas are often built on or in the skin of an aircraft.

Conformal antennas can be designed to either bear aircraft structural loads or be isolated from them. There are trade-offs associated with each configuration. Load bearing antennas are referred to as Conformal Load bearing Antenna Structure (CLAS). Those antennas that are not structural are referred to as Conformal Non-Load bearing Antennas (CNLA) [3].

CLAS antennas are a subset of aircraft components referred to as multi-function structure. Traditional design separates most load bearing structure from other systems such as armor, power systems and sensors. Multi-function structures sacrifice simplicity for weight savings by combining these systems with structural elements. In the case of a CLAS antenna this comes from combining the function of aircraft skin with the antenna. The result will be heavier than either the original skin or antenna, but can potentially be lighter than the combination due to the need for structural reinforcements such as doublers being removed or at least reduced, and the mounting structure for the antenna being discarded.

Even if the antenna is not a structural antenna it can provide benefits. The primary benefit of both CLAS and CNLA antennas is the reduction in drag. Many antennas on board aircraft are of the planar array or reflector dish type. These antennas are inherently poor aerodynamically, and are often concealed behind radomes or other fairings. These coverings do mitigate a significant amount of the drag penalty of the antenna, but may not be the fully optimal solution. Examples of structures that have drag penalties include the rotating array on the E-3 Sentry or the large cheek fairings on the RC-135 family of aircraft. Aircraft will also carry many smaller antennas with lower drag penalties such as the blade antennas used for communication.

Figure 5 USAF E-3 Sentry. Note the radome on its back. Source: AF.mil

Figure 6 USAF RC-135 electronic surveillance aircraft. Note the cheek antenna fairings and the blade antennas along the spine and at the wingtips. Source: AF.mil

The use of conformal antennas also offers benefits to RF performance. Traditional antenna arrays are often mounted at a single point, such as the nose of a fighter aircraft [3]. By using the entire aircraft surface to distribute the array, the performance can be improved. A conformal array has been found to increase range of fighter radios over traditional antennas, and the use of a single antenna for multiple systems could allow for the number of antennas to be reduced significantly. This concept could also be used to mount larger arrays such as the one proposed above for foliage penetrating radar, or possibly even ground penetrating radar.

Conformal antennas may also offer an increase in damage tolerance by virtue of being lower profile than a blade antenna or similar. Protruding antennas can be damaged by objects passing near the aircraft skin. This can include foreign objects during takeoff, landing or other low level flight, as well as ground operations such as taxi and maintenance. By mounting the antenna flush to the aircraft skin, the risk of objects colliding with the antenna is significantly reduced [3].

The tradeoff to a conformal antenna is the added complexity it introduces. The simplest form of conformal antenna to produce is the flat or planar type. However, there are few places on most aircraft where a planar antenna can be located without changing the outer mold line. Therefore, most conformal antennas will be curved in some way. For simple curvature in 1 direction, such as the fuselage tube common to most aircraft, the difficulties of making the antenna are relatively small, and the performance losses are minimal. The ideal case aerodynamically is to produce an antenna with complex curvature in 3 dimensional space to perfectly match the aircraft outer mold line. This would result in very difficult and expensive production that increase according to the complexity of the antenna shape.

The other significant hurdle to use of conformal antennas is the need for wider bandwidth. Most conformal antennas offer very low bandwidth, which is needed if an antenna is to operate as a multifunction array for multiple systems. This can be countered by either stacking antennas or increasing their thickness, but both of these solutions result in weight penalties that will have to be judged against the RF performance benefits offered [3].

In summary, the use of conformal antennas for aircraft offers an opportunity to expand the envelope of capabilities while better optimizing the aircraft for weight and aerodynamic performance. A large distributed array can offer increased RF performance, particularly in the low frequency range, with a smaller drag penalty than a more traditional mounting style.

Patch Antennas

For a conformal array to match or closely follow the aircraft skin, the antenna elements must be low profile. This requirement would suggest that the antenna elements be patch style antennas. As described by [4] and [14] a patch antenna is a low profile, lightweight directional antenna consisting of a conductive transmitting surface spaced above a ground plane by some dielectric substrate. The entire antenna can be produced through printed circuit board techniques, resulting

in ease of manufacture. The transmitting surface is usually rectangular or circular, but any shape can be used. The antenna can also be fed in a variety of ways, with a printed strip or a coaxial feed being the most common.

The patch antenna functions by creating an alternating voltage differential between the ground plane and the transmitting surface. This voltage difference results in an electric field developing in the substrate. The field frequency will be driven by the applied voltage function, and the wavelength of the field inside the antenna will be determined by the speed of light in the substrate. The electric field extends beyond the boundaries of the transmitting surface in the fringing fields. These are the source of the radiation propagating into free space.

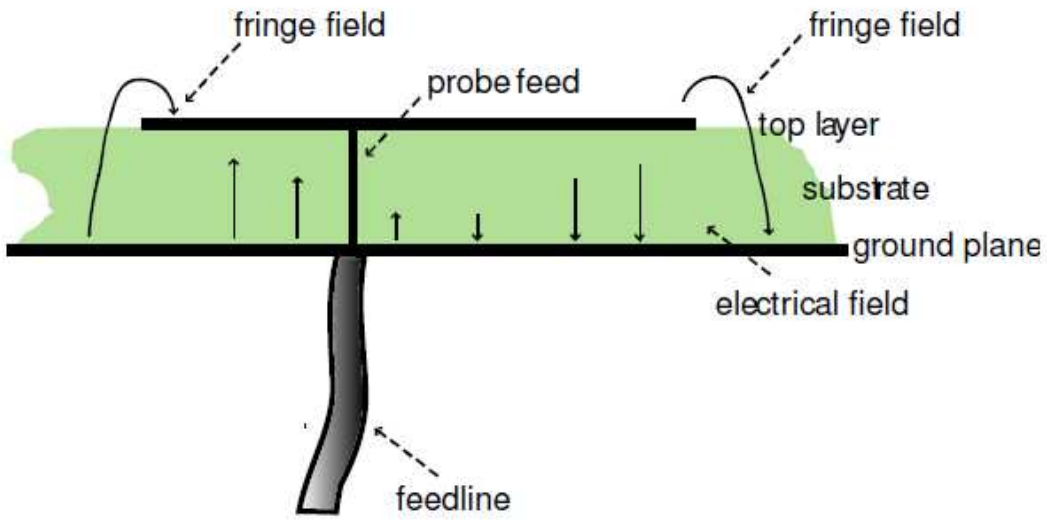

Figure 7 Cross-section of a patch antenna. [14]

The desired operating frequency of the patch will determine its dimensions. The transmitting surface should be approximately sized to half of the wavelength in the selected substrate. That is,

$$L \approx \frac{\lambda_0}{2\sqrt{\varepsilon_r}} = \frac{C}{2f\sqrt{\varepsilon_r}} \qquad 2.3$$

Where C is the speed of light in a vacuum and ε_r is the dielectric constant of the substrate material [14]. This dimension applies to rectangular and circular antennas, but more complex shapes can be used with more complicated analysis. The ground plane should also be longer than the transmitting surface in order to transmit as much energy forward as possible. Because antenna elements are often spaced at half wavelengths in arrays, the value of ε_r is important as a larger value will allow for a smaller patch, meaning the patches will have greater separation and less interaction when transmitting.

The thickness of the substrate will determine the bandwidth available to the antenna. This beamwidth determines what range of frequencies the antenna is able to transmit. The bandwidth of patch antennas is usually very narrow, in the range of 3 %. The bandwidth can be increased by thickening the substrate or by stacking several patches to give a selection of several small bands or increase the bandwidth, depending on the feed method. Both options do incur penalties to weight and profile [14].

Patch antennas have a radiation pattern that is directed primarily to the forward hemisphere, with a moderate beamwidth and a gain that can be up to 9 dB. The radiation pattern for a patch antenna is seen in Figure 8.

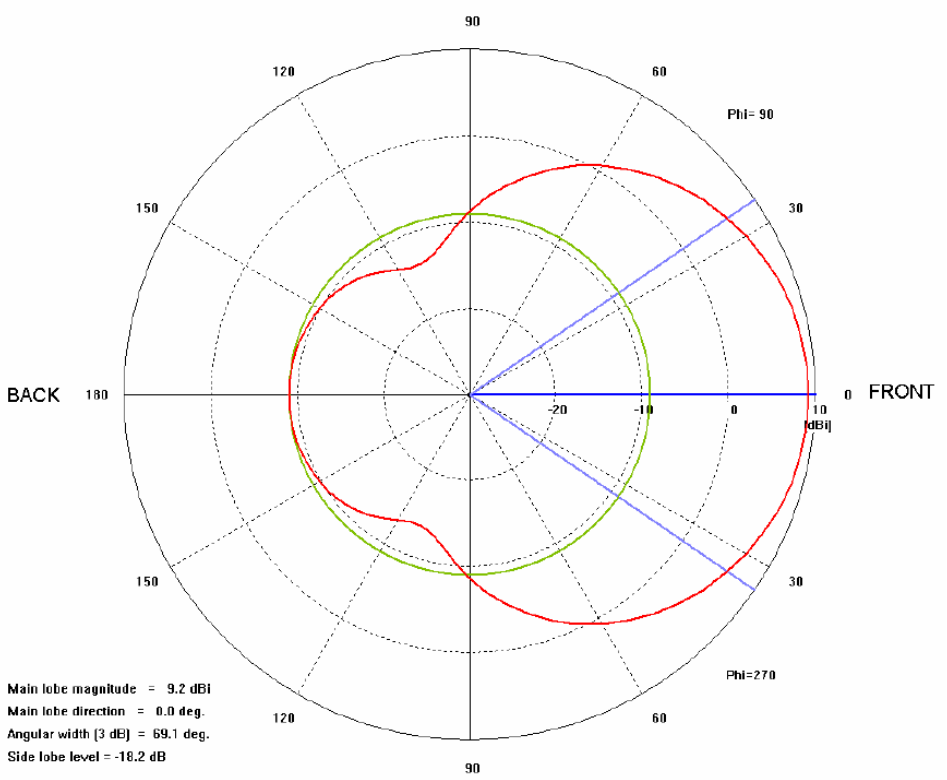

Figure 8 Typical patch antenna pattern. [14]

A conformal array of patch style antennas mounted to the underside of the aircraft is a promising solution to the challenge of integrating a low frequency FOPEN radar to a sUAV for a ground mapping mission. Such an array offers the ability to install a large, low frequency antenna on an airframe that is small enough to be transported by truck and operated without a runway.

Cruciform Antenna

As discussed earlier, the combination of narrow beamwidth and low frequency required for a FOPEN ground mapping radar requires an antenna that is very long in both the lateral and longitudinal directions. The simplest way to achieve this goal is to use as much of the aircraft's lower surface as possible. This results in a cross shaped or cruciform antenna that runs along the length of the fuselage underside and across the underside of the wing for much of the span. Using the entire span and fuselage would be ideal, but the need to include other components such as control surfaces prevents this.

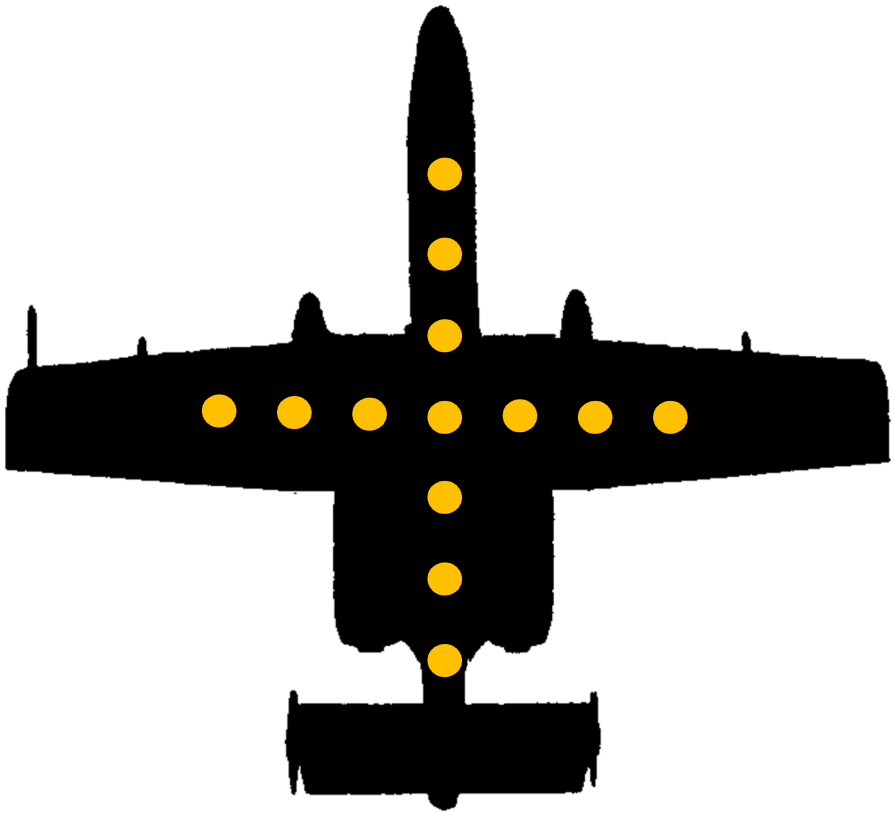

Figure 9 Cruciform array superimposed on an A-10 silhouette. Source: AF.mil

The simplest version of a cruciform antenna is a pair of crossed linear arrays seen in Figure 9. Each linear array generates a fan beam that resembles a 2 dimensional plane normal to the sub-array. These fan beams are then crossed at a 90° angle to create a beam that resembles a cross, with a slight peak at the intersection where both beams reinforce each other. This pattern can be seen in Figure 10 [6].

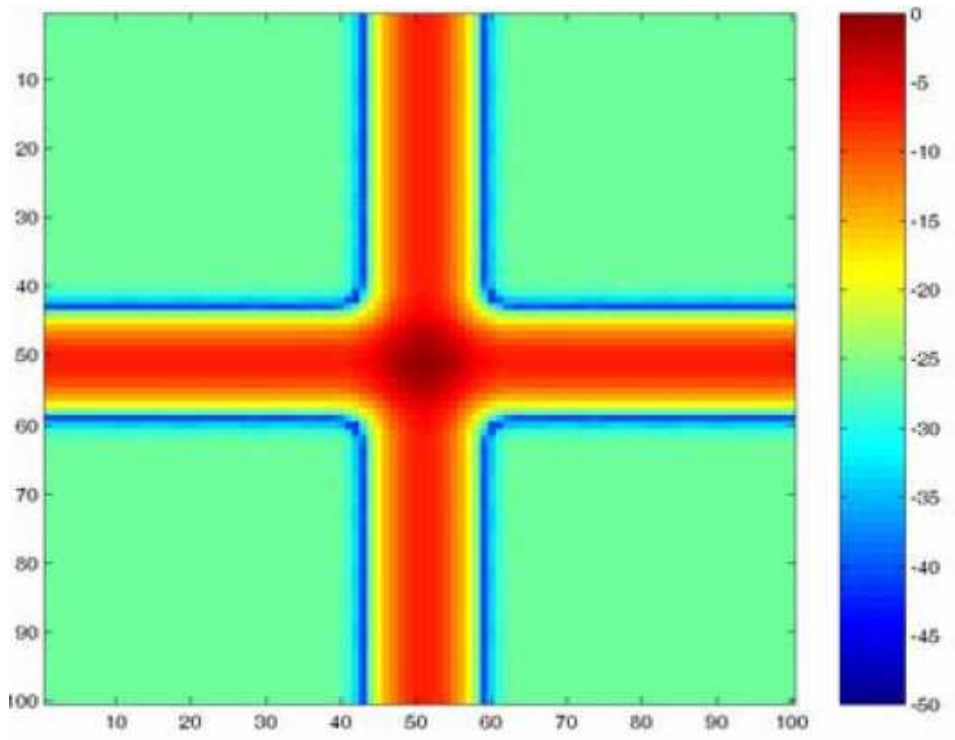

Figure 10 Generalized cruciform radiation pattern. units of dBi and degrees [6]

These fan beams can be narrowed to resemble pencil beams by adding additional rows of elements to the linear arrays, so that the antenna resembles a pair of crossed rectangular arrays. This array is very suitable to an aircraft, as it matches the basic planform, using the wings to house one array and the fuselage to house the second array. It also maximizes the number of elements in the lateral and longitudinal direction, resulting in a narrower beam.

Design Concept

In order to provide airborne FOPEN ground mapping capability for the purpose of developing elevation maps in remote locations, a sUAV with a cruciform shaped conformal array of patch antennas mounted to the underside of the aircraft is identified as a potentially viable solution. The aircraft would allow for operations to be performed quickly without the need for a large support network or runway. The conformal cruciform antenna would provide the narrow beam required for accurate measurement.

Relevant Research and Knowledge Gaps

With the design concept established, the associated challenges must now be identified and addressed. A review of studies related to the design is undertaken. In order to limit the scope of the search, a focus was placed on structural effects on the antenna. This primarily concerns wing deflection and bending and how they relate to antenna gain and beamwidth. This search allows a specific gap in knowledge to be identified. The results of the search are presented below.

Airfoil Conformal Antennas

The prospect of using a wing conformal patch array has been explored in [21], specifically a 2 dimensional patch antenna array wrapping around the entirety of the wing cross section. The goal of wrapping the antenna around the wing to match the airfoil was to allow for complete coverage forward, above and below the aircraft. The antenna arrangement meant that for any look angle, only a certain number of elements would be used. As an example, in order to look above and forward of the wing, the elements on the leading upper surface would be used. All other elements would be either masked, such as those on the lower surface, or be angled too far away to provide useful amounts of power, such as those elements on the upper surface closer to the trailing edge.

The study sought to perform a pattern synthesis for various look angles, and determine the necessary excitation for low side lobes and narrow beams in each direction. The primary conclusion was that the radiation patter side lobes are more controllable for a surface with a small radius of curvature. Beams pointing above and ahead could see their side lobes brought down 40 dB from the main lobe. A beam pointing straight ahead from the leading edge was only able to reach side lobes 23 dB below the peak. It is also important to limit how far from the direction of the main lobe the normal vector of each antenna element is allowed to deviate.

While this study does consider the effect of a wing conformal array, there is no discussion of how deflection would impact the antenna performance. Additionally, the antenna considered differs

significantly due to its configuration. The finding that an antenna with a large radius of curvature is more controllable is encouraging, as the radius of curvature for a wing under flight loads should be large, especially with regards to the antenna wavelength.

3 Dimensional Conformal Arrays

The deflection of a wing will result in the normal vector of the attached antenna array to change, resulting in a change in pointing angle. Research into this effect is done in [17] for a joined wing aircraft. In a joined wing, the aircraft has a forward and aft wing that are both swept so that they come together at or near the tip. The wings may also be set at different heights relative to the fuselage. This arrangement can be seen in Figure 11.

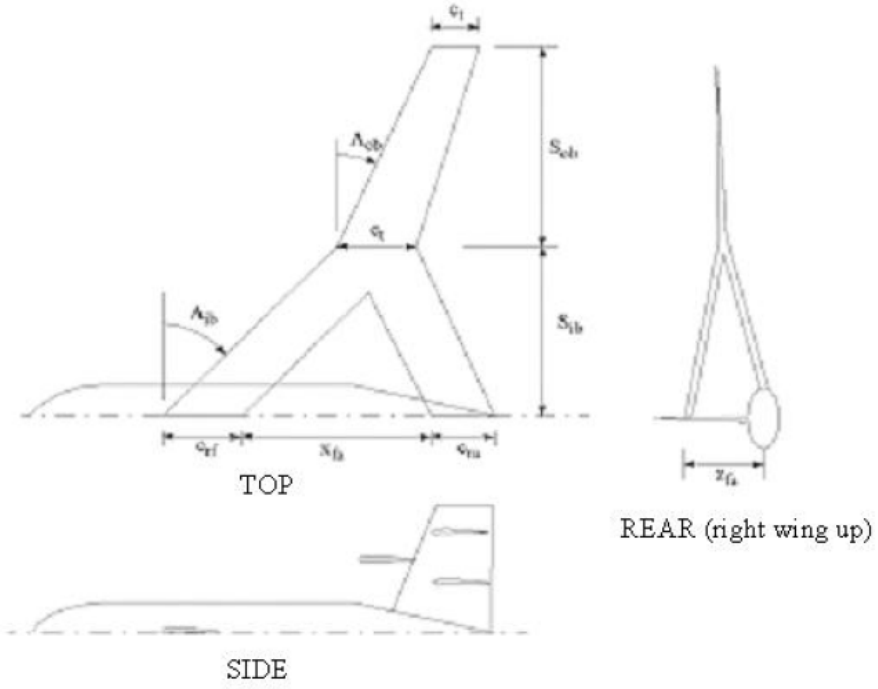

Figure 11 A joined wing aircraft [17]

A digital model of the aircraft, including load bearing antennas, was constructed and analyzed under flight loads. To simulate the antenna with regards to RF performance, an array of dipoles operating at the selected frequency of 430 MHz along the wing was simulated in both a

MATLAB program and a more specialized program, NEC-Win Plus+. Both programs used separate means of calculating the antenna performance, but only the MATLAB program accounted for translation and rotation of the elements. The two programs disagreed on the gain and the direction of the main lobe in certain conditions, but overall the MATLAB program was found to be an acceptable approximation. This, combined with its easier integrations with the structural analysis tools made it a preferred choice for analyzing the antenna in a design case.

While this study does examine the effects of aerodynamic loadings and the resultant deflection on a wing conformal antenna, there is no examination of the change in beamwidth or gain that results from this deflection. Because the array considered is only mounted on one wing, rather than dispersed along the entire underside of the aircraft, there is likely to be minimal deformation of the antenna itself. It does however suggest that such calculations can be done and that the MATLAB program may provide an acceptable numerical solution.

Deformation of Patch Antenna Elements

The deflection of a wing may deform the patch antenna elements, so the effects of bending these must be considered. A multi-band patch antenna was developed and examined by [8] regarding the effect of curving the antenna through a variety of angles, paying attention to the gain and beamwidth of the antenna.

Figure 12 Bent patch antennas. Each is approximately 45 mm square. [8]

The bending angle of the antenna was varied from 0° (planar) to 270° (far right of fig 11). The values of both gain and beamwidth were simulated and measured experimentally. It was found that gain would remain near that of the un-deformed case for smaller deflections, but would drop off beyond 90°. The beamwidth widened as the antenna was bent further, but this also varied with frequency.

The curvature angles that can be expected on the lower surface of a wing as a result of bending should not be very large relative to the cases presented above, so there is likely no need to consider the effect of bending individual elements in the determination of the radiation pattern form an array of these elements.

Deformed Arrays in Bending

The bending or deformation of a phased array can be expanded to other scenarios beyond the wing conformal array. The effects of antenna deformation with regards to satellite based arrays has been examined in [25] and the results can be applied in a similar manner to aircraft. Satellites, like aircraft, must be light weight in order to control the cost of launching them. This results in minimal structure that will experience very high loading. This means that some bending in satellite antennas is often expected.

In order to examine the effects of this deformation on satellite antennas, a model of a theoretical antenna was bent in 1 and 2 dimensions, then analysis of the radiation pattern was performed using array theory. For the 1 dimensional deformation, the array is deformed in a bent slab, according to the function

$$z = z_{max} \left({}^{x}/_{xmax}\right)^2 \qquad 2.4$$

With maximum displacements $z_{max} = 0$, $z_{max} = \lambda/2$ and $z_{max} = 1\lambda$. The deflections in X and Y are assumed to be negligible. This array is phased according to the planar case with a 24.3 dB taper applied. The taper, sometimes called aperture illumination, refers to a non-uniform power feed across the different elements, with those in the center drawing the most power and those further away drawing less according to some weighting function. This has the effect of lowering the side lobe levels at the expense of slightly widening the main lobe and can be seen in Figure 13.

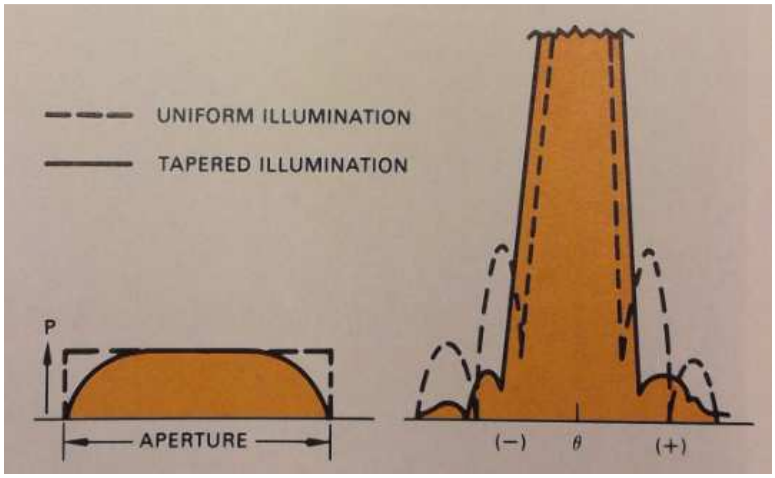

Figure 13 Effect of tapered aperture illumination [20]

The increases in deflection in the antenna resulted in a decrease in peak gain versus the planar case and an increase in beamwidth in the φ = 0° plane, but minimal effect in the φ = 90° plane other than a drop in the levels of the side lobes when compared to planar. The results are reproduced in Figures 14 through 19. These figures show plots of gain relative to the peak vs the

sine of the angle θ from broadside in both the φ=0° and φ = 90° planes for all 3 deformation cases. The primary features in each plot are the prominent main lobe and the smaller side lobes that flank it. A comparison shows that an increase in deflection results in the main lobe widening and losing some of its peak gain.

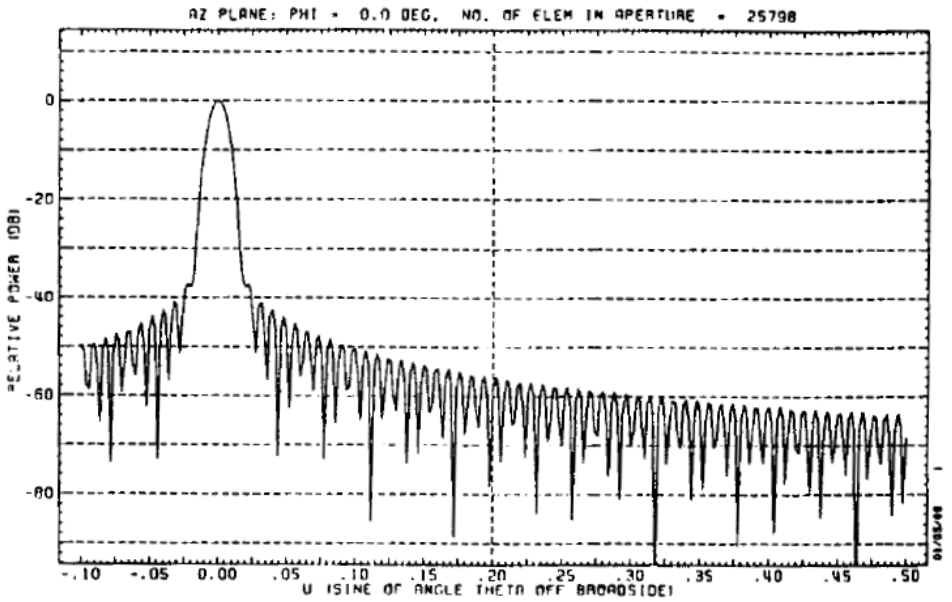

Figure 14 Undeformed radiation pattern in the φ = 0 plane [25]

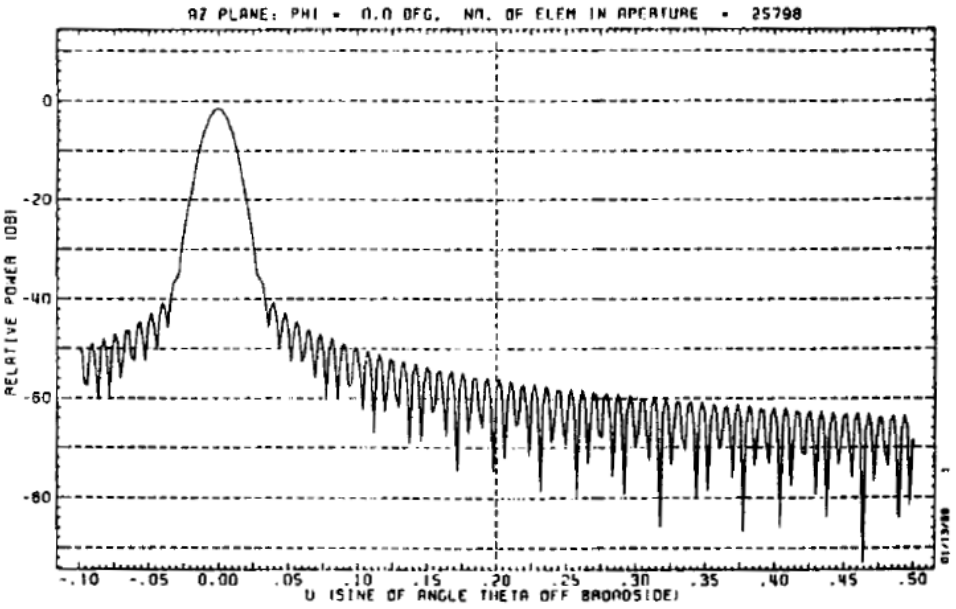

Figure 15 Radiation pattern in the φ = 0 plane for z=1/2 λ [25]

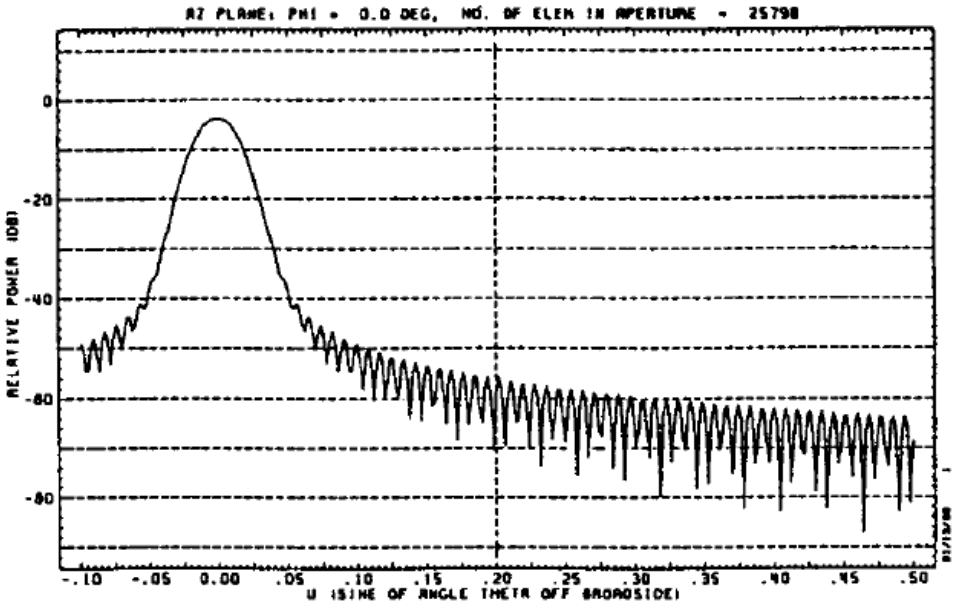

Figure 16 Radiation pattern in the φ = 0 plane for z=1 λ [25]

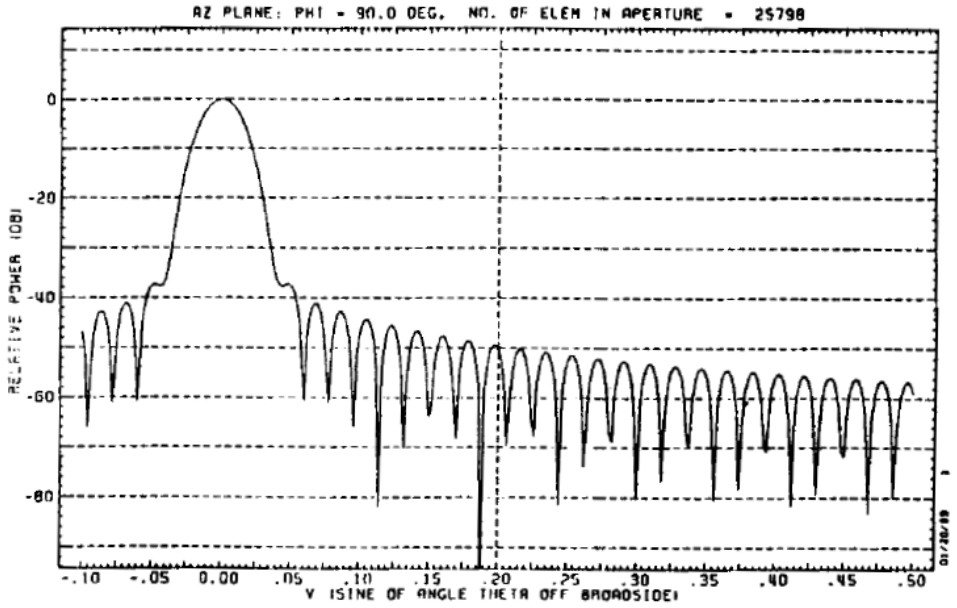

Figure 17 Undeformed radiation pattern in the φ = 90 plane [25]

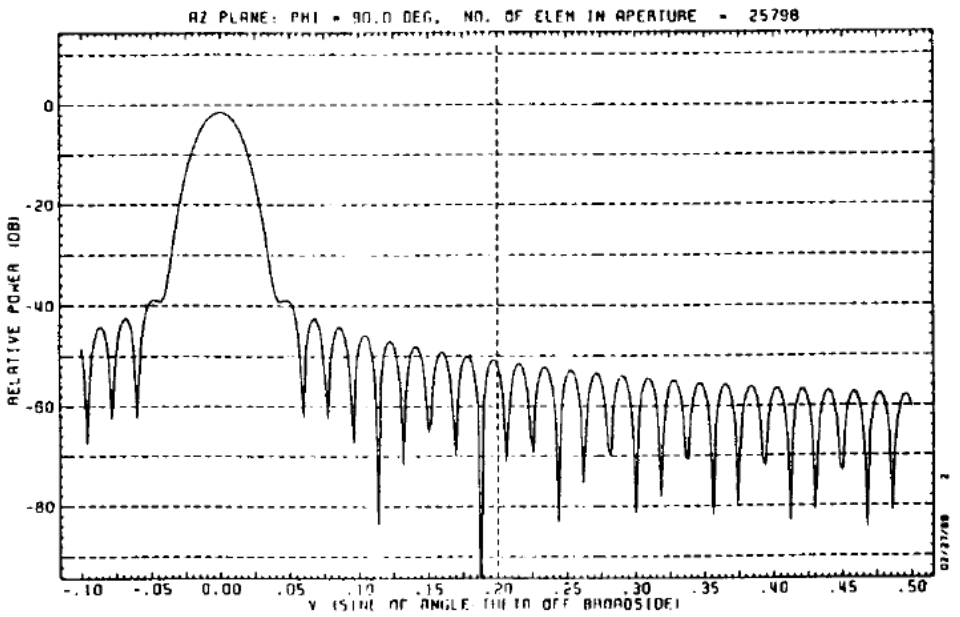

Figure 18 Radiation pattern in the φ = 90 plane for z=1/2 λ [25]

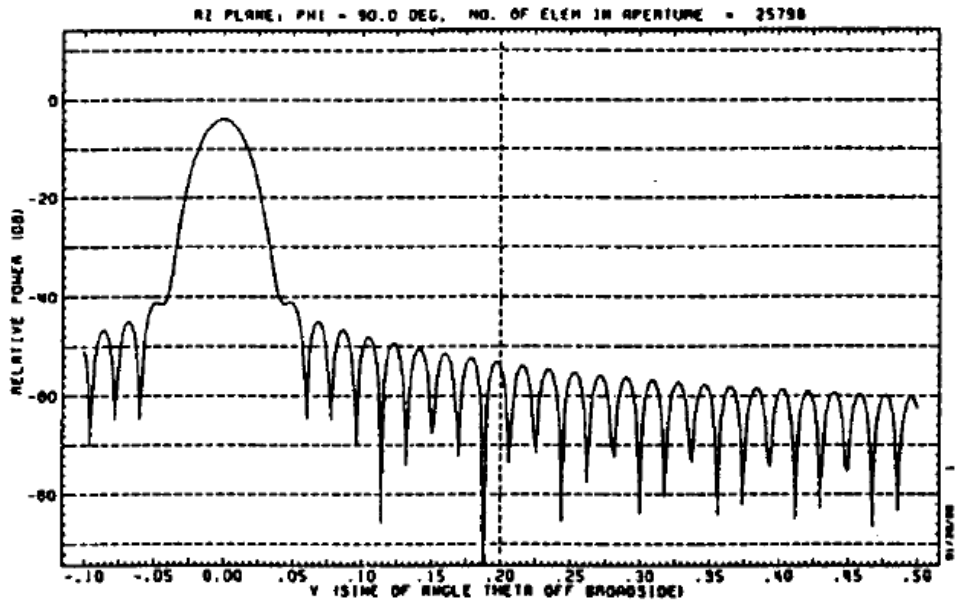

Figure 19 Radiation pattern in the φ = 0 plane for z=1 λ [25]

The results from [25] indicated that the gain and beamwidth losses will be dependent on how much the wing deflects as a percentage of the wavelength. This correlation could be applied to an antenna that is conformal to a wing in bending such as the cruciform antenna considered in this

paper. While the model discussed does not apply directly to aircraft, it can be adapted for application to an aircraft if the deflections can be determined.

Problem Statement

The possibility of wing bending resulting in the antenna losing gain and increasing beamwidth is a case that has been tangentially examined, but not fully explored with regards to aircraft. It was decided to examine the effects of wing stiffness and frequency selection on the antenna performance when subjected to small variations in wing loading that are not corrected for with phasing. Phasing is meant to correct for differences in range across the various elements, but depends on a knowledge of the exact locations of the elements relative to each other. Therefore, a small change in wing loading resulting from a maneuver, gust or fuel burn may move the elements out of location for phasing and degrade antenna performance.

The ideal solution for antenna performance is to make the wing stiffer, but doing so will drive up weight and cost as more material is used to reinforce the wing. A change in frequency may also give more tolerance to loading variation, since a set deflection will be a smaller proportion of a longer wavelength.

If the wing cannot be made so stiff that deflections do not occur, then their effects must be understood so that a means of controlling them can be implemented. To that end, the relationships between wing stiffness, frequency, variations in wing loading, and antenna performance must be understood.

CHAPTER III

METHODOLOGY

Research Plan

If a wing conformal antenna is to be integrated into an aircraft, the primary concerns for the radar antenna would be the effect of flight conditions changing the direction of the beam and the beam radiation pattern. For an antenna that is symmetric across the lower surface of the aircraft, the effect of wing deflection changing the look angle as discussed in [17] should be minimal. Any changes in angle resulting from aircraft pitch or roll can be measured by an onboard inertial measurement system or similar. Therefore, the changes in look angle can be accounted for with existing systems.

The effect of wing bending on antenna performance can, in theory, be completely compensated for with phasing. However, this requires that the locations of each element be known. Under steady flight conditions, the wing deflections and the location of the attached antenna elements can be pre-determined from static ground tests, analytic methods or digital models. This allows for the phasing to be performed for the specific load case tested.

If the aircraft has a change in lift as the result of a gust, maneuver, or fuel burn the phasing will no longer be accurate since the wing will be deflecting according to a different load, and the antenna elements will be at different locations than expected. This means the phasing will no longer be perfectly matched. For these scenarios the effectiveness of an antenna with imperfect phasing must be examined in order to determine if the resulting gain and beamwidth are acceptable or if additional tests must be performed in order to generate a database of antenna phasing values.

The objective of the research is to determine the following for a low frequency cruciform array mounted to a sUAV:

1. What relationship is there between wing stiffness and the tolerance of the antenna performance to small variations in wing loading?
2. What relationship is there between frequency selection and the tolerance of the antenna performance to small variations in wing loading?
3. Is such a configuration viable for a ground mapping application, accounting for small changes in wing loading that are not corrected with phasing?

To answer these questions, a means of connecting the wing behavior to the antenna performance must be devised. Wing behavior can be determined through analytic methods, digital models or experimental tests. As seen in [17] an approximate solution implemented through a MATLAB program can be used to calculate antenna performance and interface well with other programs such as CAD.

Overview

In order to examine the effects of aerodynamic loads and the resulting wing deflections on the wing conformal antenna as well as the sensitivity of such antennas to deflection, computer models of wings were developed in Solidworks™ CAD software using three different

construction methods: a foam wing supported by a metal spar, a stressed composite skin, and a stressed composite skin with ribs. These 3 designs represent common construction methods for lightweight aircraft and more importantly offer different structural stiffness's. All three models were evaluated under static loading conditions to determine the deflections of the lower surface. This data was then imported into a MATLAB program discussed below to determine the antenna beamwidth and gain. The wings were evaluated at a variety of loading conditions and two separate antennas were considered, operating at 1 GHz and 4GHz. The 2 frequencies were chosen to allow for a relationship between frequency and antenna performance to be made. 1 GHz is the top of the UHF band and is the highest frequency used for FOPEN applications. 4 GHz is the boundary between the S and C bands, and was chosen because it allows for an array with many more elements that is more sensitive to deflection.

Solid Modeling

Three wing models were developed in Solidworks in order to examine the effects of wing stiffness and construction methodology. The baseline comparison for the wing design was the RQ-7 Shadow operated by the US Amy. The Shadow has a 14 ft. wingspan and a maximum gross weight of 375 pounds. For this study the maximum weight was increased to 700 lb. to account for the need to mount the processing equipment associated with the radar, as well as extending the fuselage needed to provide a mounting surface for the cruciform antenna. In order to determine the strength required in the wings, the operational conditions must be considered. For a ground mapping mission, the maneuver loads will be low, so a 3g limit load is taken from [5]. A factor of safety should also be applied. This is most often 1.5, bringing the ultimate load to 4.5 g, or 3,150 lb. For composite structures, this factor of safety is increased to 1.8, making the ultimate load 3,780lb [5].

The first model is a foam wing with a solid aluminum rod spar and will be driven by the 3,150 lb. ultimate load. The spar is a solid circular rod, has a 2 in. diameter and is made of 6061-T6 aluminum. The wing itself is made of generic Styrofoam™ and is used to give the airfoil shape but is not assumed to provide any structural support. The wing was evaluated in Solidworks and the spar was found to yield at or slightly above 3,500 lb. total applied load. The area moment of inertia for the aluminum spar is measured to be 0.79 in^4. Combined with an elastic modulus of slightly over 10 MSI, the total beam stiffness term EI is 7.907e6 lb. in^2. The Styrofoam wing is assumed to contribute minimally to the overall stiffness. The wing has a total structural mass of 30 lbm. per wing. The wing can be seen in Figure 20.

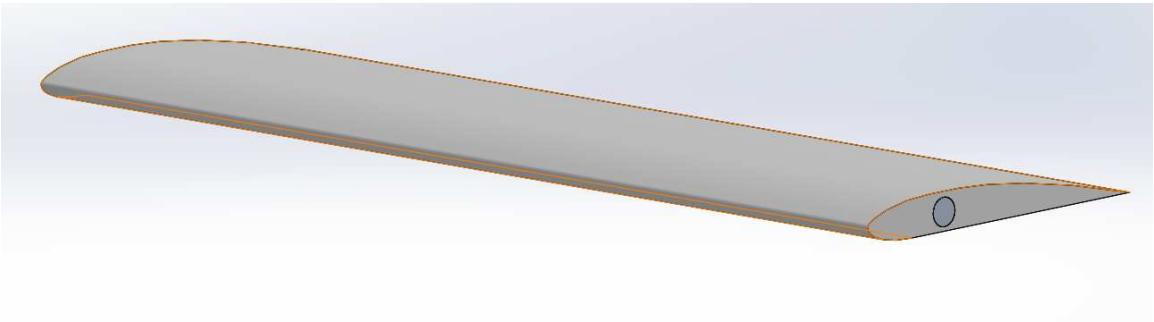

Figure 20 Foam and Spar wing

The second wing design is a glass composite stressed skin wing with a C-channel spar driven by the 3,780 lb. load. The stressed skin model, including the spar, is constructed with a composite layup consisting of a single 0°/90° ply in polyester resin. The resulting layup was 0.076 inches thick and nearly isotropic with an elastic modulus of 2.27 MSI and an ultimate strength of 35.3 ksi. The layup was developed in a vendor designed calculator [24]. Evaluation of the wing showed that it yielded slightly above 4,000 lb. The moment of inertia for the wing is 5.22 in^4. Combined with the elastic modulus of 2.27 MSI, the total beam stiffness is 11.85e6 lb. in^2. The stressed skin wing is approximately half again as stiff as the foam and aluminum spar wing. The minimal amount of material present in this wing results in the mass being 24 lbm. per wing. This

value does not include the antennas, power feed, or control surfaces and the associated components

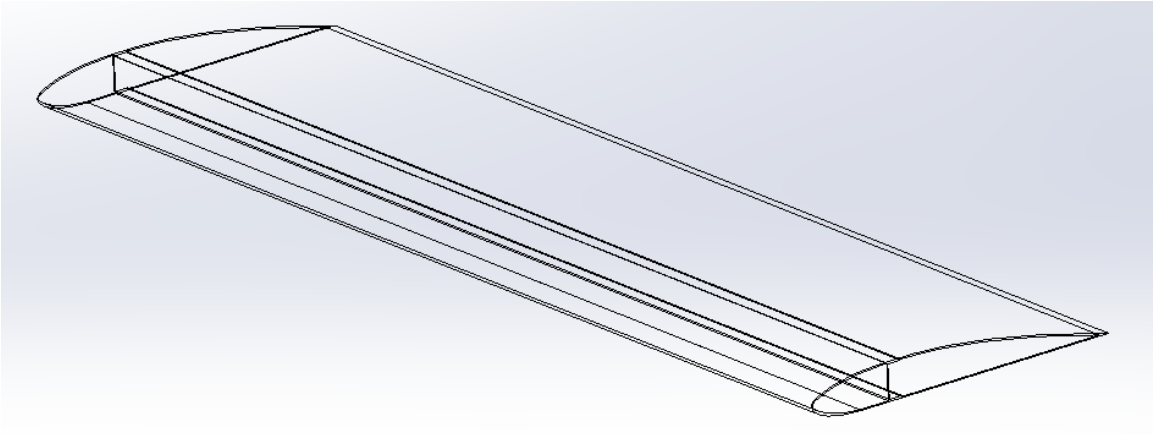

Figure 21 Stressed Skin wing

The third wing is a stressed skin wing with ribs. It is made from the same material as the second wing, but features ribs spaced at 10 in. intervals, including the ends. As with the second wing, the design was calibrated to the 3,780 lb. load. Since the cross section is the same, the ribbed wing's total beam stiffness is 11.85e6 lb. in^2. The ribs add a small amount of mass, bringing the total weight of the wing to 27.5 lbm. Once again this does not include antenna or control surface components and would likely increase. A comparison of all 3 wings is given in Table 1.

Wing Construction	Weight (per wing)	Stiffness EI (lbf. $in.^2$)	Design Load (lbf.)	Approximate Failure load (lbf.)
Foam and Spar	30 lbm.	7.907e6	3,150	3,500
Stressed Skin with C-channel spar	24 lbm.	11.85e6	3,780	4,000
Stressed Skin with spar and ribs	27.6 lbm.	11.85e6	3,780	4,000

Table 1 Comparison of wings

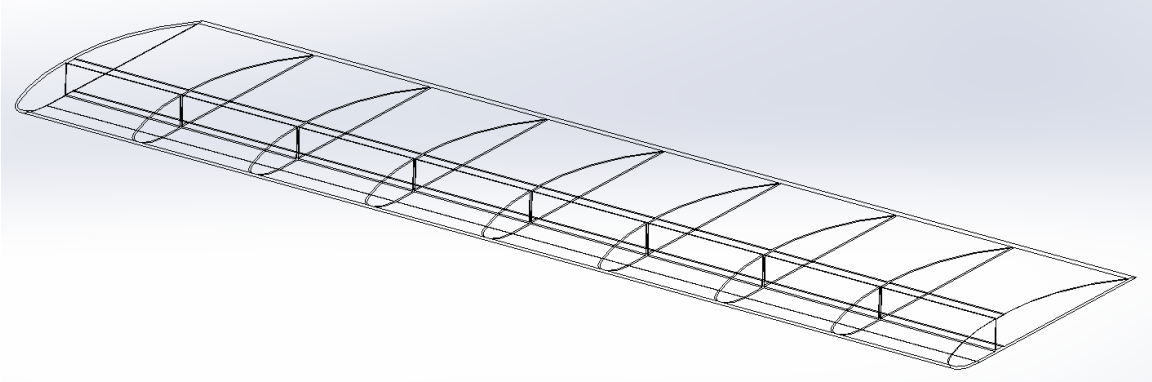

Figure 22 Stressed Skin wing with ribs

All 3 wings used an approximation of the Clark-Y airfoil with a 24" chord and an 80" span. The airfoil section is dimensioned in Figure 23. The Clark-Y was selected for the flat lower surface that the array elements would be mounted on as well as the ease of construction on flat surfaces. The Clark-Y is popular among model aircraft for performance at medium Reynolds numbers and its simplicity. As discussed in [3] the flatter the surface that a conformal antenna is mounted to, the simpler its manufacture. A conformal antenna could be applied to any wing geometry, but the flat lower surface of the Clark-Y allows for a simplified production and analysis, as the effect of distorting the individual antenna elements is removed.

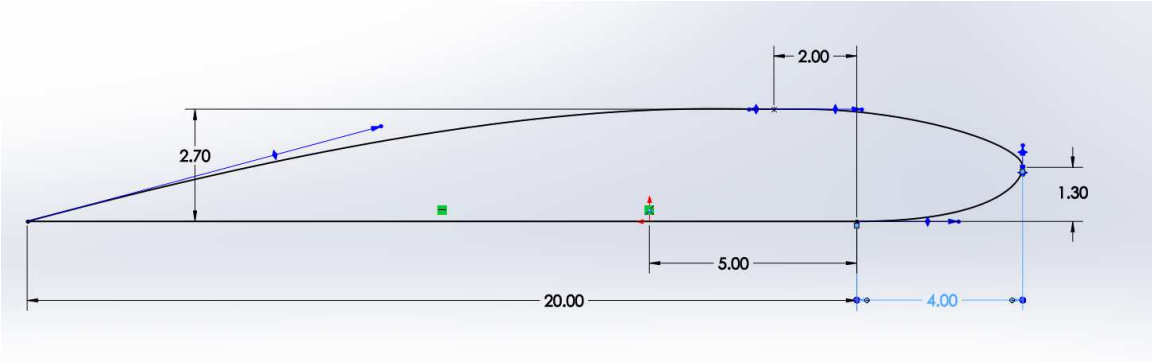

Figure 23 The Clark-Y airfoil section in Solidworks

The wings were evaluated in Solidworks™ static simulation suite for deformation under load. Solidworks uses a displacement form of a finite element method with discrete tetrahedral elements. It operates using small displacement theory and assuming linear elastic materials [18].

Solidworks was chosen due to use as the standard CAD package for OSU engineering students. As validation of the simulation, hand calculations for a basic bending case were carried out on the aluminum spar for a simple bending case using equation 3.1 and compared against the results of Solidworks. Both maximum stress values were 17.7 KSI for a moment equivalent to the 700 lb. nominal load.

$$\sigma = \frac{M\,y}{I} \tag{3.1}$$

Similar checks were made for displacement using the reference cases in [2]. The deflection for the beam under nominal load was calculated to be 7.55 inches. Solidworks returned a value of 7.58.

To define the simulation, the wing root was fixed so that it could not translate or rotate. This is to simulate the rigid attachment of the wing to the aircraft. To simulate the lift force a uniform pressure was applied to the wing's lower surface. The lower surface area is 1600 square inches. The pressure was then determined by dividing the expected lift by the area of 2 wings, or 3200 square inches. As an example, the nominal weight of the stressed skin aircraft was 700 pounds, so the pressure applied to the wing surface was 700/3200, or 0.22 psi. The pressure is not a perfect representation of the lift force a wing would experience. A more accurate depiction of lift is presented in Figure 24.

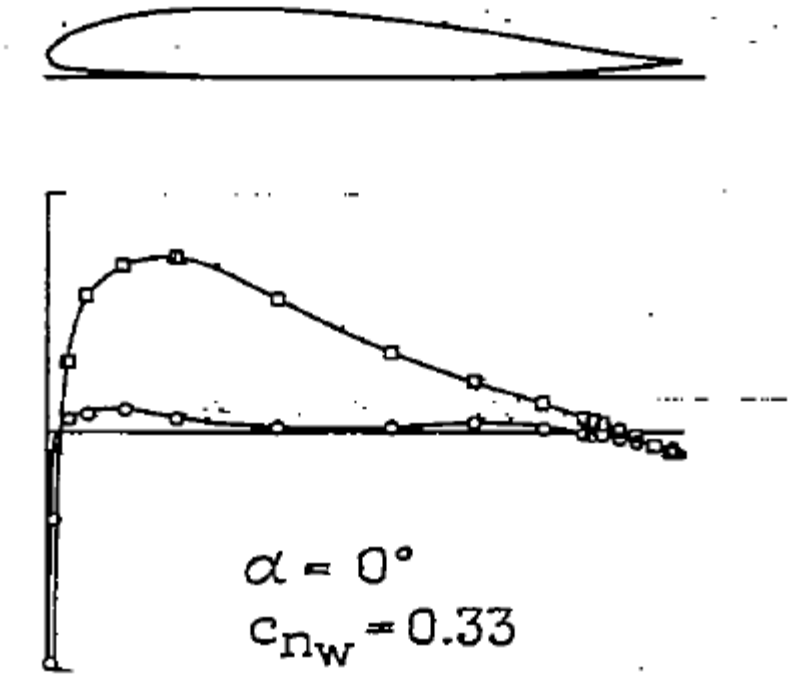

Figure 24 Pressure distribution for a Clark-Y upper and lower surface [26]

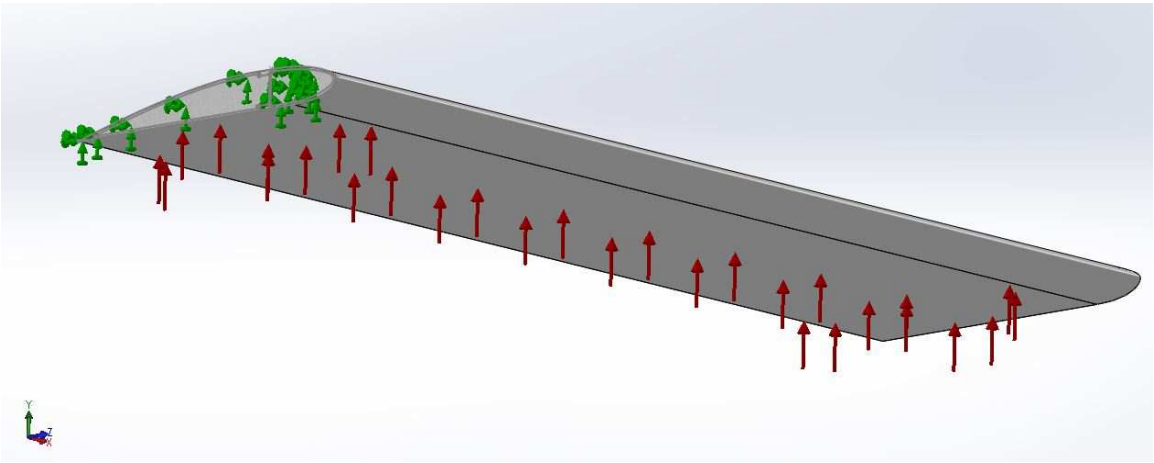

Figure 25 Wing loading parameters. Fixtures in green, loads in red

The primary difference between the two loadings is the difference in wing twist due to the different locations of the center of pressure. Since the bending of the wing will result in larger deflections, the difference in twist is neglected.

The profile of the lower surface was then taken from the deformed result using the probe tool in Solidworks™. The output is given as the original XYZ coordinates as well as the displacement in the Y direction in meters. This data is then exported as a comma delimited list (.csv). Solidworks does not give the changes in X or Z that would result from the wing bending or twisting, but such displacements are assumed to be minimal, as in [25].

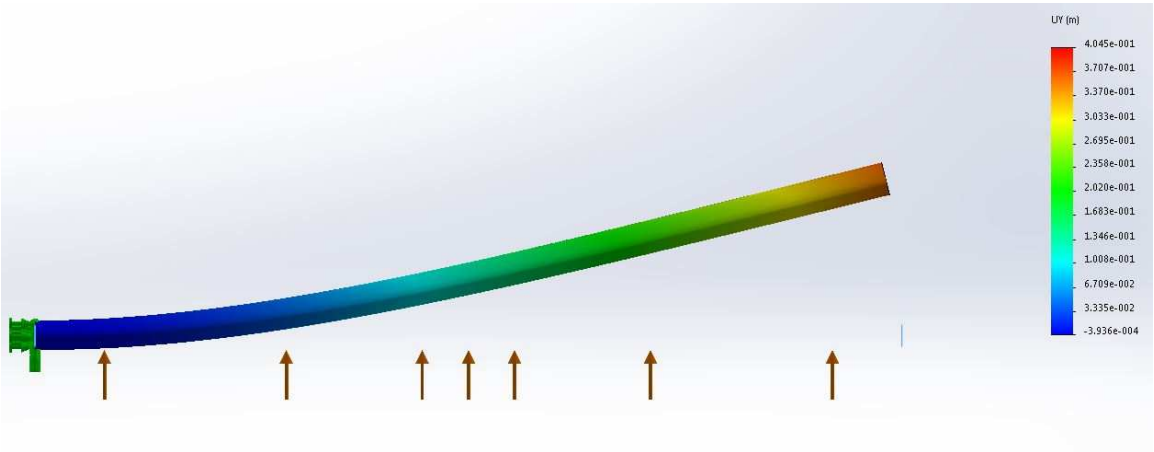

Figure 26 Wing deflection results. Y displacement shown

Power & Gain Calculations

In order to determine the antenna power, gain and radiation pattern, the two methods described in [17] are the method of moments and array theory. The method of moment refers to a general mathematical technique to approximate the solution of linear operator equations. With regards to RF applications, the element excitation is used to determine the power radiated according to the selected basis function [17]. The method of moments was not used due to the need to select a basis function to satisfy boundary conditions not defined within the problem. Array theory was chosen to determine the antenna performance and is dissed in greater detail below.

The radiation properties of an antenna are often expressed in terms of a solid angle or steradian. A steradian is essentially the three dimensional equivalent of a two dimensional radian. The

steradian is a solid angle of a sphere of radius r that has a circular surface area of r^2. The solid angle element of a sphere can be written as:

$$d\Omega = sin\theta \; d\theta \; d\varphi \tag{3.2}$$

the radiation intensity, or power per solid angle, can be found through the electric field generated by the antenna and is described by:

$$U(\theta, \varphi) = \frac{r^2}{2\eta} |E(r, \theta, \varphi)|^2 \tag{3.3}$$

Where $E(r, \theta, \varphi)$ represents the electric field function, also called radiation pattern, and η is the intrinsic impedance of the medium. In order to determine the radiation density, or power per unit area,

$$U = \; r^2 \, W_{rad} \tag{3.43}$$

Where W_{rad} is the radiation density. Therefore, radiation density can be expressed as:

$$W_{rad} = \frac{|E(r, \theta, \varphi)|^2}{2 \, \eta} \tag{3.5}$$

In order to determine the gain at each value of θ and φ the radiation intensity of the antenna's isotropic equivalent must be known, requiring the total power radiated to be determined. The total power can be calculated by

$$P_{rad} = \int_0^{2\pi} \int_0^{\pi} U(\theta, \varphi) \; sin\theta \; d\theta \; d\varphi \tag{3.6}$$

In practice it is extremely difficult to generate a continuous function for integration, so instead numerical approximations are used across a range of discrete values. These numerical approximations are dependent on the number of increments N in the θ direction and M in the φ direction. Therefore, the total power is approximated in [1] by

$$P_{rad} = \frac{\pi}{N}\frac{2\pi}{M}\sum_{j=1}^{M}\left[\sum_{i=1}^{N} U(\theta_i, \varphi_j)\, sin\theta_i\right] \quad 3.7$$

The radiation intensity of the isotropic equivalent is then calculated by dividing the total power by 4π. The gain is then expressed as the natural log of the ratio of the radiation intensity over isotropic radiation intensity and is given in dB [1].

$$U_{iso} = \frac{P_{rad}}{4\,\pi} \quad 3.8$$

$$G(\theta, \varphi) = \frac{4\pi U(\theta, \varphi)}{P_{rad}} \quad 3.9$$

Radiation Pattern Calculations

The equations presented above are dependent on knowing the radiation pattern that the antenna generates. In the coordinate system described by Figure 27 the determination of this field is described in [11] for an array antenna as

$$E = \frac{e^{-i\,k\,R_0}}{R_0}\sum_{n} a_n\, f_n(\theta, \varphi)\, e^{i\,k\,r_n \cdot \hat{\rho}} \quad 3.10$$

With

$$k = 2\,\pi/\lambda \quad 3.11$$

$$\hat{\rho} = \hat{x}\,u + \hat{y}\,v + \hat{z}\,w \quad 3.12$$

$$r_n = \hat{x}\,x_n + \hat{y}\,y_n + \hat{z}\,z_n \quad 3.13$$

$$R_0 = \sqrt{x^2 + y^2 + z^2} \quad 3.14$$

Where $\hat{x}$, $\hat{y}$, and $\hat{z}$ are the unit vectors in their respective directions, x_n, y_n, and z_n are the coordinates of element n, a_n is the excitation of element n, f_n is the radiation pattern of element n, and the direction cosines are:

$$u = sin\theta\ cos\varphi \tag{3.15}$$

$$v = sin\theta\ sin\varphi \tag{3.16}$$

$$w = cos\theta \tag{3.17}$$

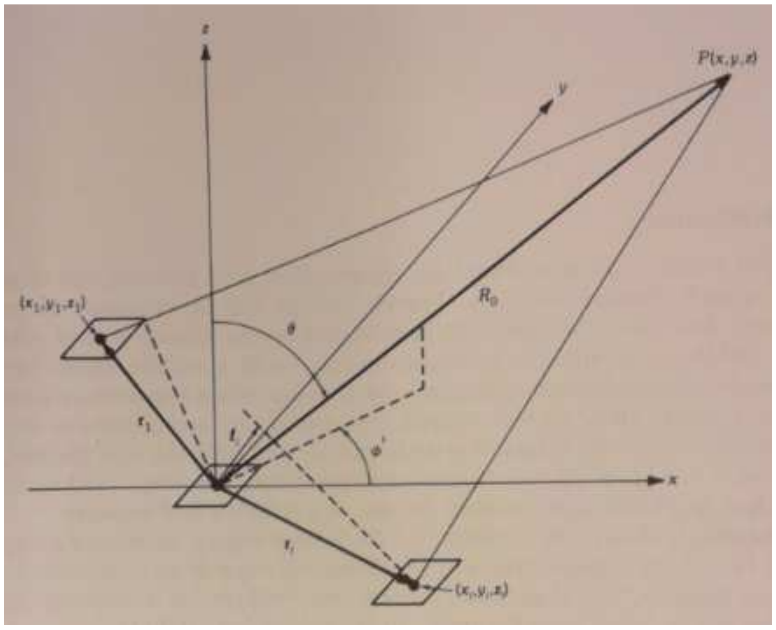

Figure 27 Coordinate system [11]

Equation 3.10 describes the impact of phasing on the antenna array. The exponential term inside the sum is a complex representation of how far out of phase each antenna element is when looking in some direction defined by θ and φ. These values are summed across all elements in the array.

The value of the antenna element radiation pattern f_n will be dependent on the antenna element's inherent directivity as well as coupling effects from nearby elements and the array edges. For simplicity they can be assumed to be isotropic radiators, with a value of 1 in all directions.

The element weighting a_n will depend on the power fed to the element according to tapered or uniform aperture illumination. The value can also be used to introduce phasing into the antenna for beam steering. This phasing can be introduced with

$$a_n = |a_n'|e^{-ikr_n \cdot \widehat{\rho_0}} \tag{3.18}$$

With $\widehat{\rho_0}$ being given by using the desired angles in the direction cosines and a_n' being the aperture illumination as discussed in Chapter II. This term greatly resembles the exponential in Equation 3.10. The weighting and the exponential should cancel each other for a perfectly phased antenna, resulting in the maximum value of the radiation pattern being at the desired angles.

MATLAB Antenna Analysis

A program called 'Radiation_Pattern.m' (See Appendix C) written in MATLAB R2016b and based on the above work of [1] and [11] was used to determine the peak gain and beamwidth. The program begins by populating the elements in 3 dimensional space using user-defined parameters and a .csv file of the wing deflection, then calculates the power and gain in every direction using the above equations.

To begin, the program is given the frequency selected for the radar as well as parameters defining the area on the wing and fuselage that can be used by the antenna. This includes the length and width of the strip on the fuselage, as well as the amount of chord and the length from the root that is available on the wing. Radiation_Pattern.m uses this data in 5 consecutive loops to place each antenna element. The first loop places the strip on the fuselage, the second and third place the elements near the root, between the fuselage strip and the wing elements, and the fourth and fifth place the elements in the wings. X and Y coordinates for each element are at half wavelength intervals. The Z coordinate is developed from a three dimensional linear interpolation of the Solidworks .csv output file. The interpolation uses the already defined X and Y coordinates to

determine a Z coordinate. The Y coordinate in Solidworks™ corresponds to the Z coordinate in Radiation_Pattern.m. This is accounted for when the interpolant function is defined from the comma delimited list. This process is shown in the flowchart below.

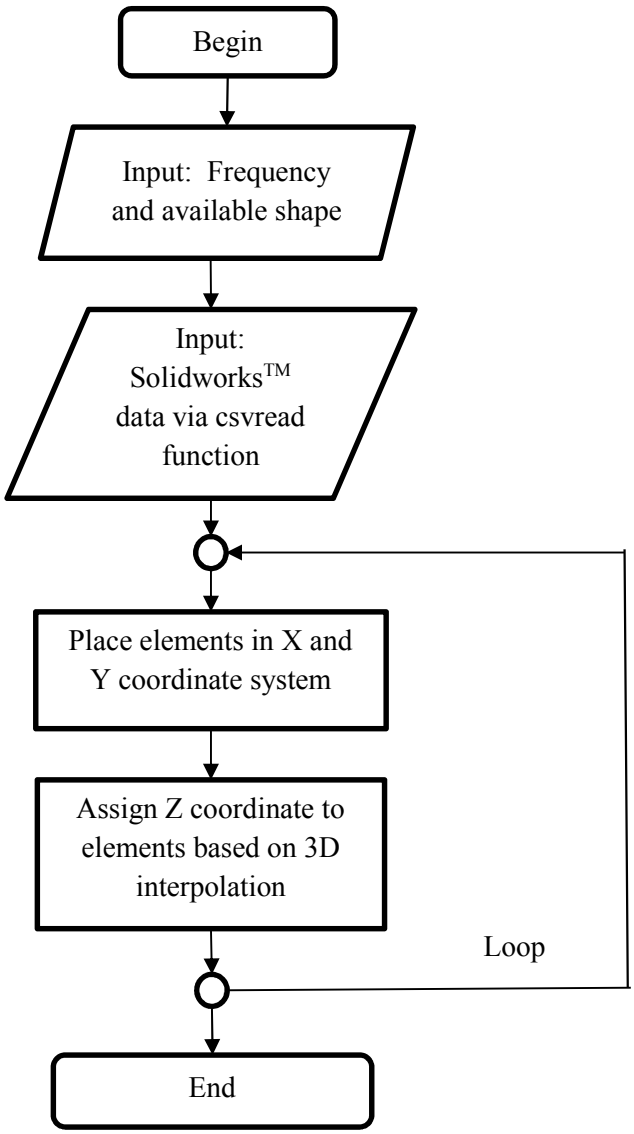

Figure 28 Element placement flowchart

To determine the phasing for each element, a second file is read in from Solidworks™. This is used to create a second interpolant function that uses the same X and Y coordinates to generate a Z coordinate that is used in phasing the array. The phasing is determined by the function:

$$a_n = |a_n'|e^{-ikr_n \cdot \widehat{\rho_0}} \quad 3.18$$

using the second interpolant function to determine the coordinates. The phasing function is similar to the radiation pattern equation defined earlier by [1]. This is to be expected since the phasing is meant to counter the effects of elements being displaced.

The files chosen for the deflections and phasing are chosen to reflect a desired condition. To establish a control, the files can be the same. This gives a point of reference for an antenna that is phased perfectly to account for its deflection. A special case of this is replacing both interpolant functions with zero, giving a planar antenna. This can be used to determine the optimum performance of an antenna. The selection of differing files for deflection and phasing would be used to reflect errors in actual versus predicted loading of the wing. These errors would be due to gusts or other perturbations to the aircraft that would result in changes to the lift generated by the wing and the corresponding deflections.

The deflection can be estimated onboard the aircraft by means of accelerometers or strain gauges on the wings. From this estimated deflection the phasing can be either calculated or taken from a look-up table. However, there will likely be some error in the deflection estimate, resulting in unmatched phasing.

After the element coordinates and phasing values have been determined, the MATLAB program calculates the total power radiated by performing equations 3.9 through 3.16 in nested loops with increments of 1° in φ and 0.1° in θ across 360° in φ and 90° in θ to give values for the entire lower hemisphere. These values are used in the sum in Equation 3.6 to give the total power radiated. The values of the power radiated found in these loops are stored for use later.

The program then repeats these loops with increments of 1° in φ and 0.1° in θ across 360° in φ and 10° in θ to give values for a 20° cone surrounding the normal axis. The total value of power radiated found above is used to determine the gain. The values of gain in both the 20° cone and

the full hemisphere are then plotted for the principal planes of φ=0° φ=45° and φ=90°. The peak gain is taken as the maximum value of the array, and will be at or very near θ=0. To find the beamwidth, the program takes the gain values calculated in the 20° cone and subtracts the peak gain to give a normalized value. The program then counts the number of values in each of the principal planes φ=0° φ=45° and φ=90° are greater than -3 dB and adds one additional increment to give a resolution of -0.02° for the beamwidth calculation. The process for the power calculations is shown in the flowchart below.

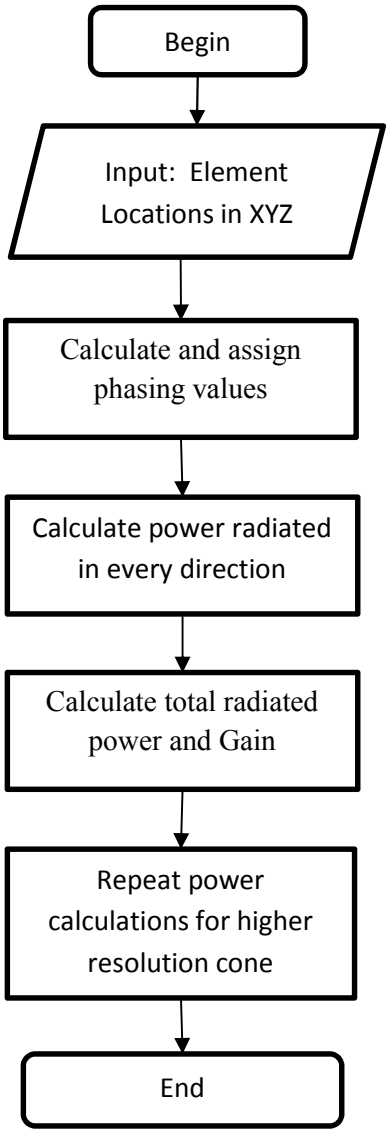

Figure 29 Power and gain calculation flowchart

Procedure

To account for many cases of phasing and loading, the wings were simulated under a number of loads. All 3 wings were evaluated with a nominal 1g load of 700 lb. This value was also used to determine phasing in all cases. To account for small changes in wing loading the wings were also evaluated for 600 lb., 650 lb., 750 lb. and 800 lb. Again, both wings were evaluated with 4GHz and 1 GHz antennas.

The 4 GHz antenna consisted of 2 crossed rectangular arrays that were each 8 by 88 elements. When crossed they gave a total of 1344 elements. The 1GHz antenna was similar, with 2 crossed rectangular arrays of 2 by 22 elements, and a total of 84 elements present. In both antennas the sub-arrays are 3.3 m long and 0.3 m wide, allowing them to fit within the aircraft wingspan and providing symmetry between the lateral and longitudinal arrays. They are also sized to use only half of the wing chord, leaving the remainder for control surfaces.

The loadings were selected for simplicity, but correspond to maneuver and gust loads that may be expected in flight. A 750 lb. applied to a 700 lb. aircraft corresponds to a 21° bank, and an 800 lb. load corresponds to a 30° bank. Assuming the aircraft flies at 60 miles per hour (88 ft/sec) during its mission, these loads represent sharp vertical gusts of 3.4 ft/sec and 6.9 ft/sec respectively [12].

During a terrain mapping mission, the aircraft may also choose to follow the terrain contours. In the original desired operating environment of Guatemala, this will require pushing down to crest hills and pulling up between hills. Keeping the 60 mph flight speed, a 650 lb. load on this aircraft represents a maneuver with a 3,400 ft. radius, and an 800 lb. load corresponds to a radius of 1700 ft. These same radii apply for a pull up maneuver between two hills [12].

The gain and beamwidth values of each wing-load-antenna combination were recorded in MS Excel, and each of the plots from the principal planes were saved in order to examine the resultant radiation pattern. The maximum deflection of the antenna elements relative to the expected values used to phase the array was also recorded as a percentage of the wavelength.

Assumptions

The model given is a simplified representation, but the goal of the research is to provide the basis for a more rigorous examination after proving the viability of the concept of a wing conformal phased array. In order to simplify the model and analysis several assumptions have been made.

Firstly, the model developed in SolidworksTM is simplified when compared to an actual aircraft wing. The bonding or other fasteners that would be present to connect the constituent pieces are not present, and the wing is considered to be a single piece. Therefore, the weaknesses in the wing introduced by these elements are not present. Also not modeled are the antenna elements themselves. In the case of the stressed skin design this is likely to have little impact, as the elements would carry relatively little load. In the foam wing, the antenna elements, as well as any protective cover that may be applied over them, may carry some significant amount of loading and impact the wing stiffness. Any damage to the patches can be checked since the strain can be taken from the model. As an example, the peak strain on the stressed skin wing is 0.0083, which is below the elongation of FR-4 epoxy, a common substrate material, at limit load [10].

The loading applied to the aircraft, as discussed above, is not a perfect representation of that which the aircraft would experience in flight. It does provide a reasonable approximation adequate for this analysis.

Several assumptions are made about the antenna elements. The primary assumption regarding their arrangement are that the elements only move vertically, with negligible displacement in the X and Y directions. While this data could possibly be extracted from the solid model, there is no simple method to integrate it into the MATLAB model. To do so would require that each test result in 3 separate .csv files that would then have to be merged individually. Since the Y displacement is the most significant to the phasing, only it is used to represent the changes.

With regards to the elements themselves, they are all assumed to be isotropic in order to remove the complexities of individual element radiation patterns and element interactions. An isotropic element is not achievable in actuality, but the patch antennas discussed in Chapter 2 offer near isotropic performance in a wide angle for the radiating hemisphere. Any rotations of the elements are assumed to be small, so the isotropic assumption holds so long as the beam is not steered to

large amounts in the θ direction. The choice to use isotropic elements also means that there is significant radiation into the back plane, in this case through the top of the wing, that would not be present with directive elements.

The model is also based on a far-field radiation pattern. The far-field refers to the region where the radiation pattern is independent from the distance to the antenna and is usually taken to begin at a range defined by

$$R = \frac{2\,D^2}{\lambda} \tag{3.19}$$

Where D is the maximum antenna dimension. For the 1 GHz antenna this range is 72.6 m and for the 4 GHz antenna it is 18.15 m. The use of the far field assumption allows the distance to the target, which is unknown for this paper, to be neglected.

Model Validation

In order to validate the Radiation_Pattern.m code, a modified version was written. It differs only in how the array is constructed. This version of the code was tested for an array identical to the one examined in [25] and compared to the results found there.

The results from [25] do not include peak gain, and all values are given as dB below peak. Therefore, it is not possible to judge the accuracy of the gain calculated. However, beamwidth can be checked. In the original model, for the 0° plane and a planar antenna, the 3 dB width on either side of peak gain was located at approximately arcsine (0.005) or 0.286°. Doubling this gives a beamwidth of 0.573°. This can be seen in Figure 30 from [25]. The modification of Radiation_Pattern.m gave a beamwidth of 0.56° for the same plane. The modified program also shows 18 side lobes within 10° of center, as does the original model. The results of the modified program are presented in Figure 31 for comparison with the results in [25].

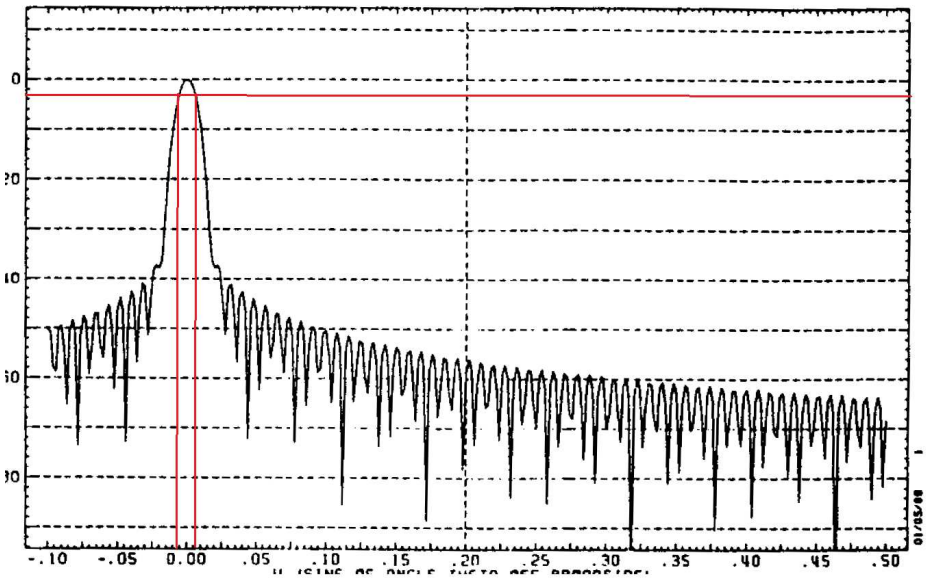

Figure 30 radiation pattern for comparison. Red lines roughly designate the -3 dB locations [25]

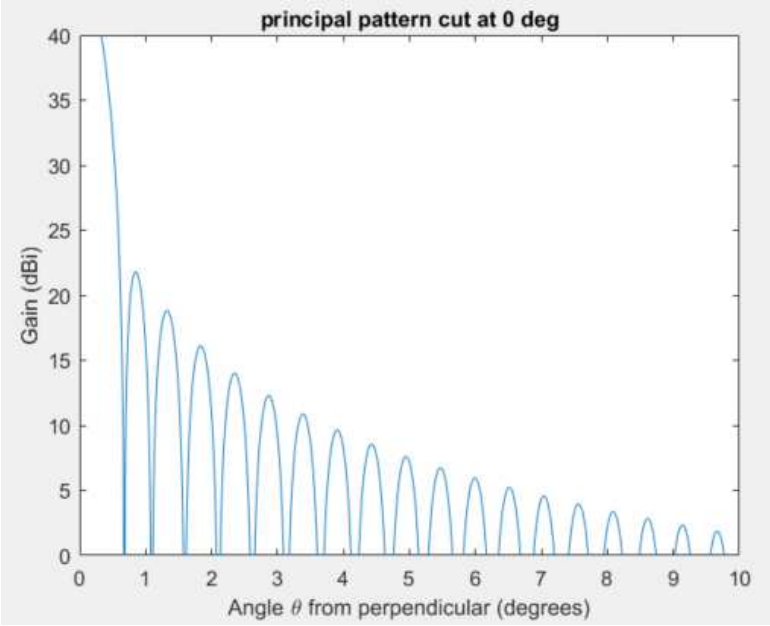

Figure 31 Radiation pattern for validation

For the 90 plane, the 3 dB width in [25] was approximately arcsine (0.0125) or 0.716°, giving a beamwidth of 1.43°. The modified program gave a beamwidth of 1.20° for the same plane. This difference is likely due to measurement error from the original plot. The modified program also shows 7 side lobes within 10° of center, as does [25].

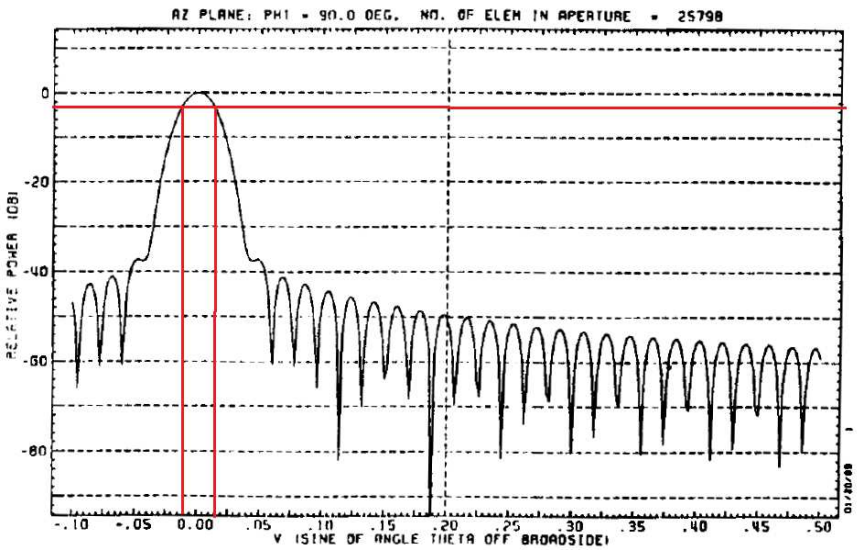

Figure 32 Radiation pattern for validation [25]

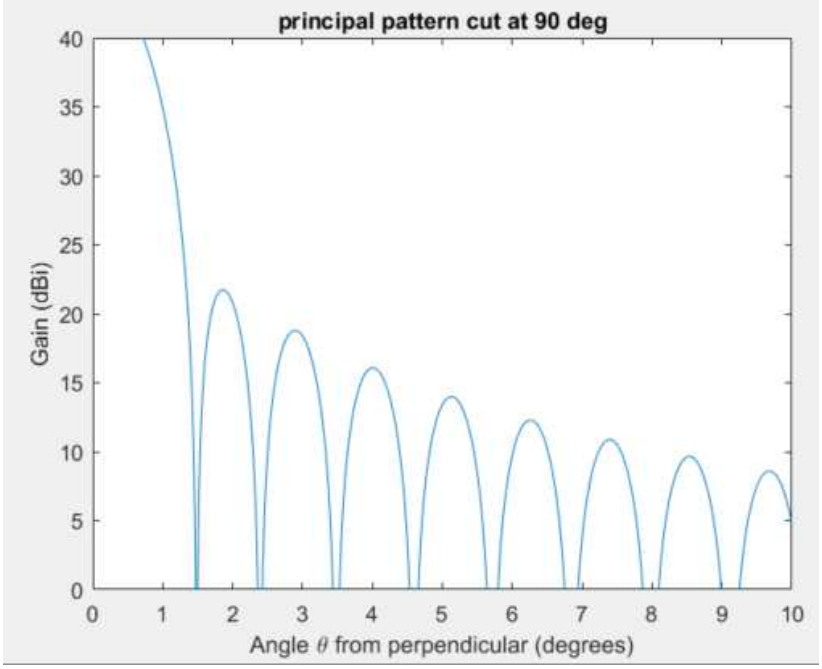

Figure 33 Radiation pattern for validation

The value of gain calculated in the modification of Radiation_Pattern.m was 44.64 dB at peak. In the 0 plane, [25] found the first side lobe to be approximately 35 dB below peak, suggesting that the modified program should calculate a side lobe of 8-10 dB. Instead, the value is near 20 dB. This is repeated in the 90 plane.

The root cause of this disparity is unknown. Both cases assume isotropic radiators, so the radiation pattern of individual elements has no effect. The array is also laid out identically, so there is no effect from elements being out of position. The exact spacing of the elements was assumed as half wavelength spacing, but it is not explicitly stated. A difference in spacing would more likely have an effect of beamwidth, not gain, so it is unlikely to be the source of the disparity.

The most likely cause is a misapplication of the Gauss taper. The function defining the taper is never given, so there may be some error. This also conforms to the results of tapered as compared to uniformly illuminated apertures seen in [20]. A tapered aperture will have a slightly wider main lobe but much lower side lobes. If the taper applied to MATLAB was not as severe, the higher side lobe levels would be expected. Accepting this conclusion, then the applied taper is incorrect, but the model itself is accurate.

To additionally validate the calculation performed in MATLAB by Radiation_pattern.m a variation was created that doubled the resolution in both the θ and φ directions. This version of the program functioned as a convergence check and was performed with the planar case of the 1 GHz antenna. The results of the original program for this case were a gain of 18.2934 dB with beamwidth being 12.36° in the 0° and 90° planes and 11.34° in the 45° plane. The convergence check returned a gain of 18.2933 dB, a beamwidth of 12.35° in the 0° and 90° planes and 11.33° in the 45° plane, suggesting that the resolution is sufficient to provide accurate gain and beamwidth calculations.

CHAPTER IV

RESULTS

Analysis of 3 different wing geometries as well as 2 different frequencies allows an assessment to be made regarding the effect of frequency and wing stiffness on the radiation pattern. Several characteristics regarding the relationship between deflections due to loading and RF performance remain constant throughout.

Firstly, the degradation in RF performance is correlated with the magnitude of the error between deflection used for phasing and deflection from applied load as a percentage of λ, not the variation in applied load. If the actual applied load results in a deflection 10% of λ above the phasing, the gain and beamwidth will be the same as if the applied load resulted in a deflection 10% of λ below the phasing. Because of this, a lower frequency system will be inherently more resistant to loading errors than higher frequency systems.

Secondly, the changes to the gain and beamwidth are very small in the range of wing loading expected for a ground mapping aircraft. The gain losses are minimal, on the order of a few hundredths or thousandths of a dB. Beamwidth is also fairly constant in this region as well, increasing by a few hundredths of a degree or remaining identical to the perfectly phased case.

The expansion in beamwidth is contained to the 90° principal plane, with some of the increases leaking into the 45° plane at extreme variations in loading. This should be expected, as the 90° plane is primarily a fan beam formed by the antenna elements on the wing. The moving of these elements out of phase results in the beam widening. The 45° plane is influenced by both the 0° and 90° planes, so it's increases in beamwidth, while smaller, correlate well with those in the 90° plane. The beamwidth in the 0° plane actually narrows somewhat at the extreme deflection errors, but such changes are relatively small, and the beamwidth remains constant for all error cases examined.

The side lobe structure is largely unchanged in the range of expected loading values, with the only noticeable change being a slight rise in the nulls for some cases. Extreme cases that are not expected.

It is also important to note that the peak gain values may not be completely accurate, as was discussed in Chapter 3. They do offer a good means of comparison between the different cases however and a means to look at the side lobe structure.

Stressed Skin Wing with 4GHz Antenna

The 4 GHz antenna used consists of 2 crossed rectangular antennas each 8 elements wide and 88 elements long spaced at half wavelengths, making each 0.3 meters wide and 3.3 meters long. The total number of elements is 1344. In a perfectly phased planar case, it has a peak gain of 30.5788 dB according to Radiation_Pattern.m, and the beamwidth is 3.08° in both the 0° and 90° planes, and 2.84° in the 45° plane. When attached to the stressed skin wing and loaded to the nominal 700 lb., the perfectly phased antenna has identical performance in beamwidth, as would be expected. The drop in gain is negligible, dropping from 30.5788 to 30.5781 dB. The radiation pattern consists of a narrow main lobe directly above a prominent first side lobe, and 3 other side lobes, each peaking near 10 dB in both the 0° and 90° planes. The 45° plane has a much more

defined main lobe, with the first side lobe peaking near 10 dB and the others having peaks between -10 and -15 dB.

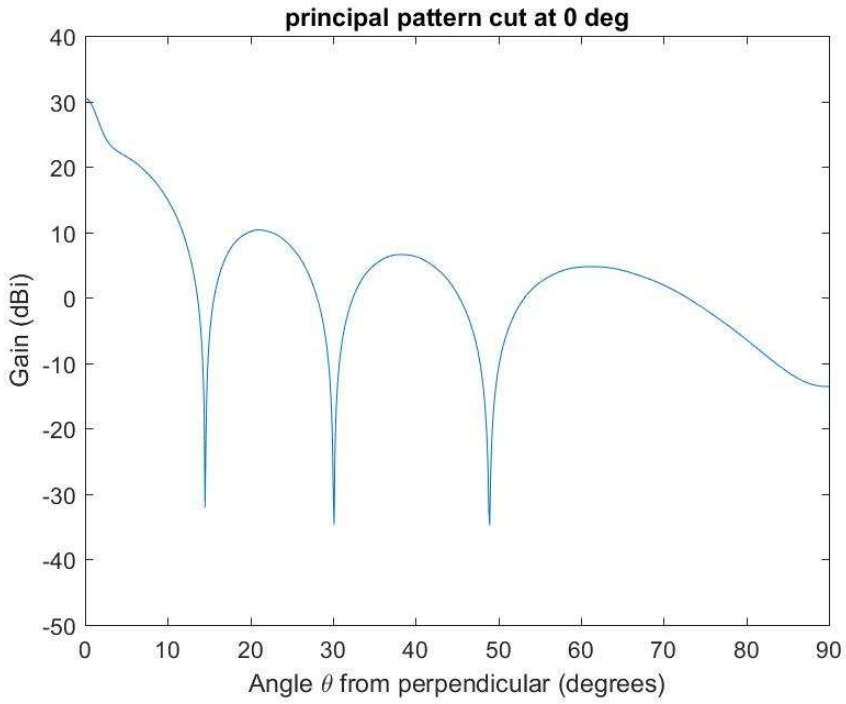

Figure 34 Nominal Radiation Pattern for stressed skin wing and 4 GHz antenna

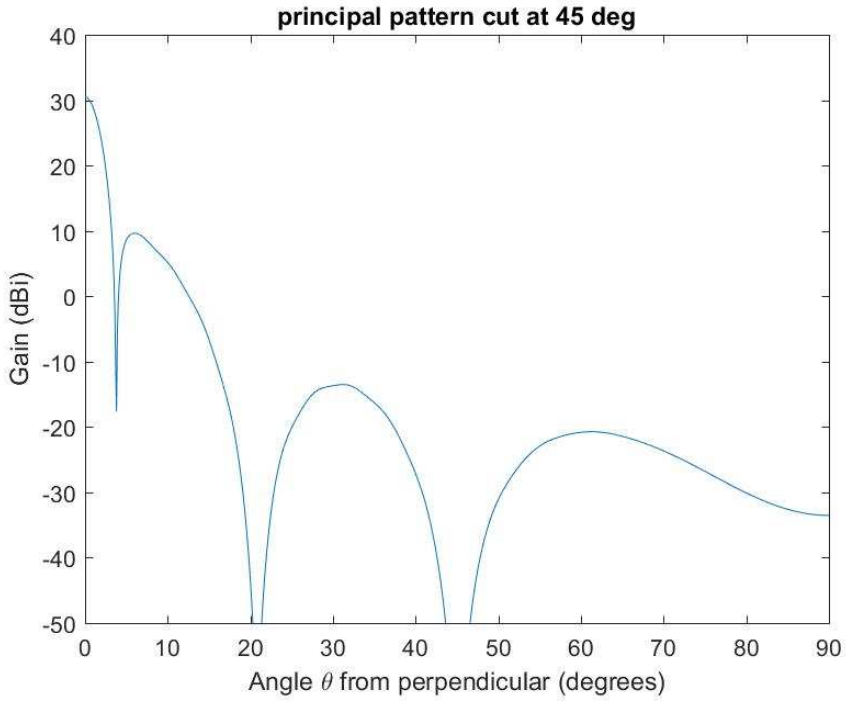

Figure 35 Nominal Radiation Pattern for stressed skin wing and 4 GHz antenna

The radiation pattern is similar to what would be expected, with the main lobe in the 0° and 90° planes coming from the overlap of the two rectangular arrays, and the side lobe levels in the 45° plane being very low.

Decreasing the loading while maintain the phasing for a 700 lb. load results in minimal performance degradation to the antenna. At 650 pounds, the maximum deflection error the antenna experiences is only 4.7% of λ. This results in the beamwidth being unchanged, and a loss of peak gain of 0.006 dB, representing an efficiency of 99.8%. At 600 pounds, the maximum deflection error is 9.4% of λ. This results in the beamwidth being unchanged in the 0° and 45° planes, and increasing slightly in the 90° plane to 3.1°, and a loss of peak gain of 0.0239 dB, representing an efficiency of 99.4%. In both cases the side lobe structure has no discernable changes.

Increasing the load results in similar changes. An increase to 750 lb. results in the maximum deflection error being 4.7% of λ, with the beamwidth unchanged and the gain dropping by 0.0059

dB. At 800 lb. the deflection error is 9.4% of λ, the beamwidth in the 90° plane increases to 3.1°, beamwidth in the 0° plane decreases to 3.06°, beamwidth in the 45° plane is unchanged, and gain drops by 0.0236 dB. The side lobe levels show little change overall in both cases.

An extreme case of zero applied load but a phasing set for a 700 lb. load results in a maximum error that is 65.5% of λ. This deflection also represents the total deflection of the wing in a 1g case. The beamwidth in the 90° plane increases to 4.44° from the original 3.08°, the beamwidth in the 0° plane decreases to 2.96°, and the beamwidth in the 45° plane increases to 3.24° from 2.84°. The gain drops to 29.6291 dB, a loss of 0.949 dB and representing an efficiency of 80%. The side lobe structure also begins to change in the 45° plane, with the nulls coming up closer to the peaks, and the first side lobe beginning to merge with the main lobe.

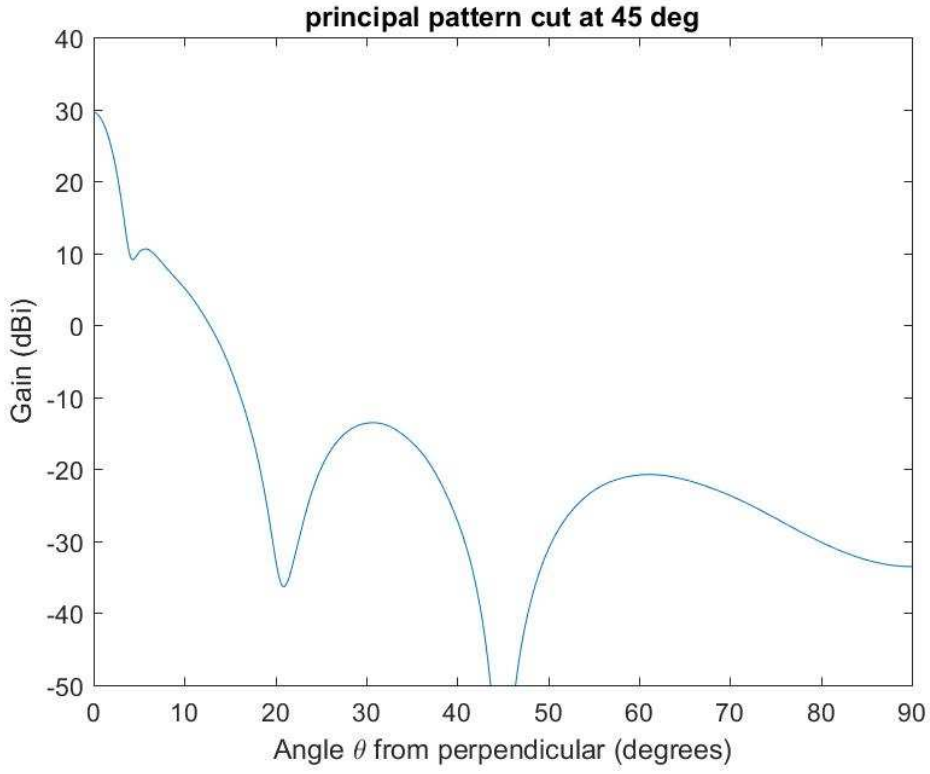

Figure 36 Zero load radiation pattern for stressed skin wing and 4 GHz antenna

Overall, there appears to be little change to antenna performance in the range of typical loading conditions. Losses to gain are minimal, and efficiency remains above 99%, while any changes to

beamwidth are minimal. The results are summarized in Table 2. Figure 37 plots loss against load.

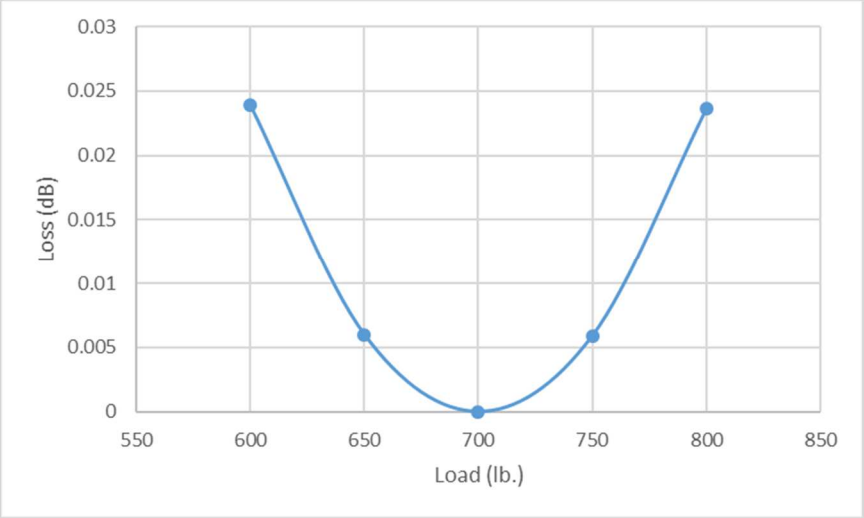

Figure 37 Load vs Loss for Stressed skin wing and 4 GHz antenna

Applied Load	Max Deflection	Gain Loss (dB)	Beamwidth in 90° plane	Beamwidth in 0° plane	Beamwidth in 45° plane
600	9.4%	0.0239	3.1°	3.08°	2.84°
650	4.7%	0.006	3.08°	3.08°	2.84°
700	0%	0	3.08°	3.08°	2.84°
750	4.7%	0.0059	3.08°	3.08°	2.84°
800	9.4%	0.0236	3.1°	3.06°	2.84°
0	65.5%	0.949	4.44°	2.96°	3.24°

Table 2 Results of Stressed Skin Wing and 4 GHz antenna

Foam and Aluminum Spar Wing with 4 GHz Antenna

The foam wing has slightly better performance when perfectly phased, with a gain of 30.5783 dB, compared to the 30.5788 dB of the planar case. Both the perfectly phased antenna on the foam wing and the planar case have beamwidth of 3.08° in the 0° and 90° planes and 2.84° in the 45° plane. As with the stressed skin wing, the radiation patterns in the 0° and 90° planes are identical, with a first side lobe very near the main lobe at approximately 20 dB and no null separating it,

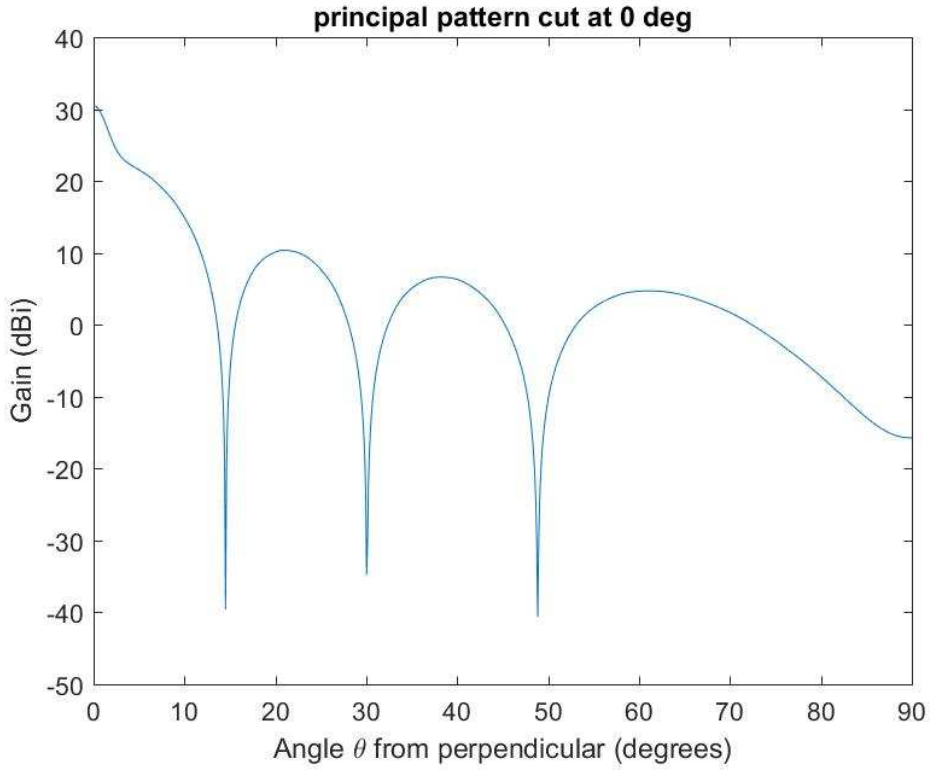

Figure 38 Nominal Radiation Pattern for foam wing and 4 GHz antenna

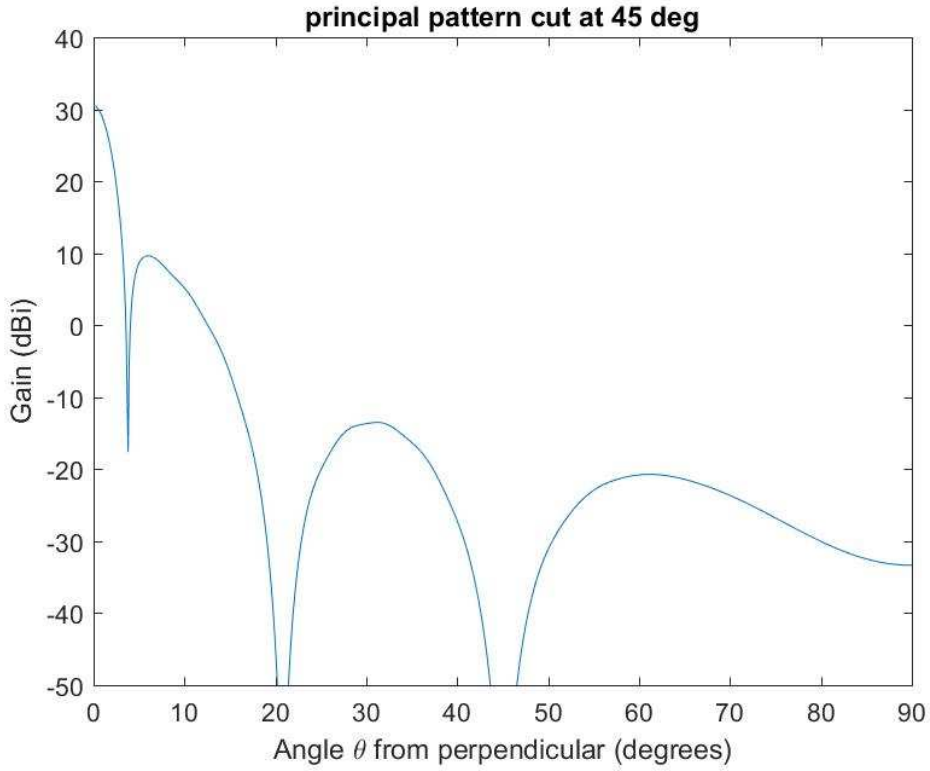

Figure 39 Nominal Radiation Pattern for foam wing and 4 GHz antenna

The deflections of the foam wing are slightly larger than the stressed skin wing at lower loads, but the deflection increases at the extreme cases near ultimate load. With a load of 650 lb. phased for the 700 lb. nominal load, the deflection is 4.9% of λ and the beamwidth is unchanged. Peak loss in negligible, 0.0063 dB. A load of 600 lb. will result in the deflection error increasing to 9.9% of λ, with beamwidth widening to 3.1° in the 90° plane and remaining 2.84° in the 45° and 3.08° in the 0° plane, with gain dropping to 30.4809 dB, for an efficiency of 99.4%. As with the stressed skin wing, changes to the radiation pattern are small enough in the 0° and 90° planes to go unnoticed. The only significant change in the 45° plane is the value of the nulls coming up.

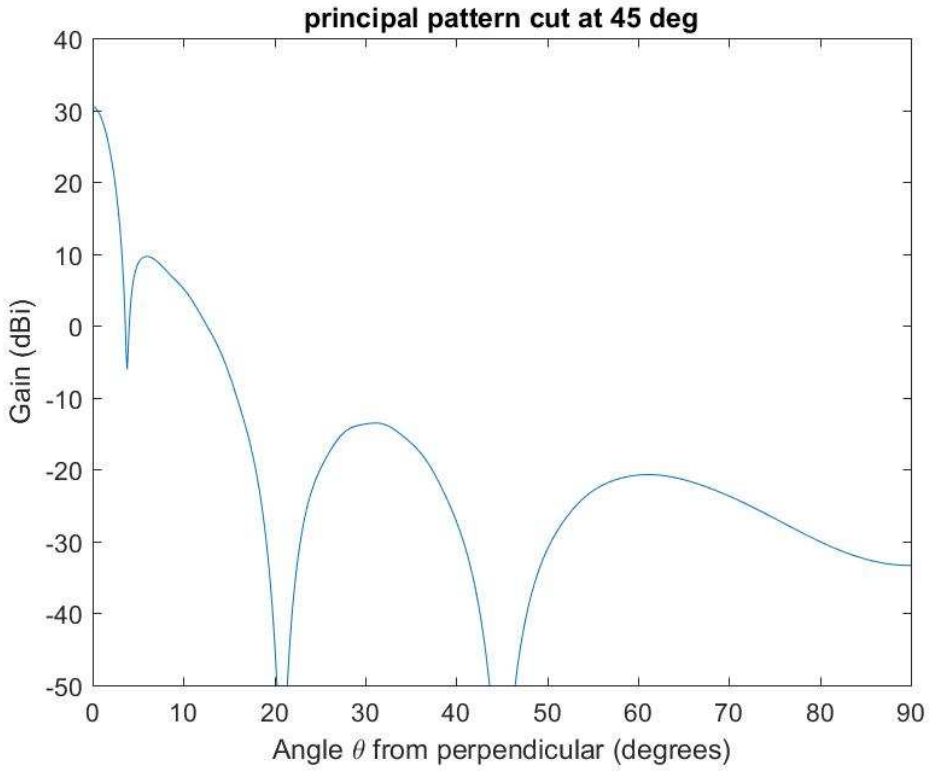

Figure 40 600 lb. radiation pattern for foam wing and 4 GHz antenna

For a no load case the deflection error is 69.9% of λ, also representing the deflection at 1g. This results in the beamwidth widening to 4.42° in the 90° plane and 3.26° in the 45° plane, narrowing to 2.94° in the 0° plane, and gain dropping by 0.9292 dB, a power ratio of 80%. The side lobes in the 0° and 90° planes are unchanged, but the first side lobe in the 45° plane is nearly merged with the main lobe.

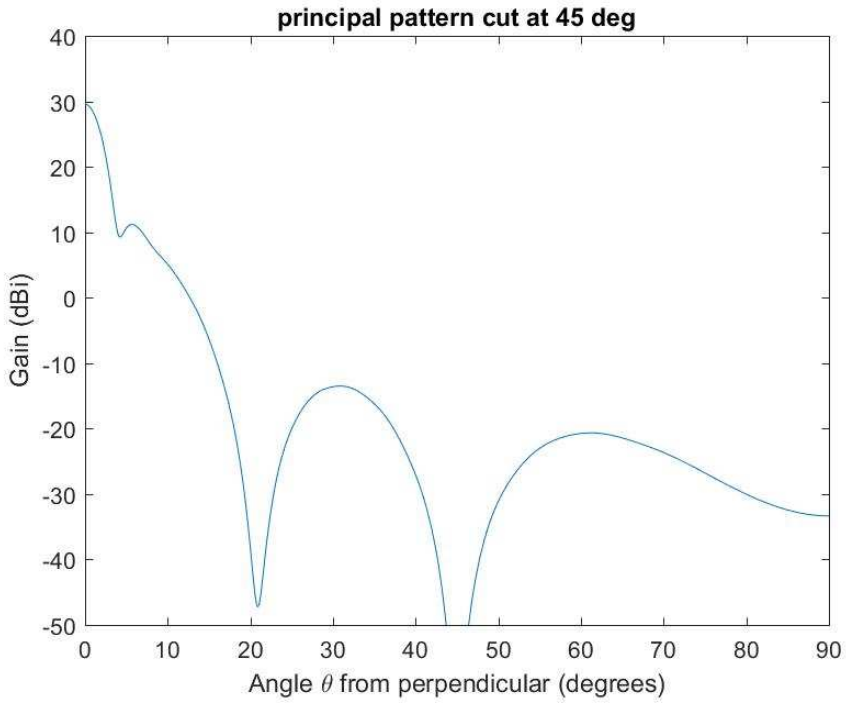

Figure 41 zero load radiation pattern for foam wing and 4 GHz antenna

Once again, increasing the load has a similar effect to decreasing the load, so long as the deflection error is the same. Loading at 750 lb. results in a max deflection error that is 5% of λ. The beamwidth does not change, but gain drops by 0.0062 dB. Increasing to 800 lb. results in a deflection error of 10% of λ, and the beamwidth in the 90° plane increasing to 3.1°, the beamwidth in the 0° plane decreasing to 3.06°, and the gain dropping by 0.0246 dB. The side lobe structure is unchanged.

The foam wing with the aluminum spar is less stiff than the stressed skin wing, and the resulting tolerance to phasing errors is slightly worse, with losses to peak gain and the deflection error being slightly higher than the stressed skin case. The plot of gain against deformation has a very similar shape to that of the same plot for the stressed skin wing and can be seen in Figure 42. Table 3 summarizes the results for the foam wing case.

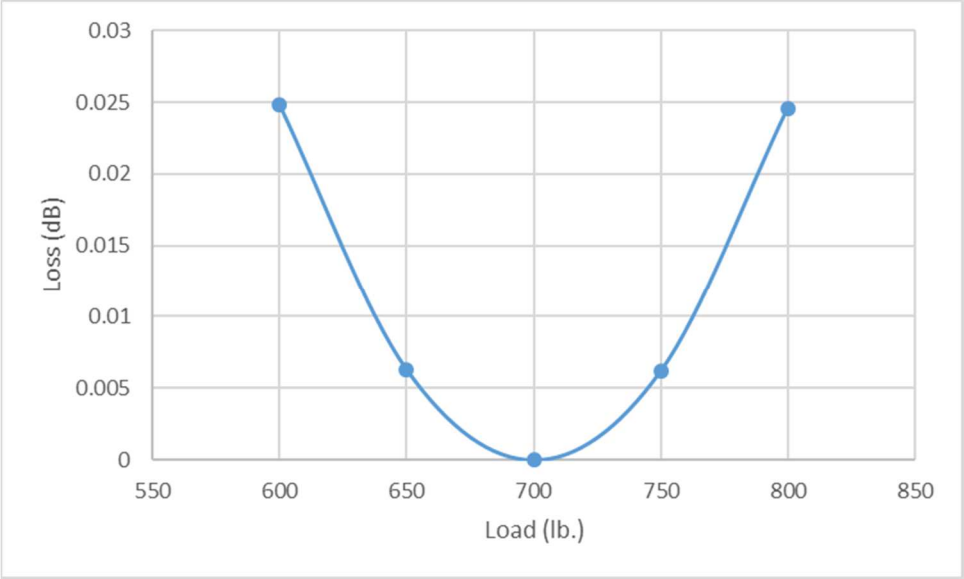

Figure 42 Load vs Loss for Foam wing and 4 GHz antenna

Applied Load	Max Deflection	Gain Loss (dB)	Beamwidth in 90° plane	Beamwidth in 0° plane	Beamwidth in 45° plane
600	9.9%	0.0248	3.1°	3.08°	2.84°
650	4.9%	0.0063	3.08°	3.08°	2.84°
700	0%	0	3.08°	3.08°	2.84°
750	5.0%	0.0062	3.08°	3.08°	2.84°
800	10.0%	0.0246	3.1°	3.06°	2.84°
0	69.9%	0.9292	4.42°	2.94°	3.26°

Table 3 Results of the Foam Wing with a 4 GHz antenna

Stressed Skin Wing with Ribs and 4 GHz Antenna

The lower surface of the stressed skin wing deforms by bending and bowing in due to the pressure applied to it and the lack of support behind the skin. This inward bowing of the stressed skin wing may reduce the effect of its greater stiffness on tolerance to loading variation by

increasing the deflection error of some elements, resulting in both the foam and stressed skin wings having very similar results. This is a result of how the lift force is applied to the model, and is likely not representative of reality.

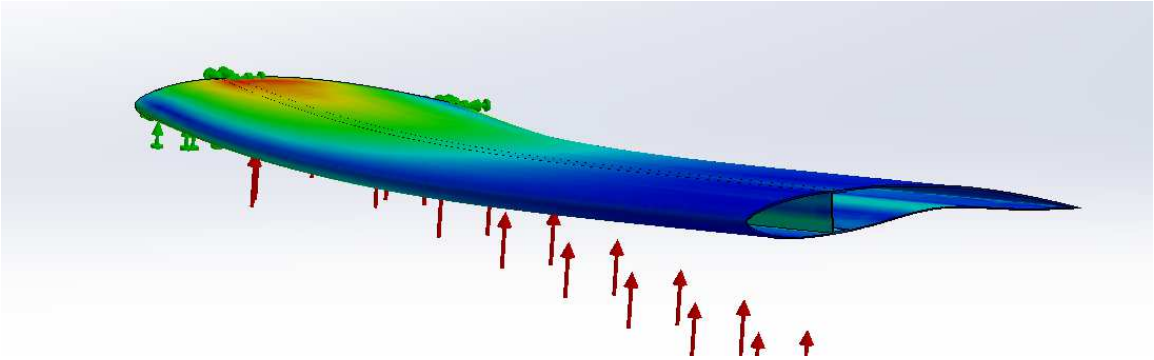

Figure 43 Deformation of the stressed skin wing

The deformations with the ribs in place show a similar amount of bending to the original stressed skin model, but the wing retains its cross section much better, and as a result the maximum deflection error is smaller. This is a much better representation of wing behavior.

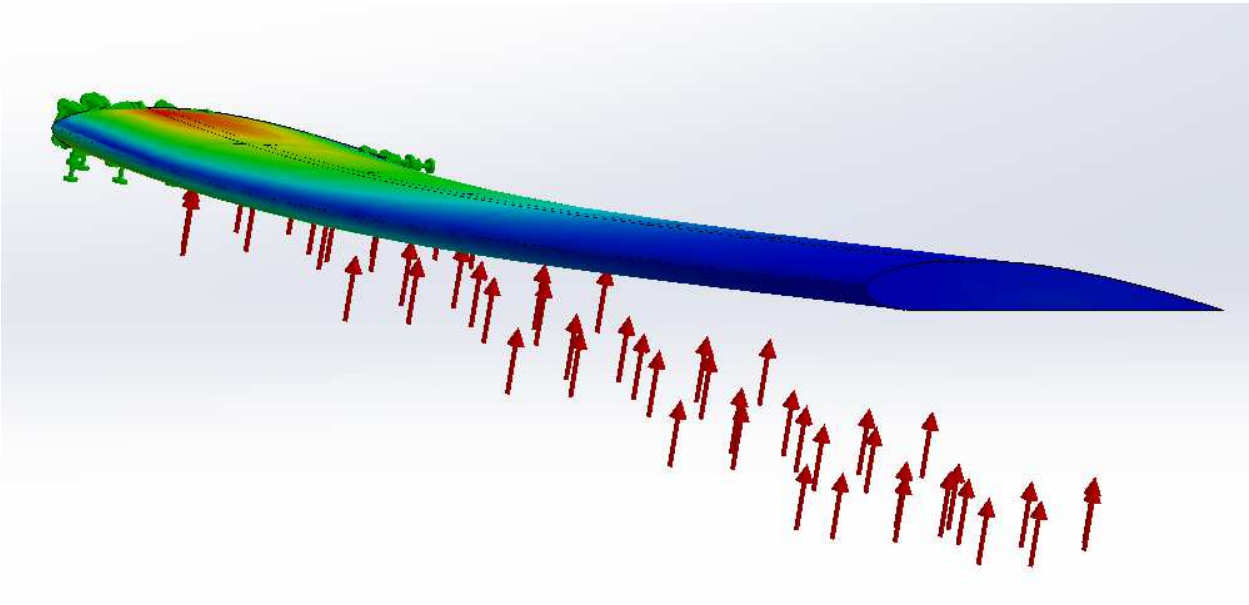

Figure 44 Deformation of the ribbed wing

For a perfectly phased case, the performance is similar to that of the stressed skin and foam cases. Gain is 30.5787 dB. Beamwidth is the same as the other cases, 3.08° in both the 0° and 90°

planes and 2.84° in the 45° plane. The radiation pattern is similar to the others as well, with the first side lobe just over 20 dB, and 3 others at approximately 10 dB in the 0° and 90° planes, with the first side lobe at 10 dB and two others at -10 dB in the 45° plane.

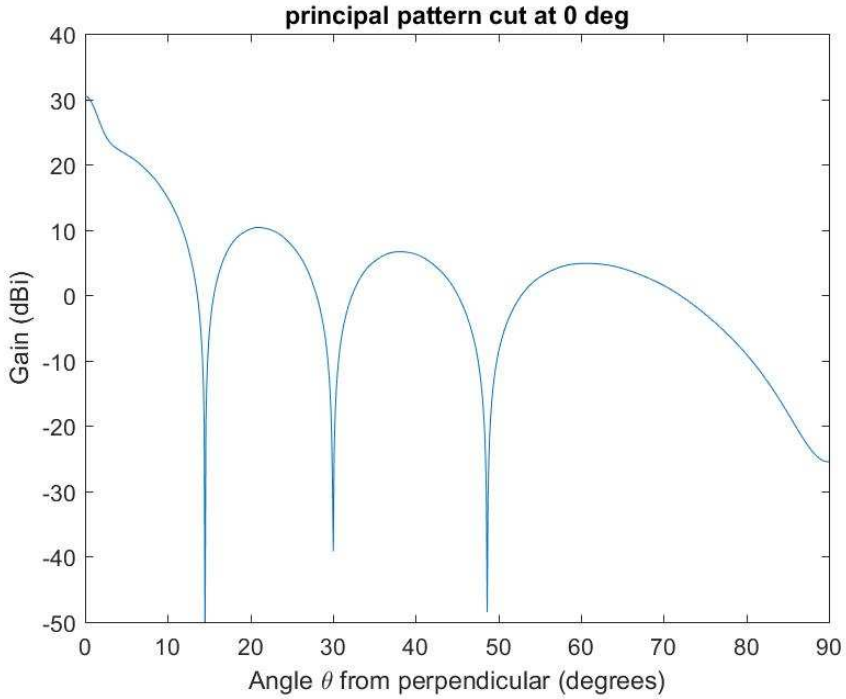

Figure 45 Nominal radiation pattern for ribbed wing and 4 GHz antenna

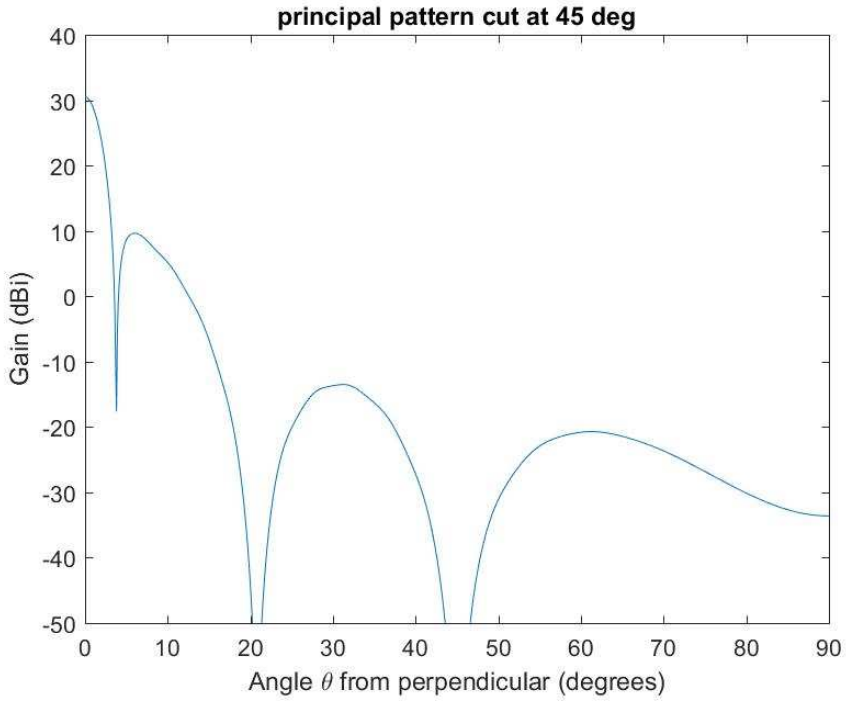

Figure 46 Nominal radiation pattern for ribbed wing and 4 GHz antenna

For a load of 600 lb. the deflection is 8.2% of λ, as opposed to 9.4% for the wing without ribs. Gain is 30.5601 dB, beamwidth is 3.1° in the 90° plane, 3.08° in the 0° plane and 2.84° in the 45° plane. The loss of 0.0187 dB corresponds to a 99.5% efficiency. A load of 650 lb. results in a deflection error that is of 4.1% of λ, gain of 30.574 dB and beamwidth of 3.8° in the 0° and 90° planes and 2.84° in the 45° plane. The loss is 0.0047 dB, for an efficiency of 99.9%. The antenna patterns show no significant differences from the perfectly phased case besides a rise in the nulls.

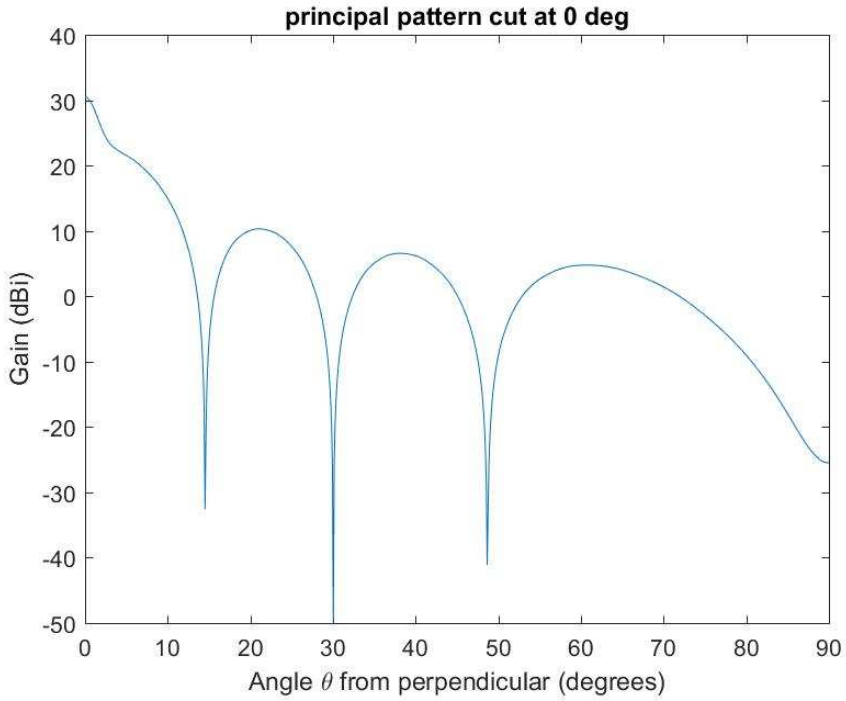

Figure 47 600 lb. radiation pattern for ribbed wing and 4 GHz antenna

Increasing the load has a similar effect to decreasing the load, so long as the deflection error is the same. Loading at 750 lb. results in a max deflection error that is 4.1% of λ. The beamwidth does not change, but gain drops by 0.0046 dB, representing an efficiency of 99.9%. Increasing to 800 lb. results in a deflection error that is 8.2% of λ, and the beamwidth in the 90° plane increasing to 3.1°, the beamwidth in the 0° and 45° plane remaining constant, and the gain dropping by 0.0186 dB, making the antenna 99.5% efficient. The side lobe structure is largely unchanged.

In the no load case, the gain drops to 29.8226 dB, beamwidth widens to 4.16° in the 90° plane and 3.18° in the 45° plane and narrows to 2.96° in the 0° plane. The maximum deflection error is 57.6% of λ and represents the deflection at 1g. As a reference, the original stressed skin wing had a maximum deflection of 65.5% of λ and a gain of 29.6291 dB. The beam was wider, 4.44° in the 90° plane and 3.24° in the 45° plane. The radiation pattern is similar to the other 4 GHz cases, with no discernable change in the 0° and 90° planes beside the main lobe widening, and the nulls in the 45° plane coming up.

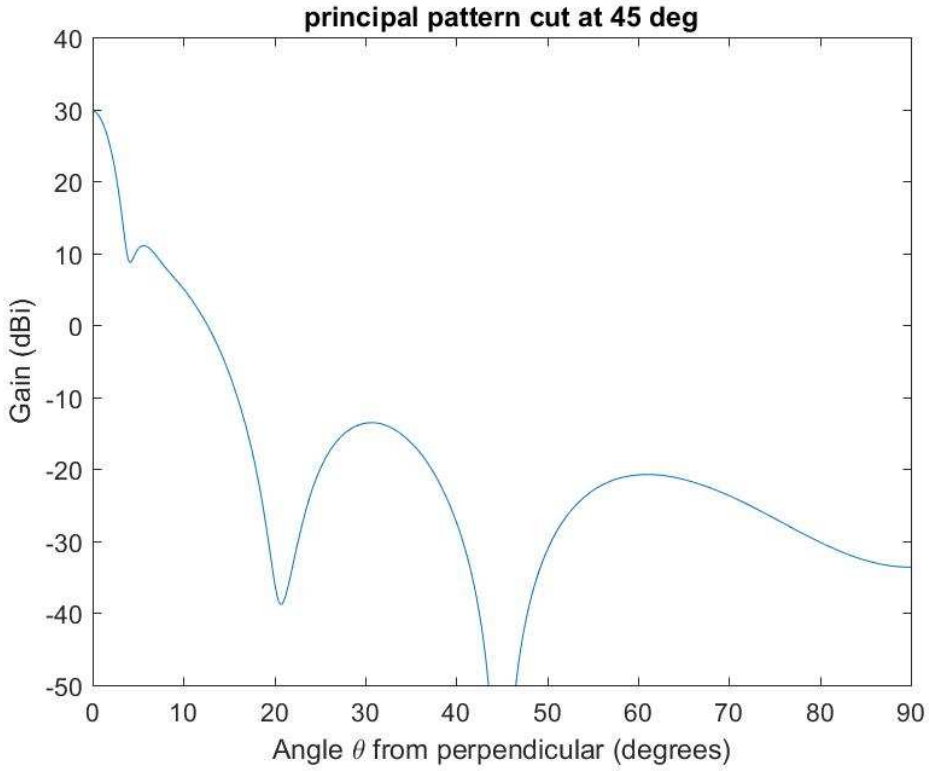

Figure 48 No load radiation pattern for ribbed wing and 4 GHz antenna

Overall, the addition of the ribs improves the tolerance to loading by allowing the wing to better retain its shape. The plot of load against loss shows a similar shape to the preceding cases, with the magnitude for the losses being somewhat smaller. The results for the ribbed wing are summarized in Table 4.

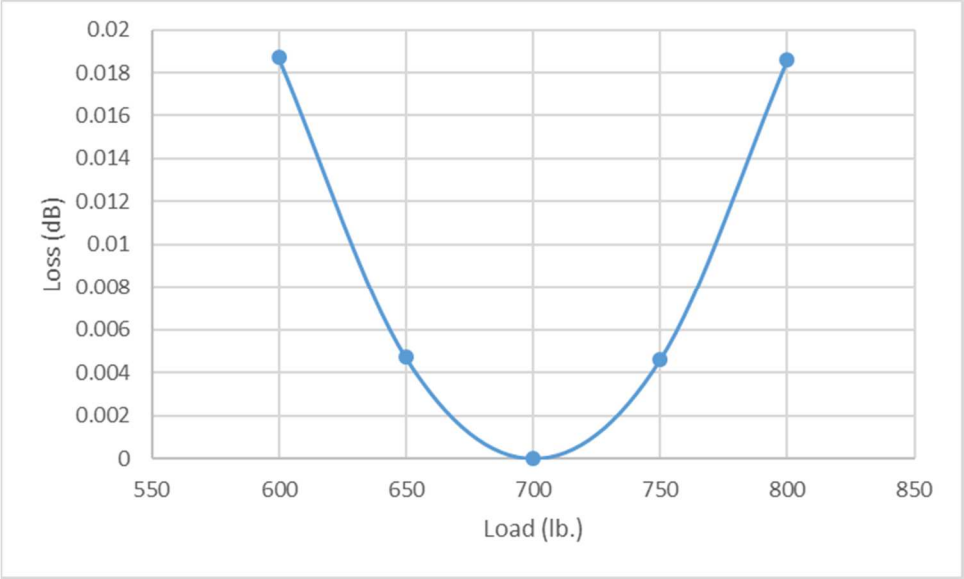

Figure 49 Load vs Loss for ribbed wing and 4 GHz antenna

Applied Load	Max Deflection	Gain Loss (dB)	Beamwidth in 90° plane	Beamwidth in 0° plane	Beamwidth in 45° plane
600	8.2%	0.0187	3.1°	3.08°	2.84°
650	4.1%	0.0047	3.08°	3.08°	2.84°
700	0%	0	3.08°	3.08°	2.84°
750	4.1%	0.0046	3.08°	3.08°	2.84°
800	8.2%	0.0186	3.1°	3.08°	2.84°
0	57.6%	0.7561	4.16°	2.96°	3.18°

Table 4 Results for the ribbed wing with 4 GHz antenna

Stressed Skin Wing with 1 GHz Antenna

The 1 GHz antenna used consists of 2 crossed rectangular antennas each 2 elements wide and 22 elements long spaced at half wavelengths, making each 0.3 meters wide and 3.3 meters long. The total number of elements is 84. In a perfectly phased planar case, it has a peak gain of 18.2934

dB according to Radiation_Pattern.m, with a beamwidth is 12.36° in both the 0° and 90° planes, and 11.34° in the 45° plane. When attached to the stressed skin wing and loaded to the nominal 700 lb., the perfectly phased antenna has identical performance in beamwidth, as would be expected. The drop in gain is negligible, dropping from 18.2931 to 18.2925 dB. The radiation pattern consists of the main lobe and a single side lobe at around 10 dB and running through most of the plane in both the 0° and 90° planes, with the side lobe leveling off in the 0° plane and dropping to a null in the 90° plane. The 45° plane has a much more defined main lobe, with the first side lobe peaking near 0 dB and having a defined null unlike the other pattern.

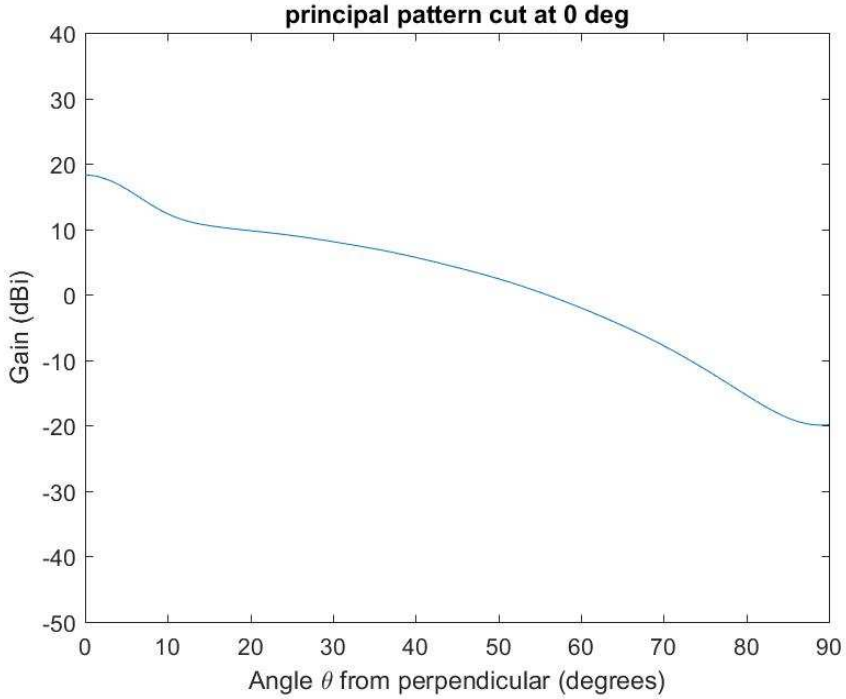

Figure 50 Nominal Radiation pattern for stressed skin wing and 1 GHz antenna

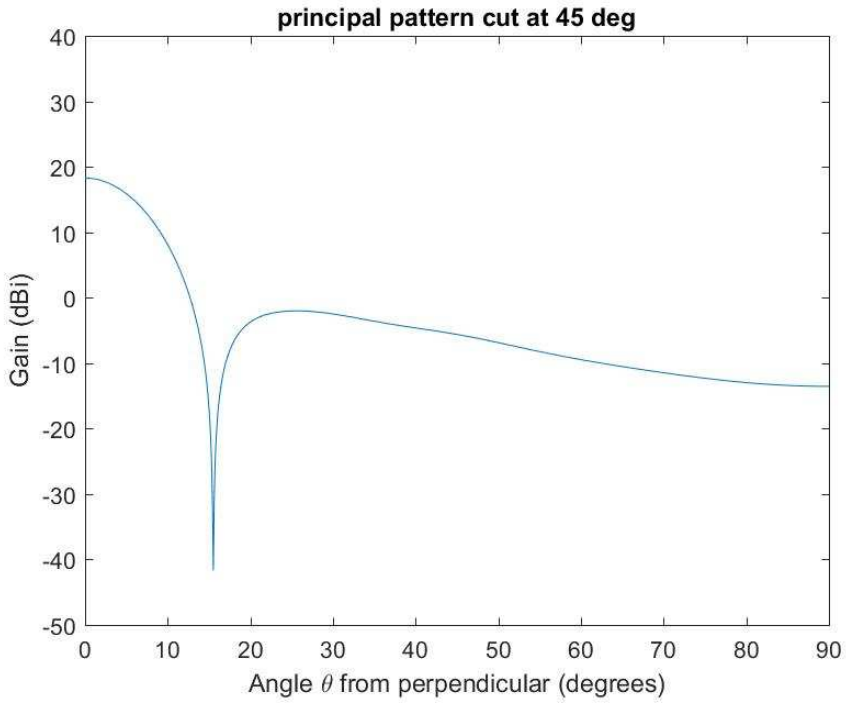

Figure 51 Nominal Radiation pattern for stressed skin wing and 1 GHz antenna

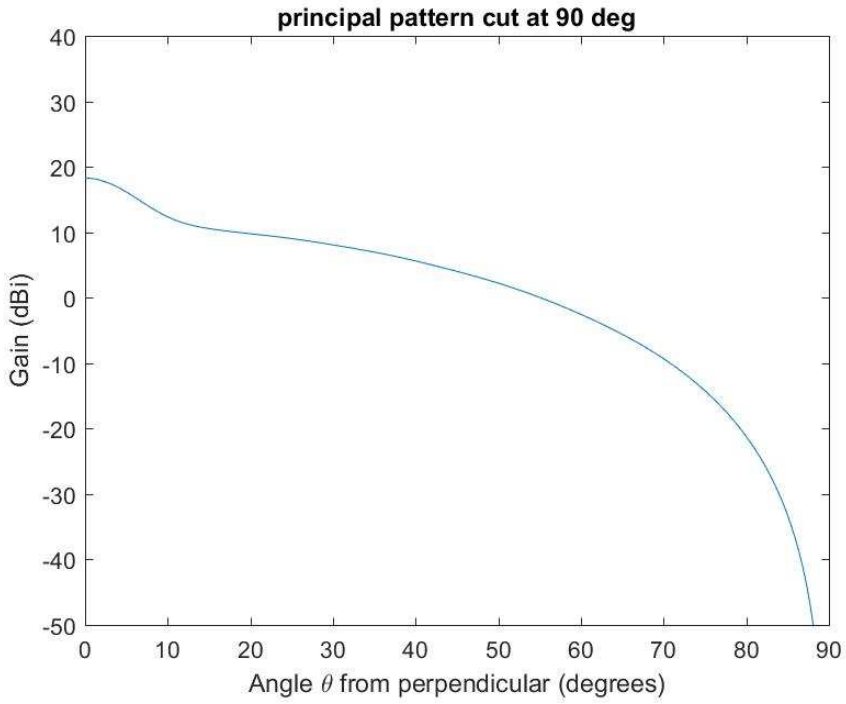

Figure 52 Nominal Radiation pattern for stressed skin wing and 1 GHz antenna

The radiation pattern is similar to what would be expected, with the main lobe in the 0° and 90° planes coming from the overlap of the two rectangular arrays, and the side lobe levels in the 45°

plane being very low. Because there are so few elements there is only a single side lobe in each plane.

Decreasing the loading while maintain the phasing for a 700 lb. load results in miniscule performance degradation to the antenna. At 650 pounds, the maximum deflection error the antenna experiences is only 1.1% of λ. This results in the beamwidth being unchanged, and a loss of peak gain of 0.0005 dB, representing an efficiency of 99.98%. At 600 pounds, the maximum deflection error is 2.2% of λ. This results in the beamwidth once again being unchanged in all 3 planes, and a loss of peak gain of 0.0017 dB, representing an efficiency of 99.96%. In both cases the side lobe structure has no discernable changes.

Increasing the load results in similar changes. An increase to 750 lb. results in the maximum deflection error being 1.1% of λ, with the beamwidth unchanged and the gain dropping by 0.0003 dB. At 800 lb. the deflection error is 2.2% of λ, the beamwidth in the 0° plane decreases to 12.34°, beamwidth in the 90° and 45° planes are unchanged, and gain drops by 0.0013 dB, making the antenna 99.97% efficient. The side lobe structure is unchanged in the 0° and 90° planes, but the 45° plane again shows changes, with the null coming up. The side lobe levels show little change overall.

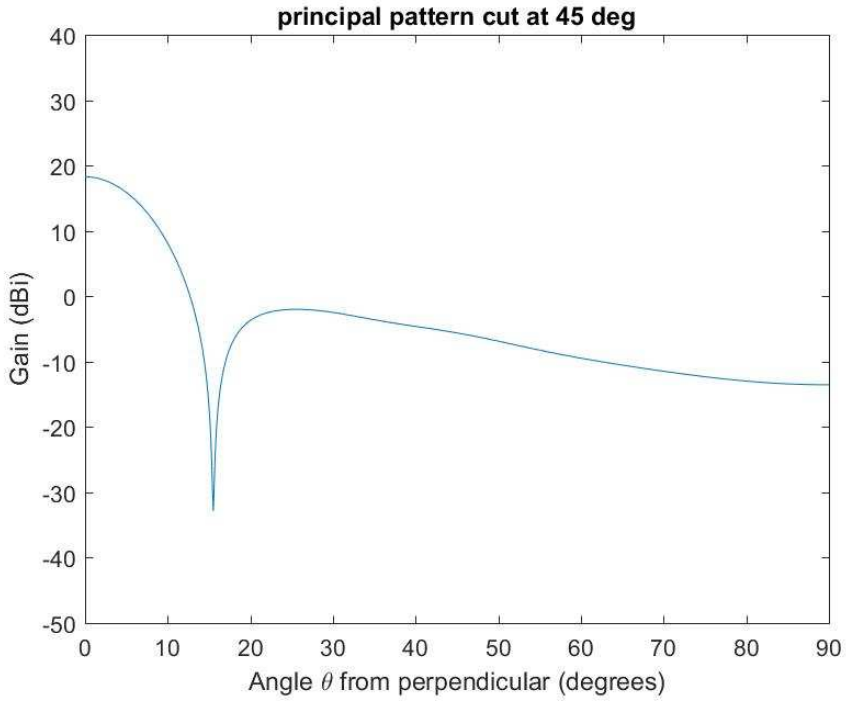

Figure 53 800 lb. load radiation pattern for stressed skin wing and 1 GHz antenna

An extreme case of zero applied load with a phasing set for a 700 lb. load results in a maximum error that is 15.1% of λ. This 15.1% also represents the normal deflection at 1g. The beamwidth in the 90° plane increases to 12.72° from the original 12.36°, the beamwidth in the 0° plane increases to 12.38°, and the beamwidth in the 45° plane increases to 11.44° from 11.34°. The gain drops to 18.219 dB, a loss of 0.0735 dB and representing a 98% efficient antenna. The side lobe structure also begins to change in the 45° plane, with the null coming up closer to the peaks.

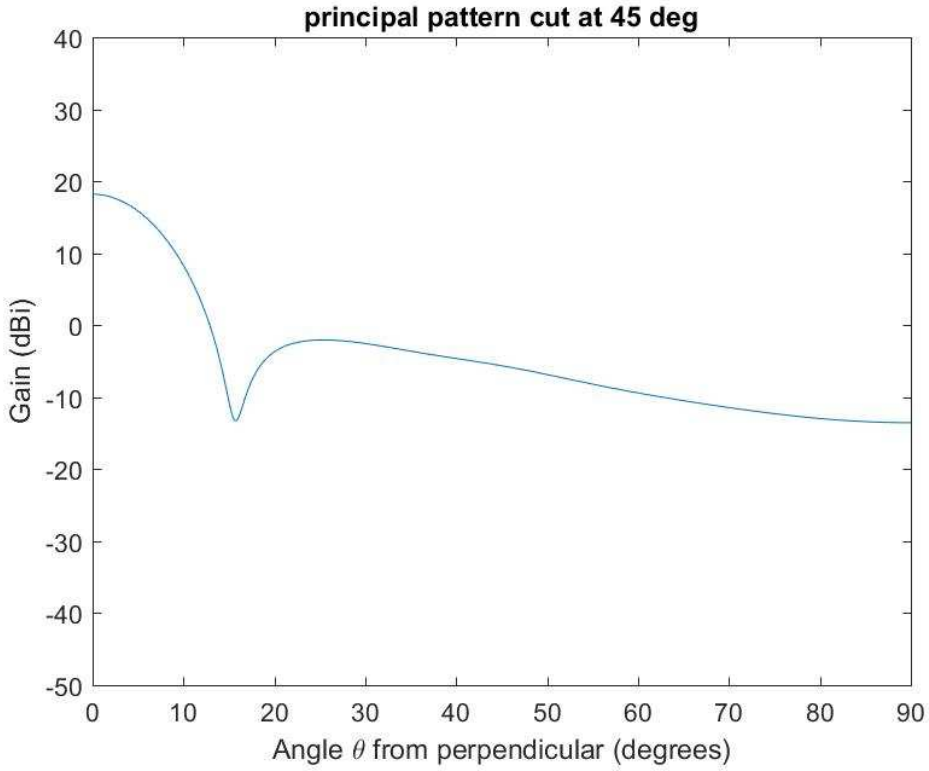

Figure 54 Zero load radiation pattern for stressed skin wing and 1 GHz antenna

In the case of the 1 GHz antenna, the deflections are much smaller because of the larger wavelength as compared to the 4 GHz antenna. Because of this, the deflections remain small, even for very large loading conditions. The plot of deflection against loss shows a similar curve to the 4 GHz case, but does not progress as far through the deflections due to the larger wavelength. For loading near the nominal the losses are practically negligible because the deflections are so small. Because the deflection error is such a small fraction of wavelength, the losses to gain are very small, and the beamwidth holds across almost all expected loading conditions. The plot of loss against load shows the shape expected, but with a much lower magnitude as compared to the 4 GHz antennas and a shallower increase on the positive loading side of the curve. The results are summarized in Table 5.

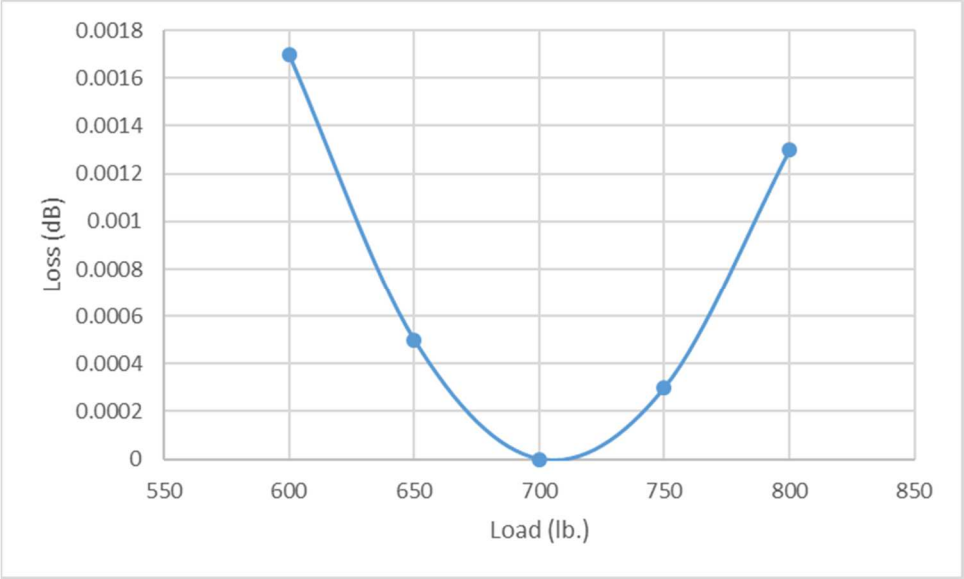

Figure 55 Load vs Loss for Stressed Skin wing with 1 GHz antenna

Applied Load	Max Deflection	Gain Loss (dB)	Beamwidth in 90° plane	Beamwidth in 0° plane	Beamwidth in 45° plane
600	2.2%	0.0017	12.36°	12.36°	11.34°
650	1.1%	0.0005	12.36°	12.36°	11.34°
700	0%	0	12.36°	12.36°	11.34°
750	1.1%	0.0003	12.36°	12.36°	11.34°
800	2.2%	0.0013	12.36°	12.34°	11.34°
0	15.1%	0.0735	12.72°	12.38°	11.44°

Table 5 Results for Stressed skin wing with 1 GHz antenna

Foam and Aluminum Spar Wing with 1 GHz Antenna

The foam wing has slightly better performance when perfectly phased, with a gain of 18.2931 dB, compared to the 18.2934 dB of the planar case. Both the perfectly phased antenna on the foam wing and the planar case have beamwidth of 3.08° in the 0° and 90° planes and 2.84° in the 45°

plane. As with the stressed skin wing, the radiation patterns in the 0° and 90° planes are almost identical, with a first side lobe very near the main lobe at approximately 10 dB, no null separating it from the main lobe, and a taper to -30 dB in the 0° plane and a drop to zero power in the 90° plane. In the 45° plane the pattern is similar to the stressed skin case, with a much more defined side lobe at 0 dB and tapering off to -12 dB.

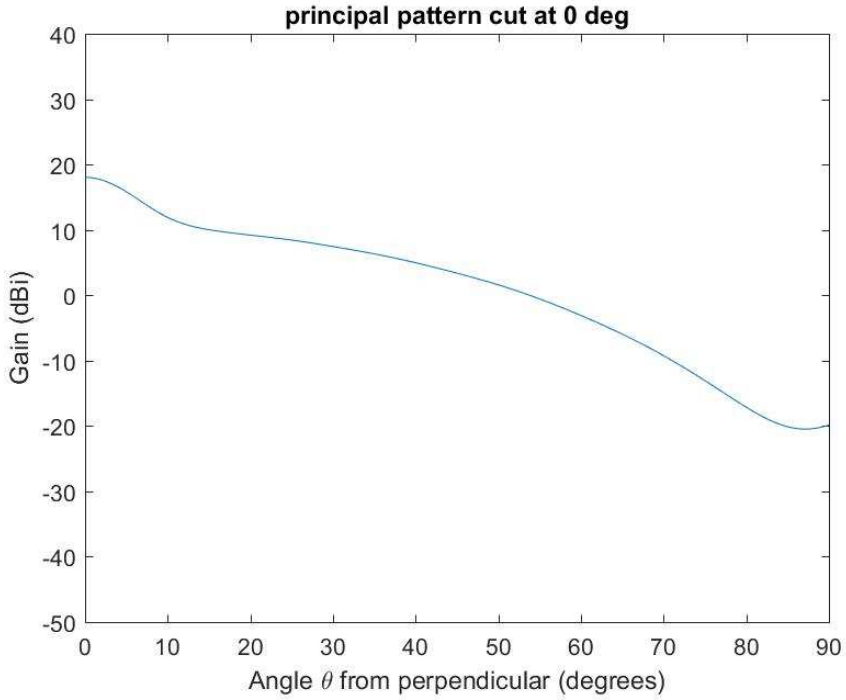

Figure 56 Nominal radiation pattern for foam wing and 1 GHz antenna

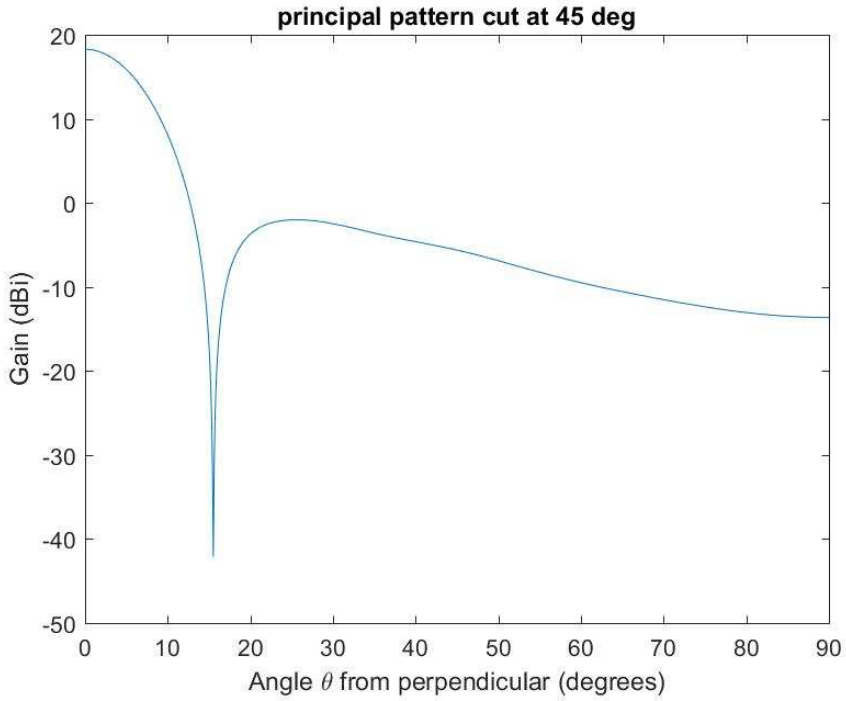

Figure 57 Nominal radiation pattern for foam wing and 1 GHz antenna

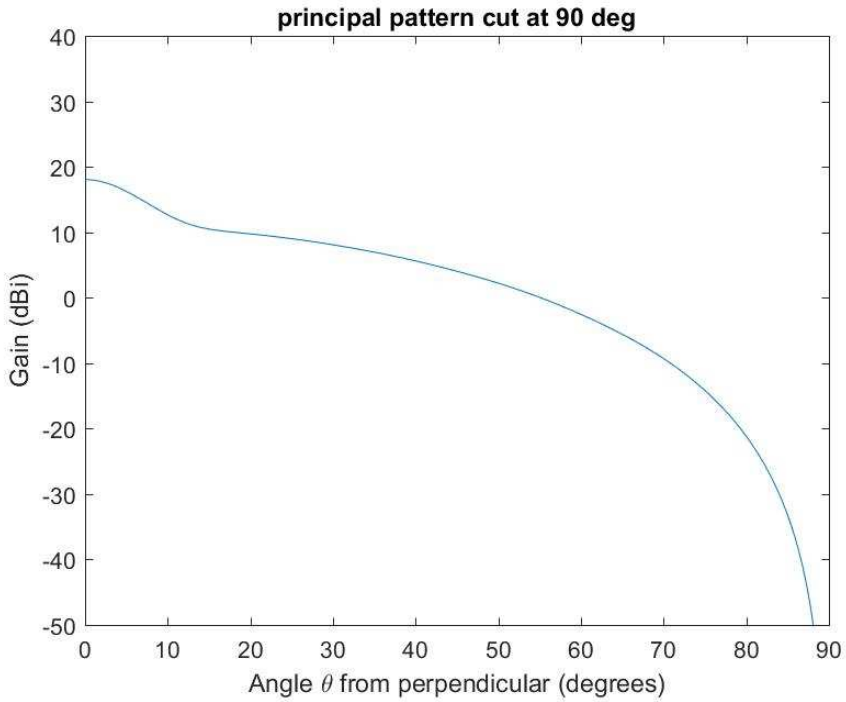

Figure 58 Nominal radiation pattern for foam wing and 1 GHz antenna

The deflections of the foam wing are, once again, slightly larger than the stressed skin wing. With a load of 650 lb. phased for the 700 lb. nominal load, the deflection is 1.2% of λ and the beamwidth is unchanged. Peak loss in miniscule, 0.0005 dB for an efficiency of 99.99%. A load of 600 lb. will result in the deflection error increasing to 2.3% of λ, with beamwidth again holding constant in all 3 planes, and gain dropping to 18.2914 dB, for an efficiency of 99.96%. As with the stressed skin wing, changes to the radiation pattern are small enough in the 0° and 90° planes to go unnoticed. The only significant change in the 45° plane is the value of the null coming up.

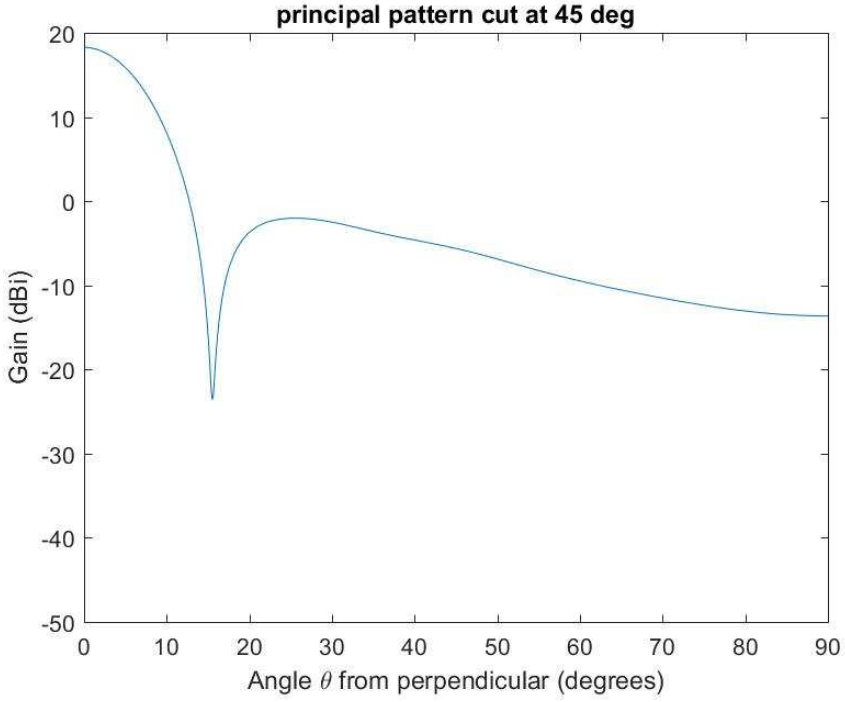

Figure 59 600 lb. load radiation pattern for foam wing and 1 GHz antenna

Once more, increasing the load has a similar effect to decreasing the load, so long as the deflection error is similar. Loading at 750 lb. results in a maximum deflection error that is 1.1% of λ. The beamwidth does not change, but gain drops by 0.0004 dB. Increasing to 800 lb. results in a deflection error of 2.3% of λ, with the beamwidth again remaining unchanged, and the gain dropping by 0.0014 dB. The side lobe structure is unchanged in both cases.

For a no load case the deflection error is 16% of λ, which is also the deflection for the 1 g case. This results in the beamwidth widening to 12.74° in the 90° plane and 11.46° in the 45° plane, narrowing to 12.34° in the 0° plane, and gain dropping by 0.0747 dB, making the antenna 98.3% efficient. The side lobes in the 0° and 90° planes are unchanged, but the null in the 45° plane continues to rise and begins to approach -10 dB.

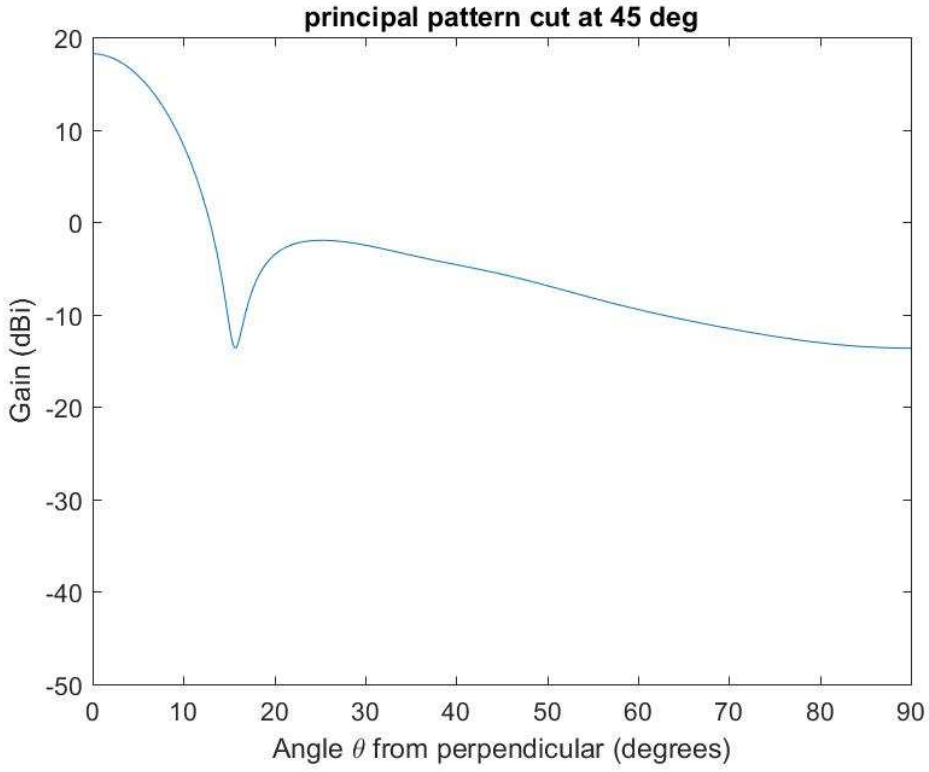

Figure 60 Zero load radiation pattern for foam wing and 1 GHz antenna

As with the 4 GHz cases, the maximum deflection error is smaller for the stressed skin wing but performance is similar, with beamwidth remaining constant throughout in the foam wing and the stressed skin wing having slightly lower losses. Similarly to the 1 GHz stressed skin case, the sensitivity to loading is shallower on the positive loading side of the curve. The results are summarized in Table 6.

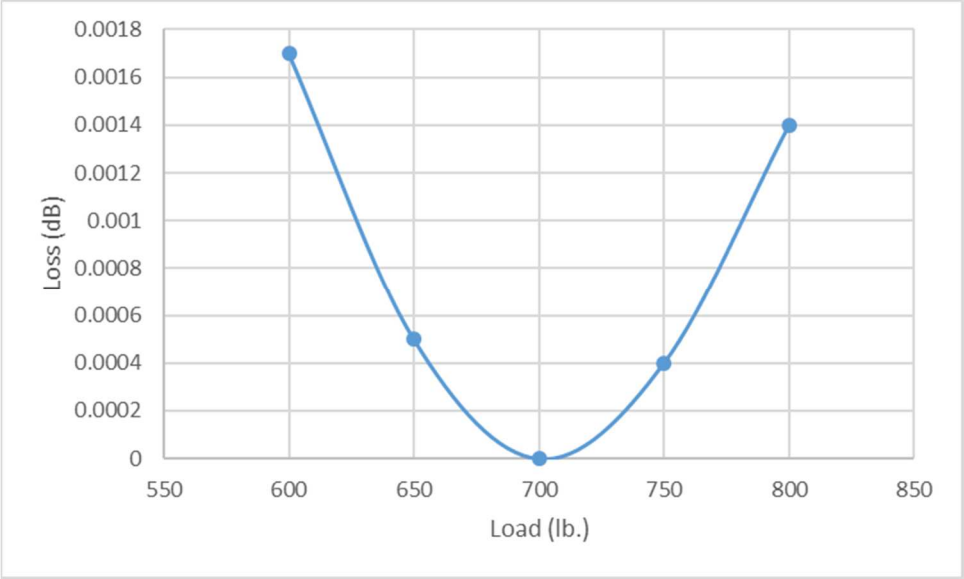

Figure 61 Load vs Loss for Foam wing and 1 GHz antenna

Applied Load	Max Deflection	Gain Loss (dB)	Beamwidth in 90° plane	Beamwidth in 0° plane	Beamwidth in 45° plane
600	2.3%	0.0017	12.36°	12.36°	11.34°
650	1.2%	0.0005	12.36°	12.36°	11.34°
700	0%	0	12.36°	12.36°	11.34°
750	1.1%	0.0004	12.36°	12.36°	11.34°
800	2.3%	0.0014	12.36°	12.36°	11.34°
0	16.0%	0.0747	12.74°	12.34°	11.46°

Table 6 Results of Foam wing and 1 GHz antenna

Stressed Skin Wing with Ribs and 1 GHz Antenna

For a perfectly phased case, the performance is similar to that of the stressed skin and foam cases. Gain is 18.2933 dB. Beamwidth is the same as the other cases, 12.36° in both the 0° and 90°

planes and 11.34° in the 45° plane. The radiation pattern is similar to the others as well, with the first side lobe just over 10 dB, and trailing off after 60° in the 0° and 90° planes, with the first side lobe at 0 dB and a very sharp null in the 45° plane.

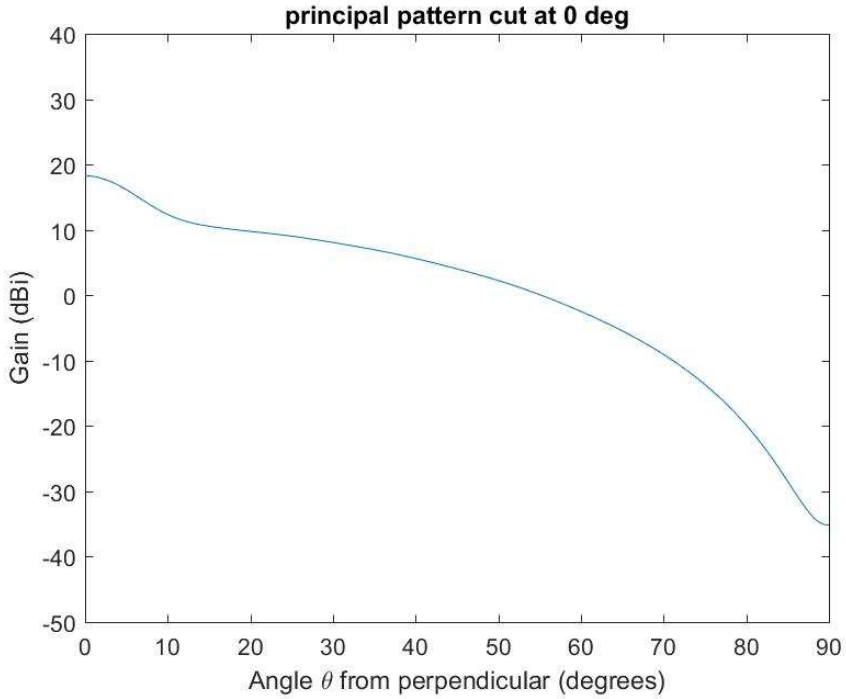

Figure 62 Nominal radiation pattern for ribbed wing and 1 GHz antenna

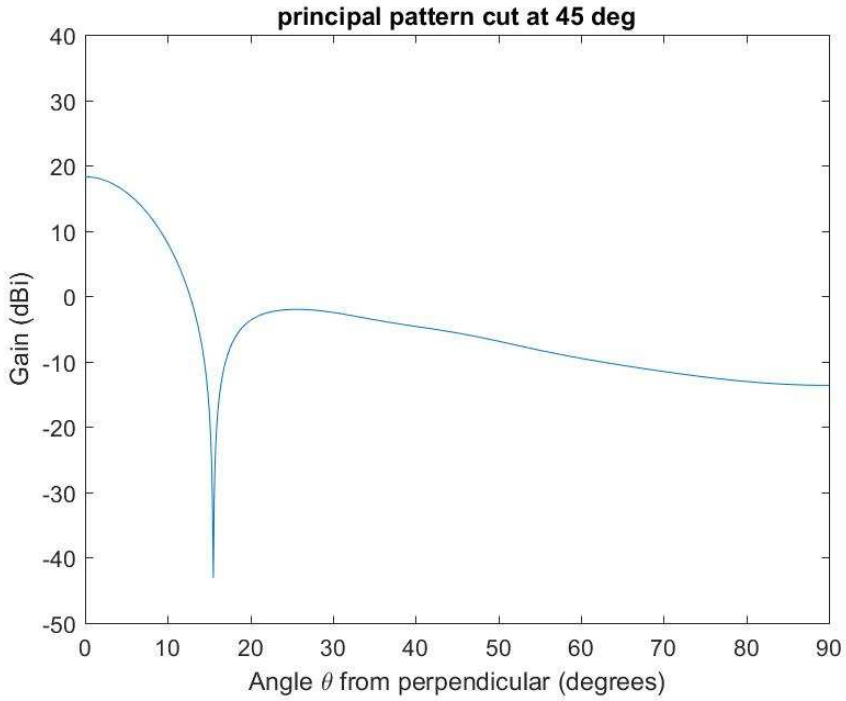

Figure 63 Nominal radiation pattern for ribbed wing and 1 GHz antenna

For a load of 600 lb. the deflection is 1.9% of λ, loss is 0.0013 dB, beamwidth remains 12.36° in the 0° and 90° planes and 11.34° in the 45° plane. The loss of 0.0013 dB corresponds to 99.97% efficiency. A load of 650 lb. results in a deflection error that is of 0.9% of λ, gain of 18.2929 dB and beamwidth remaining constant. The loss is 0.0004 dB, for an efficiency of 99.99%. The antenna patterns show no significant differences from the perfectly phased case besides a rise in the null in the 45° plane.

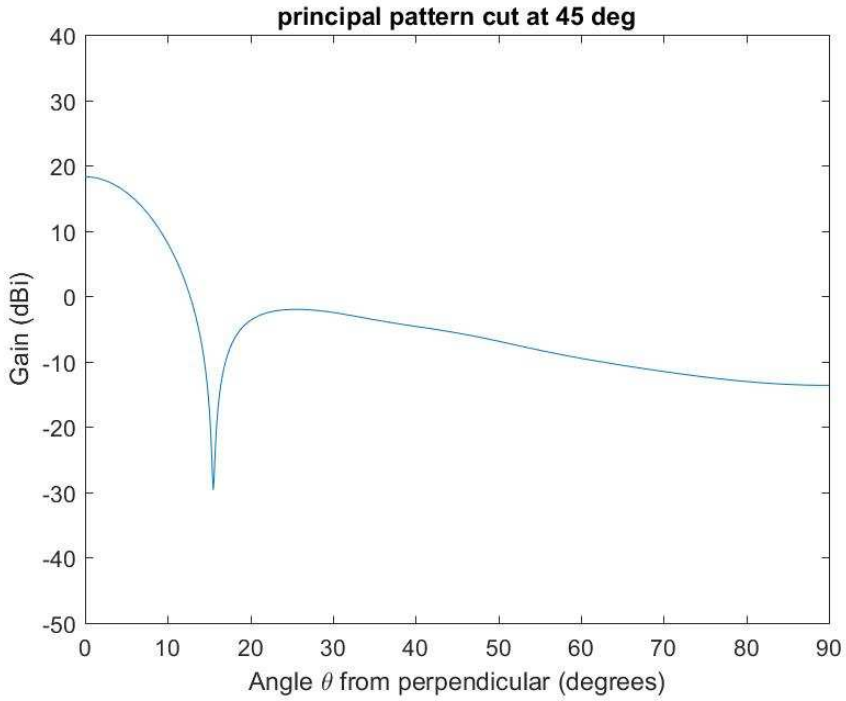

Figure 64 600 lb. radiation pattern for ribbed wing and 1 GHz antenna

Increasing the load, as with the previous 5 cases, has a similar effect to decreasing the load. Loading at 750 lb. results in a max deflection error that is 0.9% of λ. The beamwidth does not change, but gain drops by 0.0003 dB, representing an efficiency of 99.99%. Increasing to 800 lb. results in a deflection error that is 1.9% of λ, the beamwidth in all 3 planes remaining constant, and the gain dropping by 0.0011 dB, making the antenna 99.97% efficient. The side lobe structure is largely unchanged.

In the no load case, the gain drops to 18.2362 dB, beamwidth widens to 12.64° in the 90° plane and 11.44° in the 45° plane and narrows to 12.32° in the 0° plane. The maximum deflection error is 13.5% of λ, as is the total deflection at 1g. The radiation pattern is similar to the other 1 GHz cases, with no discernable change in the 0° and 90° planes beside the main lobe widening, and the null in the 45° plane coming up to almost -10 dB.

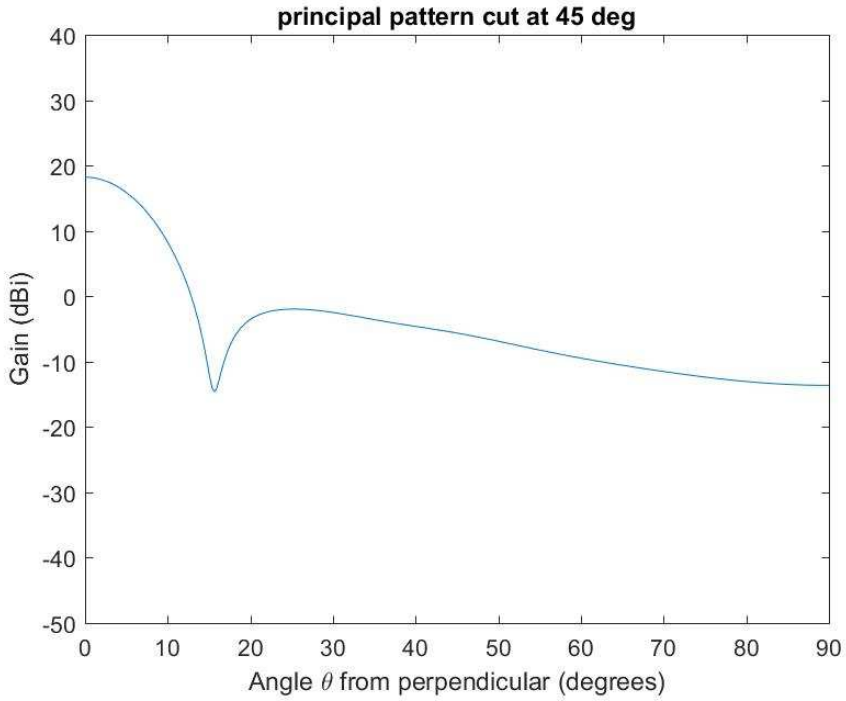

Figure 65 No load radiation pattern for ribbed wing and 1 GHz antenna

Overall, the addition of the ribs once again improves the tolerance to loading by allowing the wing to better retain its shape, but this improvement is lessened by the long wavelength of the system. The plot of load against loss shows a similar shape to the preceding cases, with the sensitivity being shallower on the positive loading side of the curve, and the magnitude of the losses being somewhat smaller. The results for the ribbed wing are summarized in Table 7.

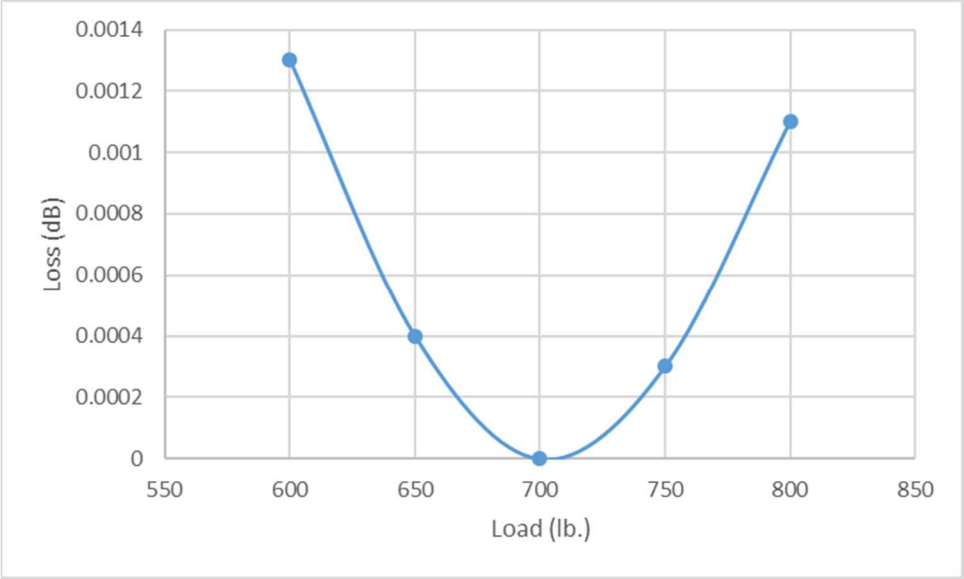

Figure 66 Load vs Loss for ribbed wing and 1 GHz antenna

Applied Load	Max Deflection	Gain Loss (dB)	Beamwidth in 90° plane	Beamwidth in 0° plane	Beamwidth in 45° plane
600	1.9%	0.0013	12.36°	12.36°	11.34°
650	0.9%	0.0004	12.36°	12.36°	11.34°
700	0%	0	12.36°	12.36°	11.34°
750	0.9%	0.0003	12.36°	12.36°	11.34°
800	1.9%	0.0011	12.36°	12.36°	11.34°
0	13.5%	0.0571	12.64°	12.32°	11.44°

Table 7 Results for the ribbed wing with 1 GHz antenna

CHAPTER V

CONCLUSIONS

Analysis of the 6 cases for a low frequency wing conformal cruciform antenna array was done to provide insight into the relationships between frequency selection, wing construction and stiffness, loading and antenna performance. Specifically, the aim was to answer the following:

1. What relationship is there between wing stiffness and the tolerance of the antenna performance to small variations in wing loading?
2. What relationship is there between frequency selection and the tolerance of the antenna performance to small variations in wing loading?
3. Is such a configuration viable for a ground mapping application, accounting for small changes in wing loading that are not corrected with phasing?

In addition to the specific relationships relevant to these questions, some general relationships were found as well.

Firstly, the degradation of antenna performance is correlated with the difference in element positions used to phase the array and the actual positions as a percentage of wavelength, not the loading applied. Since the applied load does directly affect the actual element positions it does have an effect on the antenna performance, but there is no difference between a load above nominal and one that is below nominal so long as the error in deflection is the same.

Secondly, for the small changes in loading expected, the changes to gain and beamwidth are very small. Beamwidth does not widen by more than 0.02°, and the antenna gain indicated that they were still more than 99% efficient in transmitting as compared to the perfectly phased case. This is especially true for the 1 GHz case, where changes to beamwidth are isolated and gain corresponds to efficiencies of 99.9% or more. The gain losses in particular can be neglected as they will fall below the level of the ambient electronic noise the system will pick up.

Effect of Wing Stiffness

The 3 wings evaluated exhibited different degrees of stiffness and resistance to deformation under loading. The foam wing with the aluminum spar was the most flexible wing, and therefore deformed the most. The stressed skin wing was stiffer by almost half, but its underside was unsupported and would bow in under load. The ribbed wing retained the bending stiffness but added support to prevent this bowing inward.

Since most changes in beamwidth were below the resolution of the MATLAB model to detect, the losses from peak gain against loading offer the best insight into the relationship between loading, wing stiffness and antenna performance.

The foam and stressed skin wings have very similar curves, despite the differences in stiffness. The ribbed wing has a better tolerance to loading, and its losses are approximately 80% of the losses on the other 2 wings. This would suggest that a stiffer wing will better resist the effects of uncorrected loading. The lower surface of the stressed skin wing deformed inward, increasing how far out of phase it was and negating its stiffness advantage over the foam wing, whereas the ribbed wing did not suffer this penalty and was able to take full advantage of the stiffness inherent to its design.

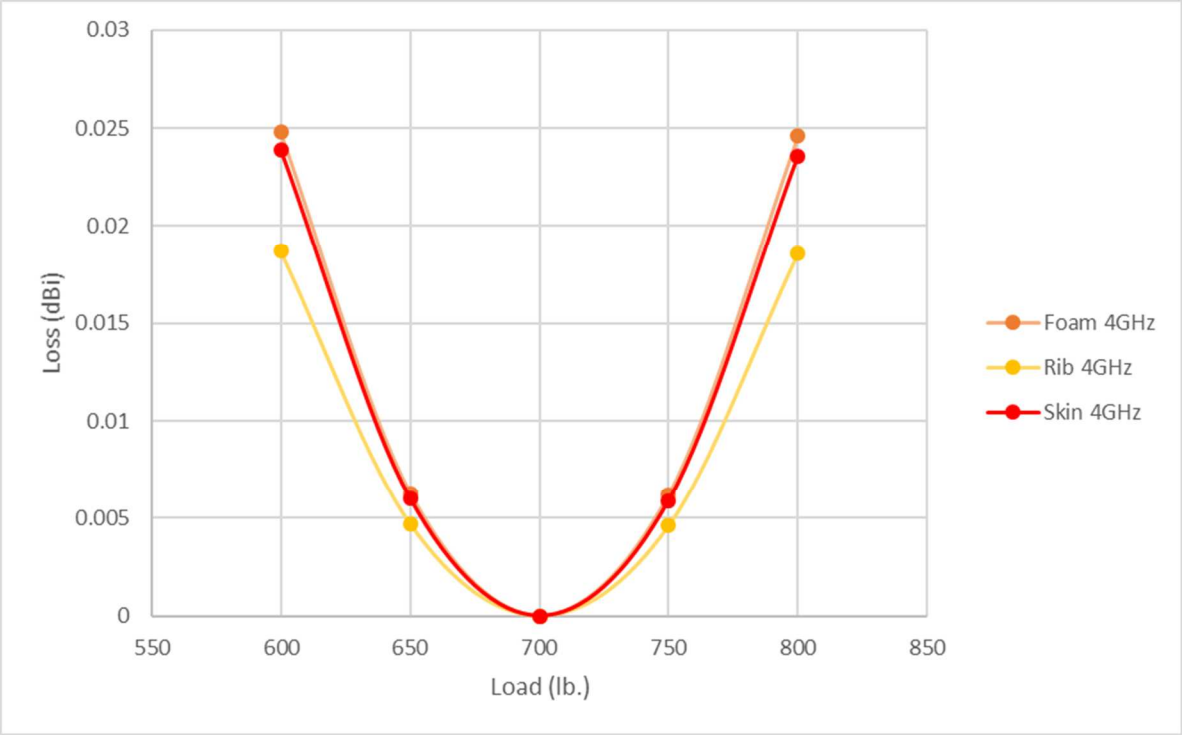

Figure 67 Loss vs Load for all 3 wings at 4 GHz

The relationship between the 3 wings can be seen in Figure 67, which combines the loss vs loading curves for all 3 wings operating at 4 GHz. The curves for the foam and stressed skin wings are very close to each other, but the curve for the ribbed wing sits below the other 2.

Effect of Frequency

Since the degradation of the antenna performance depends on the deflection error as a percentage of wavelength, the selection of a lower frequency and longer wavelength will improve he antenna tolerance to loading. This is because a set deflection error resulting from a specific loading of the wing will be a smaller proportion of the wavelength than for a higher frequency. The result of this can be seen when comparing the plots of load and loss across the 1 GHz antennas and the 4 GHz antennas.

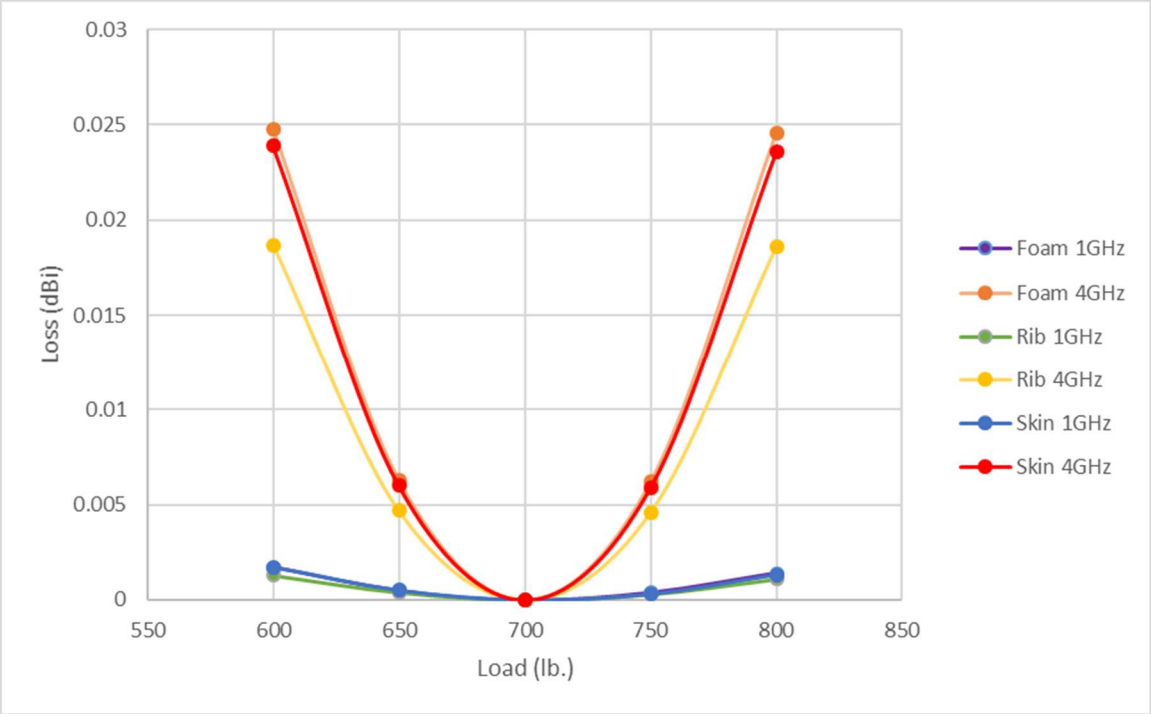

Figure 68 Load vs Loss across 1 GHz and 4 GHz

The losses in the 1 GHz antennas are nearly an order of magnitude below the losses of the 4 GHz antennas.

Additionally, the 1 GHz antennas showed a slightly shallower increase in losses for loadings above 1 GHz not seen in the 4 GHz case. This source of this is difficult to identify, and can be seen in Figure 69, where all 3 wings show lower losses for the loadings above nominal than for those below.

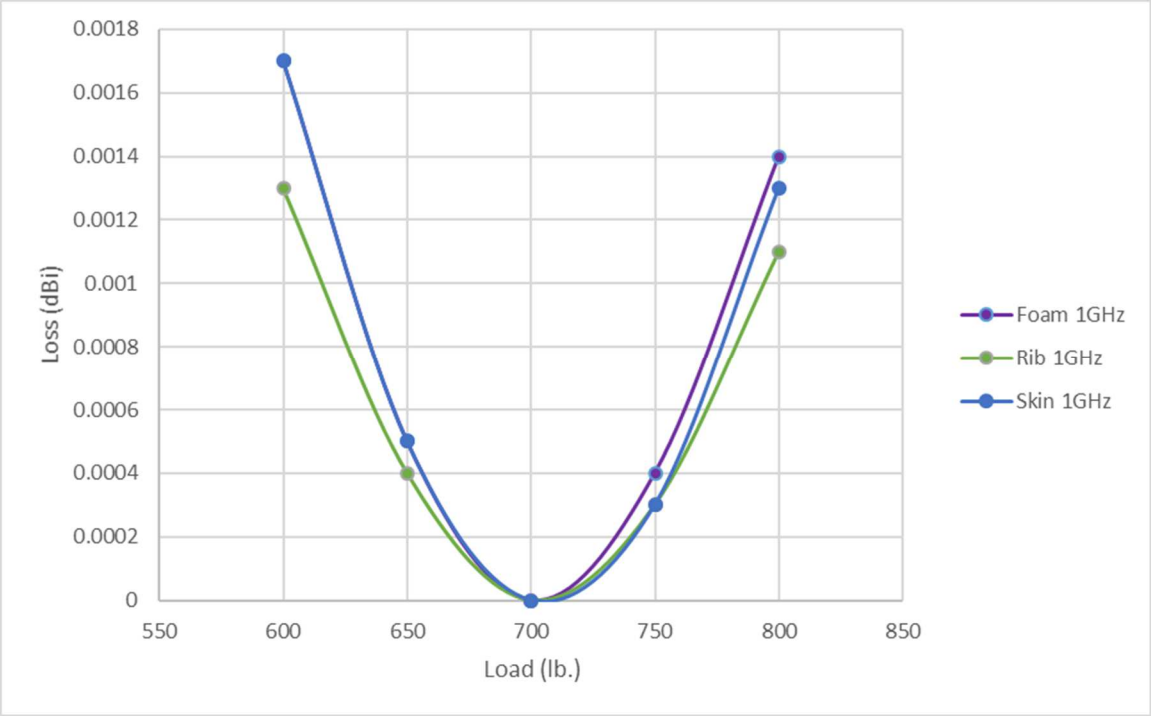

Figure 69 Loss vs Load for 1 GHz antenna

Lastly, the lower frequency antennas fit fewer elements aboard the aircraft, meaning that they have a different side lobe structure compared to the higher frequency systems. This can be seen by comparing the radiation patterns for the perfectly phased cases of both the 1 GHz and 4 GHz antennas. The 1 GHz antenna in Figure 70 has the single long side lobe whereas the 4 GHz antenna in Figure 71 has a single side lobe attached to the main lobe, and 3 others that are more distinct.

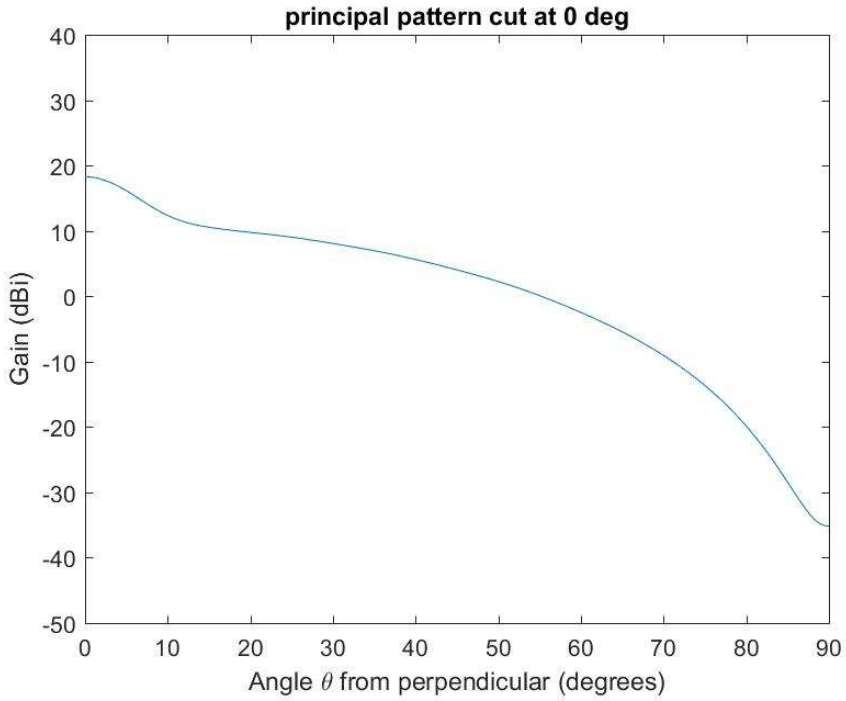

Figure 70 Nominal radiation pattern at 1 GHz

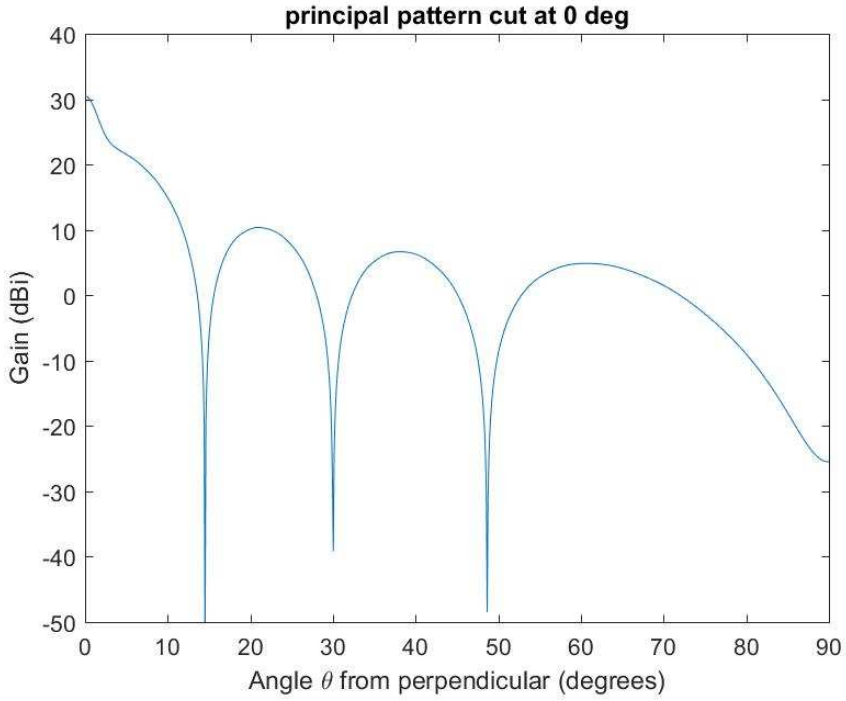

Figure 71 Nominal radiation pattern at 4 GHz

Viability for Ground Mapping

With the original motivations of this study being the requirement to perform ground elevation modeling with a low frequency radar system mounted to a sUAV, the performance of the systems shown must be evaluated.

Overall, the antenna performance is inconclusive. The beamwidth of 12.36° in the 1 GHz antennas is able to offer 6 m area resolution at an altitude of 27 m and 3 m resolution form an altitude of 13 m, but both these values are well below the far-field distance of 72.6 m. The gain is acceptable, and would be improved in actuality by the use of antenna elements with directivity as opposed to the idealized isotropic elements used here.

The greatest effect of a gust may be a change in altitude increasing the size of the patch being mapped. A change from 27 meters to 30 meters will increase the resolution from 6 meters to 6.5 meters. Similarly, a change from 13 to 15 meters elevation will increase the resolution from 3 meters to 3.25 meters. This effect may also be caused by drift in altitude due to the autopilot or control system.

The primary issue is the side lobe levels. Most of the side lobes sit around 8-10 dB below the main lobe, meaning that they may not be low enough to wash out clutter. For example, a metal roof located beside a patch being overflown is more reflective than the ground directly below and could return a signal that washes out the main lobe return.

Implications

With the changes to antenna performance being so small, the effect of wing stiffness is not a significant factor at low frequencies. Designers can build the wing to a certain strength instead of designing to both strength and stiffness. At higher frequencies or in arrays with sparser spacing

the effect of stiffness becomes a more important factor and must be considered. Additionally, the selection of a longer wavelength radar relative to the aircraft dimensions gives the system a much better tolerance to loading errors. The choice of a lower frequency does require that fewer elements be present on the aircraft, resulting in a lower gain and a less desirable radiation pattern.

Future Work

Due to time constraints and a need to control the scope of this project, there are several related areas that merit further study, but were not considered. These include:

1) A more rigorous CAD model incorporating the antenna elements so that the stresses in the elements as well as the effects of CLAS antennas on wing stiffness can be examined.
2) Including the directivity and normal vector of each element in the calculations as opposed to isotropic radiators, in order to provide a more accurate calculation of gain and beamwidth.
3) Examination of pattern synthesis to account for the change in normal vector of each element and to allow for beam steering.
4) Examination of ease of manufacture for various construction methods as well as any additional benefits they may offer to antenna performance beyond tolerance to deformation such as maintenance, damage tolerance and antenna power feed.
5) Examination of other means to predict deflection such as analytic models, onboard strain gauges, and aircraft testing.
6) More rigorous simulations of aerodynamics and lift in order to develop a complete force distribution and resulting deflections.
7) Determining the effects of small errors in material properties or small defects in construction on the antenna performance.

REFERENCES

1. Balanis, C. A. *Antenna Theory: Analysis and Design*. John Wiley & Sons, Inc., 1997
2. Budynas, Richard G., J. Keith. Nisbett, and Joseph Edward. Shigley. *Shigley's Mechanical Engineering Design*. New York, NY: McGraw-Hill Education, 2015. Print.
3. Callus, Paul J. *Conformal Load-Bearing Antenna Structure for Australian Defense Force Aircraft*. Australian Government Department of Defense. 2007
4. Ciso Corporation, "Antenna Patterns and Their Meaning" White Paper, 2007
5. Civil Aviation Safety Authority Australia, "Design Standards: Unmanned Aerial Vehicles – Aeroplanes" 2000
6. Cortambert, Jean-Marc, et al. "The Cruciform Array and Associated Signal Processing," IEEE Radar Conference, 2005
7. Dielectric Corporation, "G-10/FR-4/G-11 (Glass-Epoxy) General Material Properties" http://www.dielectriccorp.com/downloads/thermosets/glass-epoxy.pdf
8. Geng, J. P. et al. "The Development of Curved Microstrip Antenna With Defected Ground Structure," *Progress In Electromagnetics Research* 53-73, 2009
9. Josefsson, Lars and Patrik Persson *Conformal Array Antenna Theory and Design*. Wiley-Interscience, 2006

10. Khan, Anzar and Rajesh Nema, "Analysis of Five Different Dielectric Substrates on Microstrip Patch Antenna" *International Journal of Computer Applications* (0975-8887), 2012
11. Mailloux, R. J. "Periodic arrays." *Antenna Engineering Hand-book* chapter 13, McGraw-Hill, 1981.
12. Megson, T. H. G. Aircraft Structures for Engineering Students. Elsevier, 2013.
13. Neubauer, Martin et al., *Structural Design Aspects and Criteria for Military UAV*, EADS, 2007
14. Orban, D. and G. J. K. Moernaut "The Basics of Patch Antennas, Updated," *RF Globalnet Newsletter*, 2009
15. Robinson, Clarence A. "Radar Counters Camouflage" *Signal Magazine*. 2007
16. Simons, Martin, *Model Aeroplane Aerodynamics*, Model & Allied Publications 1978. Chapter 7 - 9, Aerofoil Sections.
17. Smallwood, Ben P. *Structurally Integrated Antennas on a Joined-Wing Aircraft.* MS Thesis, Air Force Institute of Technology, Wright-Patterson AFB OH, 2003
18. Solidworks Corporation "Finite Element Analysis" http://www.solidworks.com/sw/products/simulation/finite-element-analysis.htm
19. SRC inc. "FORESTER Radar Fact Sheet" 2012
20. Stimson, George W. *Introduction to Airborne Radar*. SciTech Publishing, 1998.
21. Steyskal, Hans. *Pattern Synthesis on a Conformal Wing Array*. Air Force Research Laboratory. 2001
22. Sze, Lim Tien et al., "High Resolution DEM Generation Using Small Drone for Interferometry SAR" *International Conference on Space Science and Communication*. 2015
23. Tsunoda, S. I. et al. "Lynx: A high-resolution synthetic aperture radar" *SPIE Aerosense*, 1999

24. VectorLam Cirrus, “Laminate Design and Analysis Software”
25. Wang, H. S.C. “Performance of Phased –Array Antenna with Mechanical Errors” *IEEE Transactions on Aerospace and Electronic Systems* 28-2 1992
26. Wenzinger, Carl J. “Pressure Distribution Over a Clark Y-H Airfoil with a Split Flap” NACA Technical Notes No. 627
27. Wilbur, G. and P. Weckler (2016, March 3). Personal Interview.

APPENDICES

Appendix A: Glass Fiber Composite Properties

ID	Lay-up, Top to Bottom Product	Fiber Content %	vol / wt	Top Up/Dn u/d/m/h	Rotation deg.	Fiber Wt. oz/sq.yd	Layer Thickness	Fiber lb/sq.ft	Resin lb/sq.ft	Total lb/sq.ft	Fiber $/lb	Fiber $/sq.ft	Resin $/sq.ft	Total $/sq.ft	Layer #	
Ve	E-LTM 3610	49 %	Wt	Hom.	0	44.84	0.076	0.31	0.33	0.636	$ -	$ -	$ -	$ -	1	
		-	Wt	Hom.	0	-	-	-	-	-	$ -	$ -	$ -	$ -		
		-	Wt	Hom.	0	-	-	-	-	-	$ -	$ -	$ -	$ -		
		-	Wt	Hom.	0	-	-	-	-	-	$ -	$ -	$ -	$ -		
		-	Wt	Hom.	0	-	-	-	-	-	$ -	$ -	$ -	$ -		
		-	Wt	Hom.	0	-	-	-	-	-	$ -	$ -	$ -	$ -		
		-	Wt	Hom.	0	-	-	-	-	-	$ -	$ -	$ -	$ -		
		-	Wt	Hom.	0	-	-	-	-	-	$ -	$ -	$ -	$ -		
		-	Wt	Hom.	0	-	-	-	-	-	$ -	$ -	$ -	$ -		
		-	Wt	Hom.	0	-	-	-	-	-	$ -	$ -	$ -	$ -		
		-	Wt	Hom.	0	-	-	-	-	-	$ -	$ -	$ -	$ -		
		-	Wt	Hom.	0	-	-	-	-	-	$ -	$ -	$ -	$ -		
		-	Wt	Hom.	0	-	-	-	-	-	$ -	$ -	$ -	$ -		
		-	Wt	Hom.	0	-	-	-	-	-	$ -	$ -	$ -	$ -		
		-	Wt	Hom.	0	-	-	-	-	-	$ -	$ -	$ -	$ -		
		-	Wt	Hom.	0	-	-	-	-	-	$ -	$ -	$ -	$ -		
		-	Wt	Hom.	0	-	-	-	-	-	$ -	$ -	$ -	$ -		
		-	Wt	Hom.	0	-	-	-	-	-	$ -	$ -	$ -	$ -		
		-	Wt	Hom.	0	-	-	-	-	-	$ -	$ -	$ -	$ -		
		-	Wt	Hom.	0	-	-	-	-	-	$ -	$ -	$ -	$ -		
	in this table by clicking on an existing				Laminate :	44.8	0.076	0.311	0.33	0.64	Lam :	$ -	$ -	$ -	1	# Layers
	name and selecting a property from				Core / Solids :	-	-	-			Core:	$ -	$/lb :	$ -		Adjustment
	the list that pops up.				Total :	44.8	0.076	0.311								

Laminate Comparison Table — Table Units: US

Laminate # ->	1	
Laminate	Current Laminate	
Thickness	0.076	in.
Mf	48.93 %	by Wt.
Density	101.0	lb/cu.ft
Fiber Wt.	0.31	lb/sq.ft
Resin Wt.	0.33	lb/sq.ft
Laminate Wt.	0.64	lb/sq.ft
Vf	31.16 %	by Vol.
0º Modulus, Ex	2.27	MSI
90º Modulus, Ey	2.27	MSI
Poisson Ratio, PRxy	0.16	
Shear Modulus, Gxy	0.45	MSI
0º Ten. Ult. Stress	35.3	KSI
0º Comp. Ult. Stress	35.3	KSI
90º Ten. Ult. Stress	37.2	KSI
90º Comp. Ult Stress	38.6	KSI
Shear Ult. Stress	10.3	KSI
0º Flex. Ult. Stress	46.1	KSI
90º Flex. Ult. Stress	46.1	KSI
Layer Cost-1	$ 0.00	/sq.ft
Layer Cost-3	$ 0.00	/sq.ft

Appendix B: Nominal Radiation Patterns

Stressed Skin Wing 4 GHz

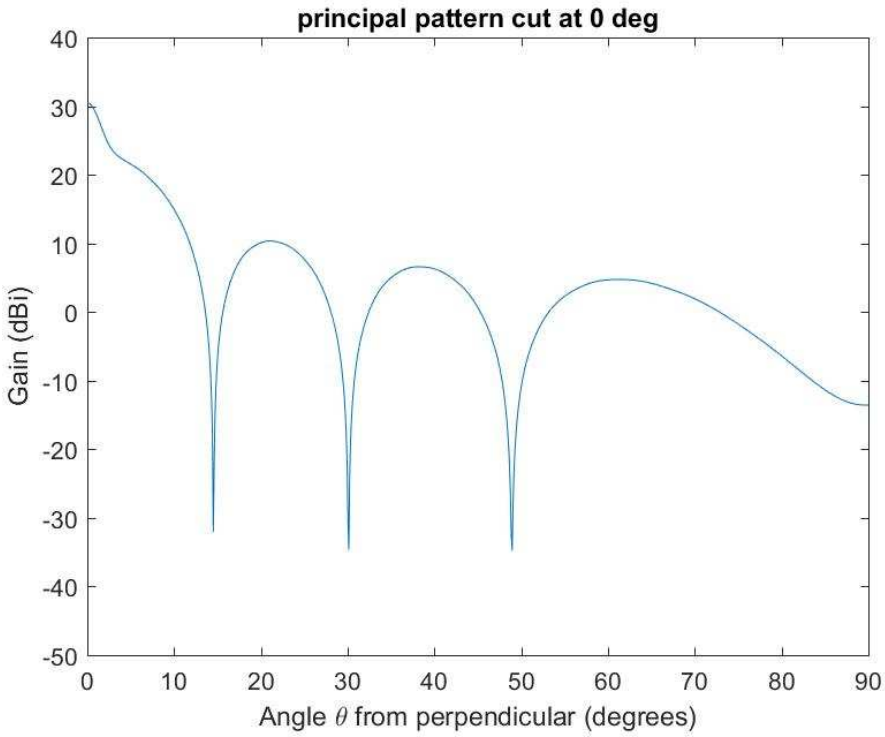

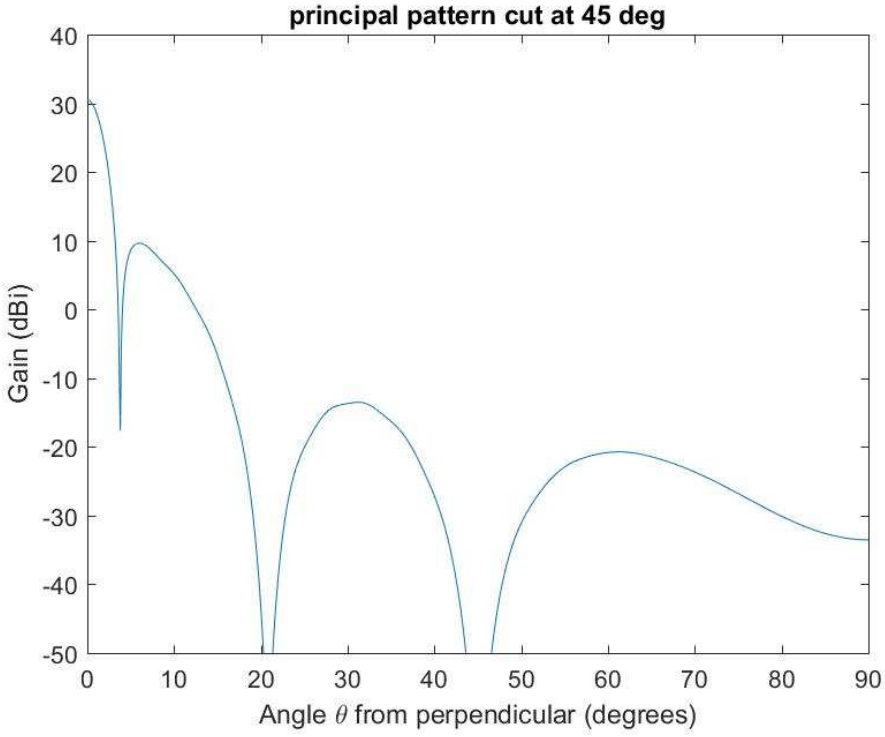

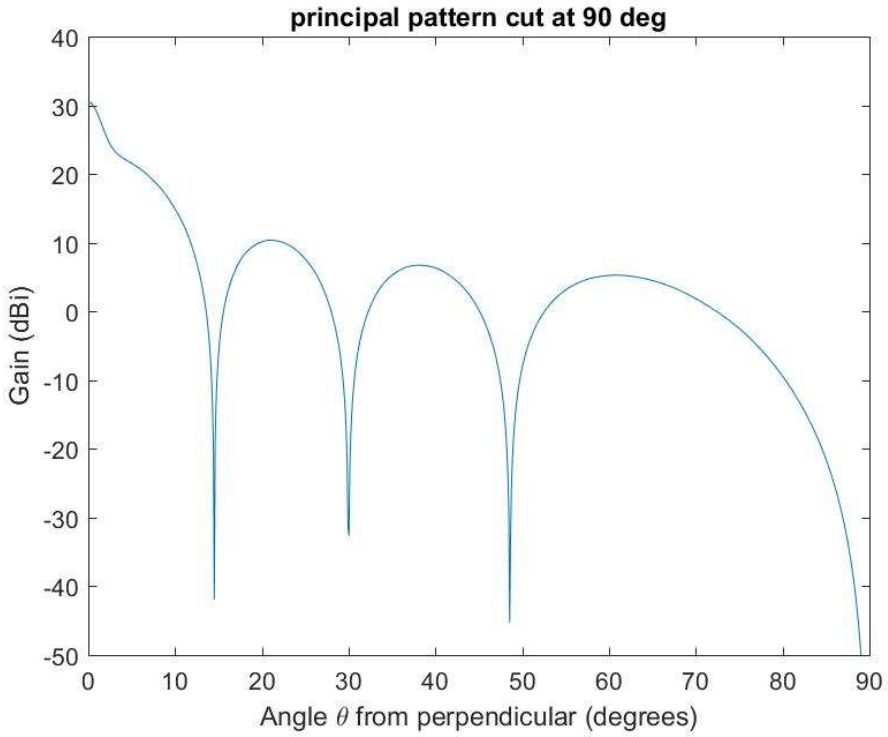

Foam Wing with 4 GHz Antenna

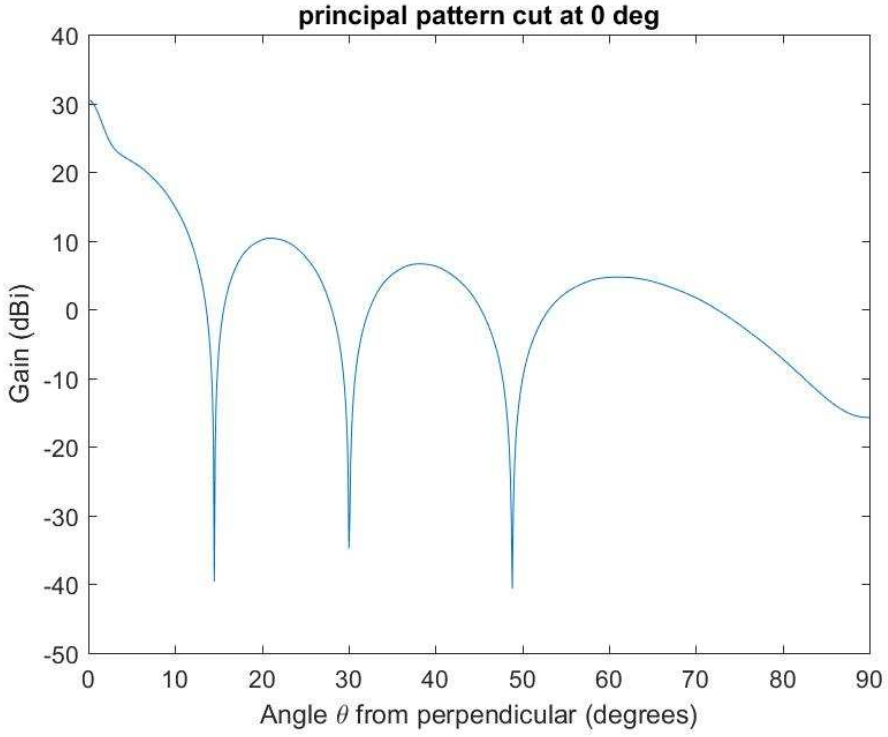

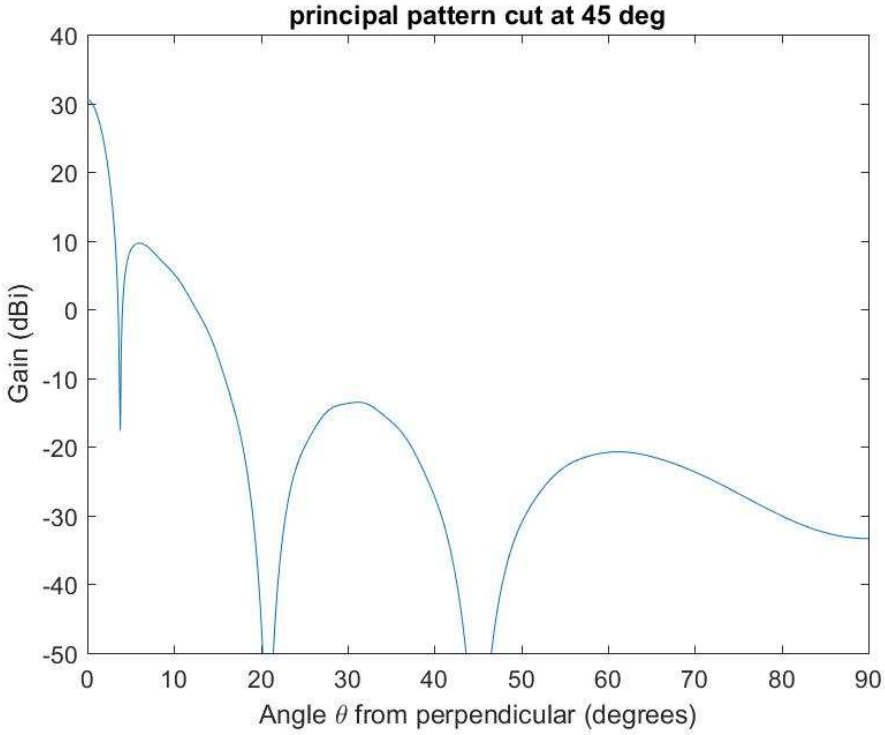
principal pattern cut at 45 deg
Gain (dBi)
Angle θ from perpendicular (degrees)
40
30
20
10
0
-10
-20
-30
-40
-50
0
10
20
30
40
50
60
70
80
90

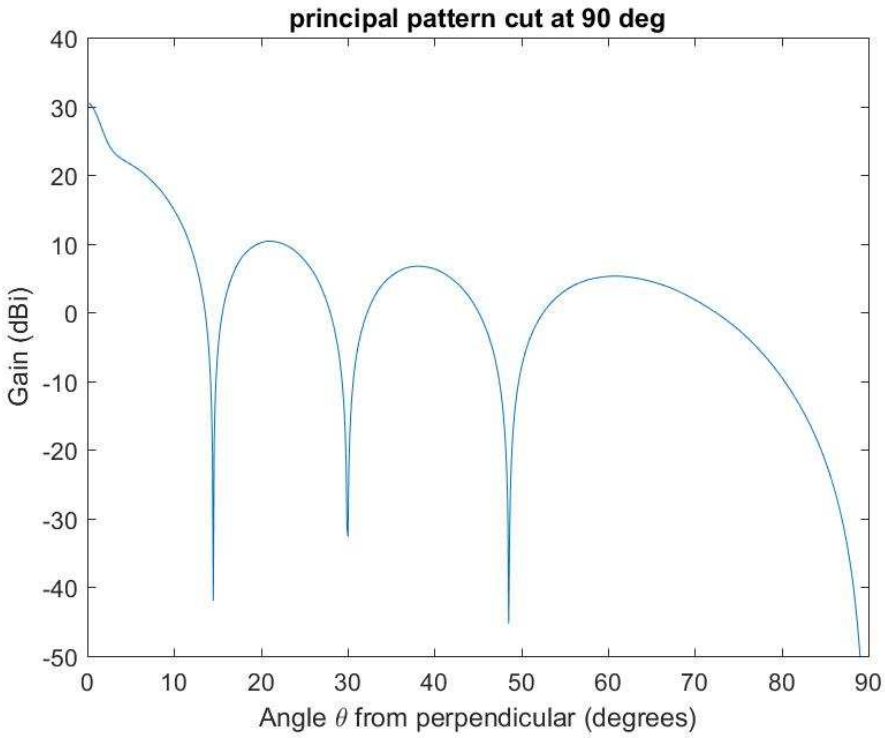
principal pattern cut at 90 deg
Gain (dBi)
Angle θ from perpendicular (degrees)
40
30
20
10
0
-10
-20
-30
-40
-50
0
10
20
30
40
50
60
70
80
90

Ribbed Wing with 4 GHz Antenna

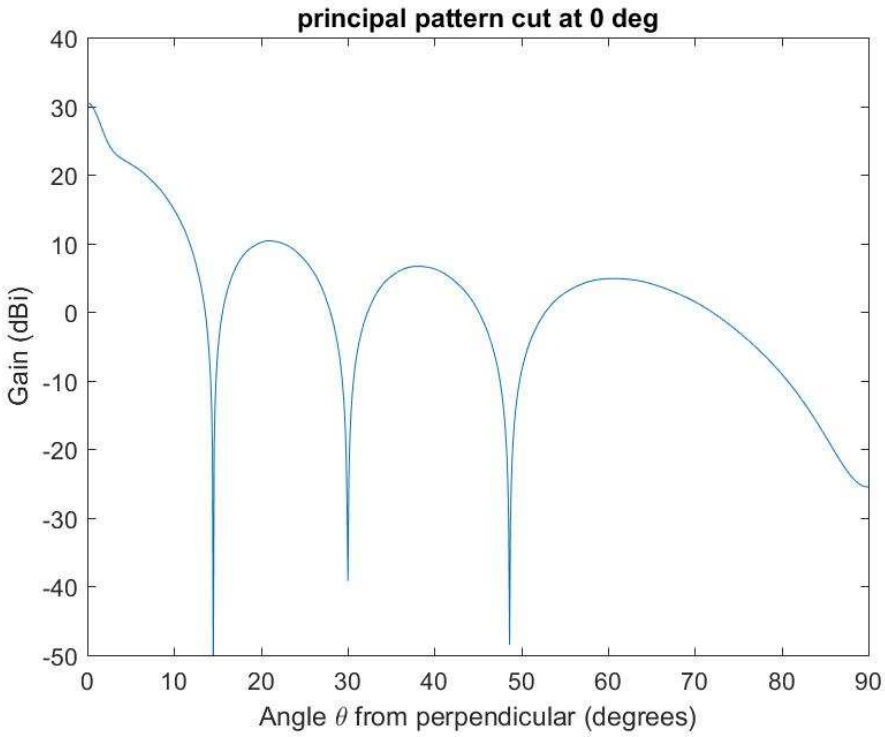

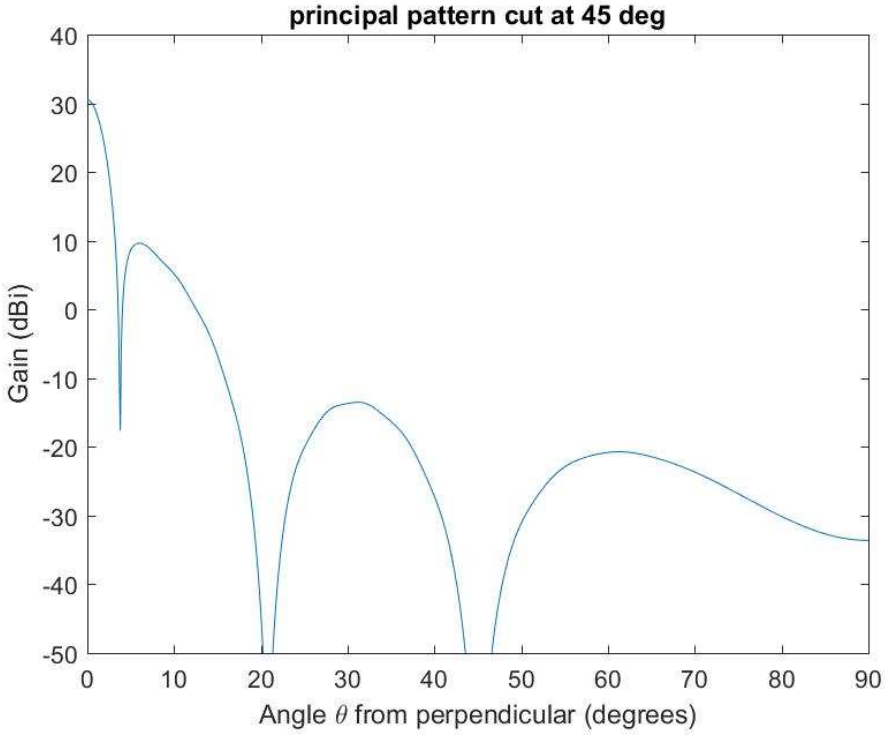

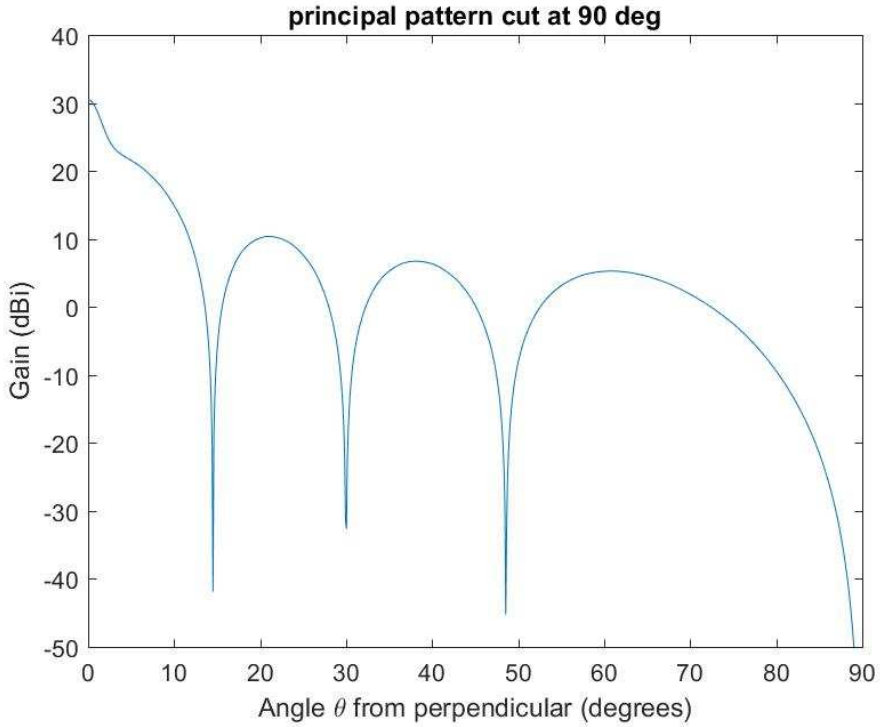

Stressed Skin Wing with 1 GHz Antenna

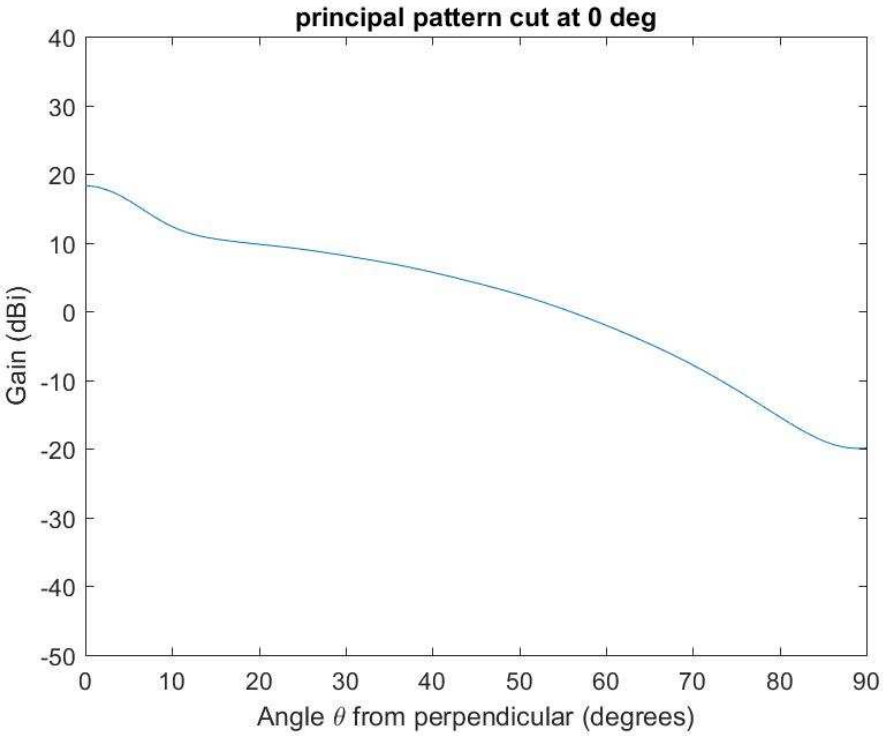

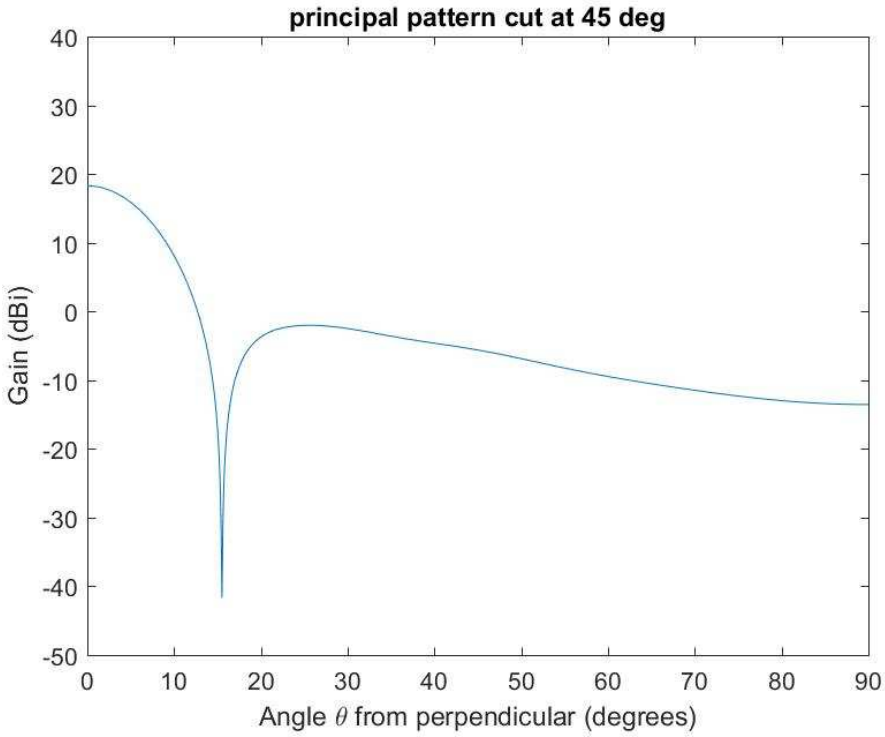
principal pattern cut at 45 deg
Gain (dBi)
Angle θ from perpendicular (degrees)
40
30
20
10
0
-10
-20
-30
-40
-50
0
10
20
30
40
50
60
70
80
90

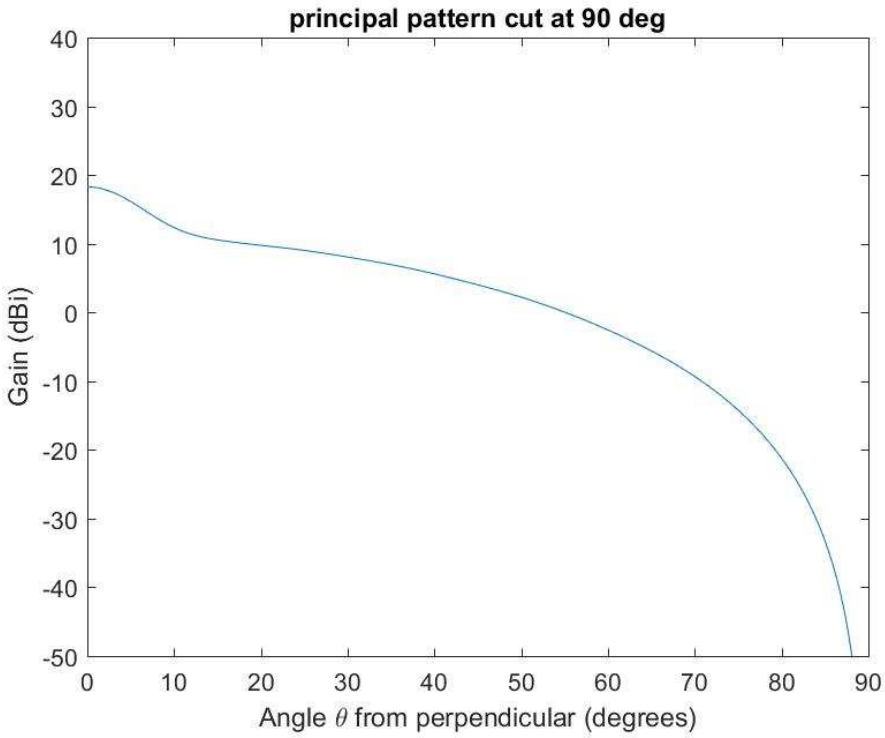
principal pattern cut at 90 deg
Gain (dBi)
Angle θ from perpendicular (degrees)
40
30
20
10
0
-10
-20
-30
-40
-50
0
10
20
30
40
50
60
70
80
90

Foam Wing with 1 GHz Antenna

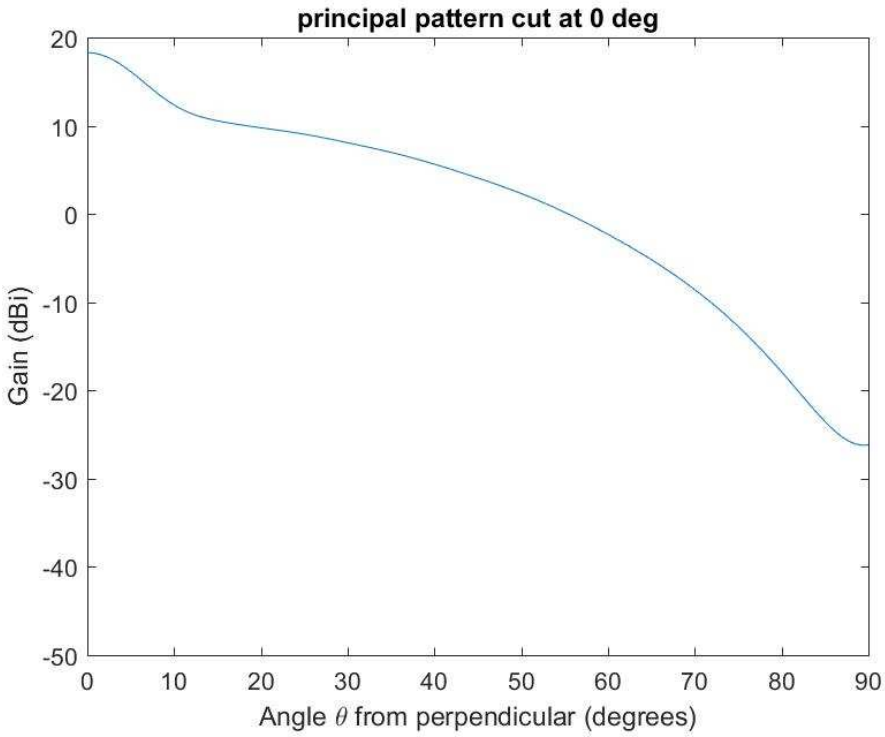

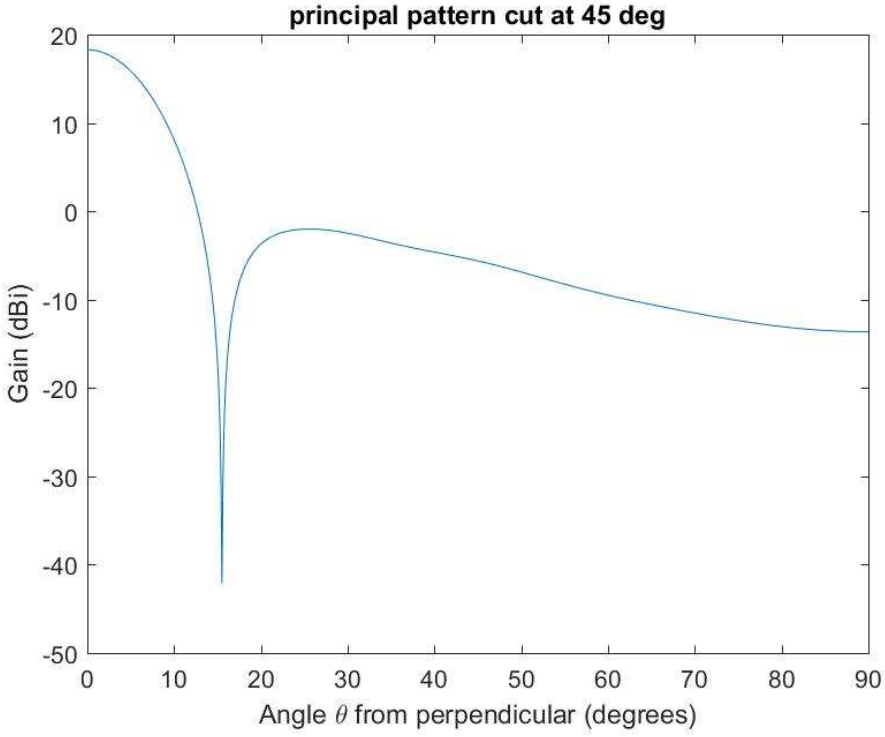

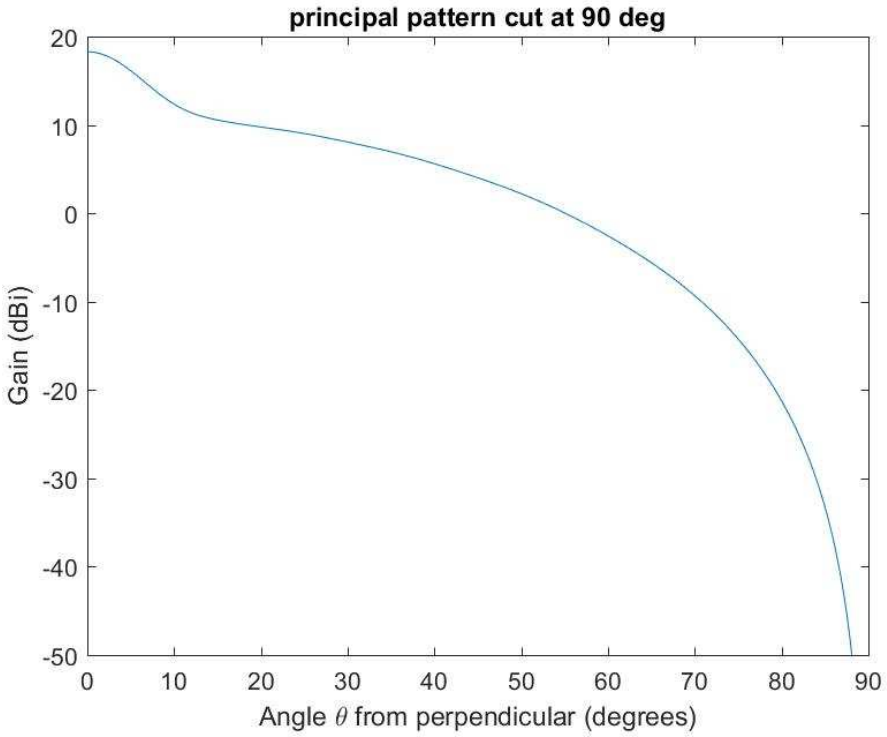

Ribbed Wing with 1 GHz Antenna

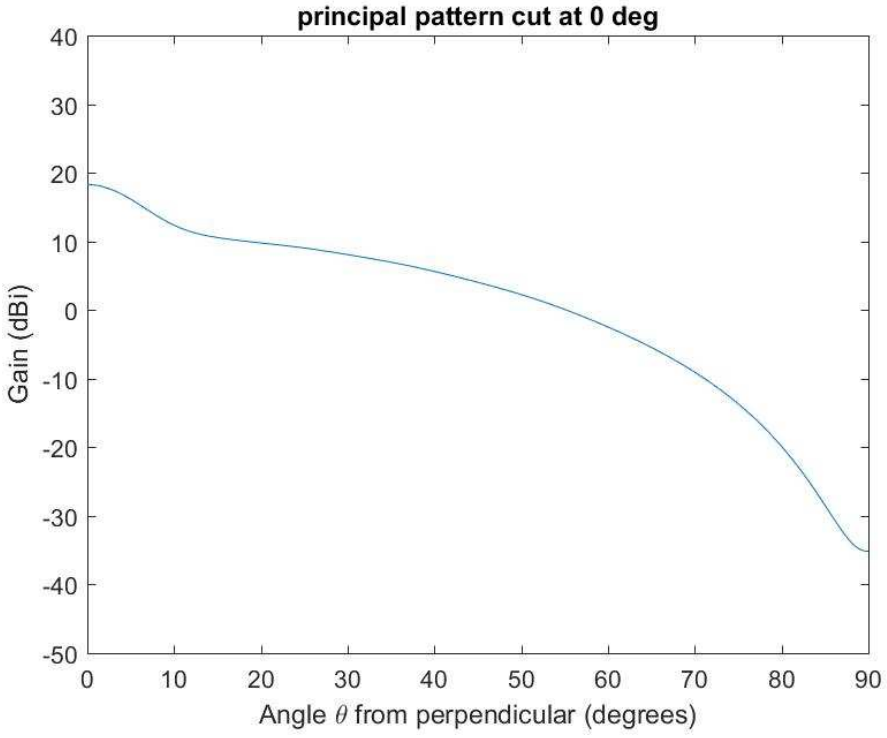

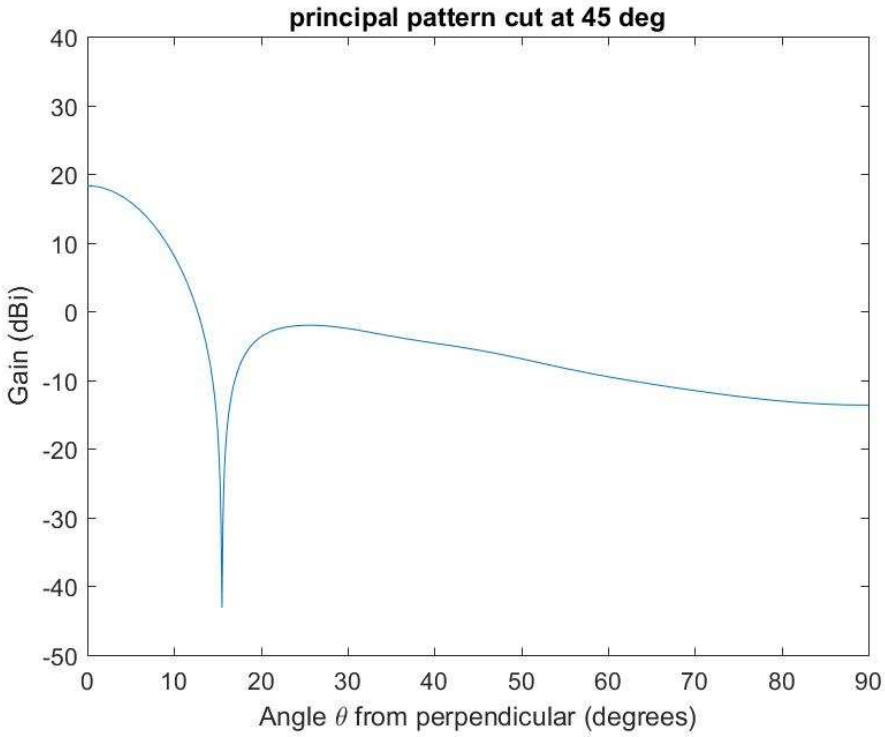
principal pattern cut at 45 deg
Gain (dBi)
Angle θ from perpendicular (degrees)
40
30
20
10
0
-10
-20
-30
-40
-50
0
10
20
30
40
50
60
70
80
90

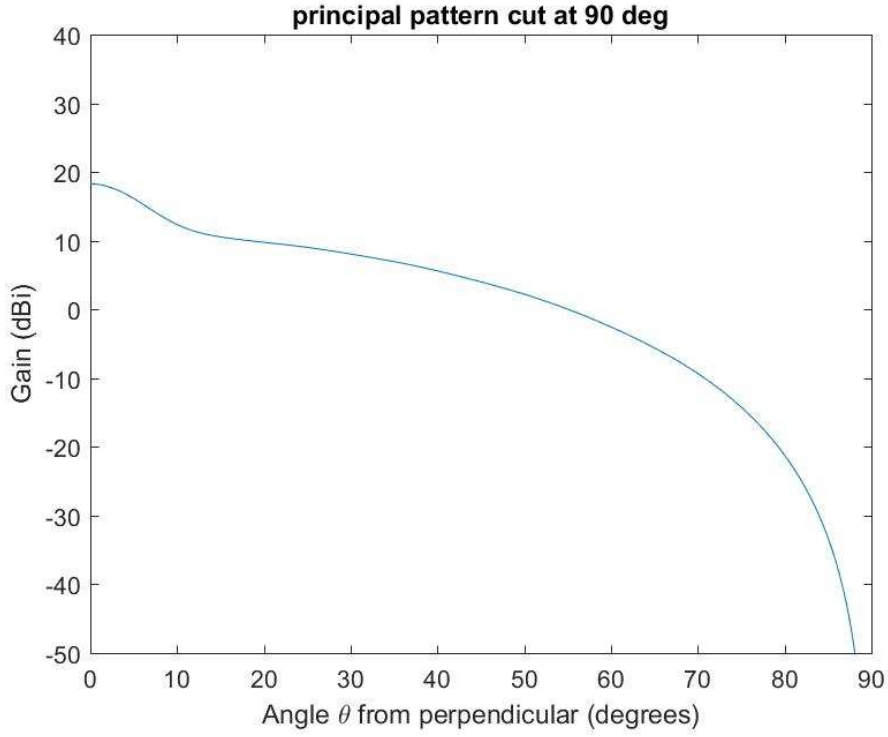
principal pattern cut at 90 deg
Gain (dBi)
Angle θ from perpendicular (degrees)
40
30
20
10
0
-10
-20
-30
-40
-50
0
10
20
30
40
50
60
70
80
90

```
%program to analyze radiation pattern of a cruciform antenna on an aircraft
%lower fuselage & wing by reading in the CAD data
%Adapted from work by Balanis [1] and Mailloux [2]

freq=1*10^9;          %corresponds ot X band
lambda=3*10^8/freq;    %from v=f*lambda
dx=0.5*lambda;         %half wavelngth spacing
dy=0.5*lambda;

uChord=1*lambda;   %useable amound of wing chord in m
uSpan=5*lambda;   %usable amount of span on each wing from root outwards in
m
totWidth=0.3048;  %total fuselage width in m
uLength=2*uSpan+totWidth;  %usable amount of fuselage length in m
uWidth=uChord;  %usable amount of fuselage width in m
%totSpan=1.828;    %total span of each wing from root outwards in m

%NOTE: spanwise out the wing is Y-direction, chordwise out the nose is X-
direction

nxw=floor(uChord/dx);             %number of elements chordwise on each wing
nyw=floor(uSpan/dx);              %number of elements spanwise on each wing
nxr=floor(uChord/dx);             %number of elements lenghtwise in each root
nyr=floor((totWidth-uWidth)/(2*dx));%number of elements spanwise in each root
nyc=floor(uWidth/dx);             %number of elements chordwise on center section
nxc=floor(uLength/dx);            %number of elements spanwise on center section

Nw=nxw*nyw;
Nr=nxr*nyr;
Nc=nxc*nyc;
N=2*Nw+2*Nr+Nc;  %total number of elements

xmax=uLength/2;
ymax=(2*uSpan+totWidth)/2;         %max distances from center
k=2*pi/lambda;

xw=5*1i*xmax/(400*pi*1i-243)^0.5;      %element weighting variables
yw=5*1i*ymax/(400*pi*1i-243)^0.5;

curve=csvread('S600.csv',8,0);
```

```
phasing=csvread('R700.csv',8,0);

CADX=curve(:,3);
CADY=curve(:,2);
CADZ=curve(:,5);
%coordinate systems don't alight, re-assign in surface interpolation
F=scatteredInterpolant(CADZ, CADX, CADY);

%create interpolation ofr erroneous phasing
phaseX=phasing(:,3);
phaseY=phasing(:,2);
phaseZ=phasing(:,5);
Ph=scatteredInterpolant(phaseZ, phaseX, phaseY);

ePhase=zeros(N,1);
coord=zeros(N, 3);
n=1;

%nested loops to position elements in center of cross along fuselage
for row=1:nyc
   for col=1:nxc
      coord(n,1)=dx*(col-0.5*(nxc+1));
      coord(n,2)=dx*(row-0.5*(nyc+1));
      coord(n,3)=0;
      ePhase(n,1)=0;
      n=n+1;
   end
end

%nested loops to position elements in left root area
for row=1:nyr
   for col=1:nxr
      coord(n,1)=dx*(col-0.5*(nxr+1));
      coord(n,2)=dx*(row-0.5*(nyc+1)-nyr);
      coord(n,3)=0;
      ePhase(n,1)=0;
      n=n+1;
   end
end

%nested loops to position elements in right root area
for row=1:nyr
   for col=1:nxr
```

```
        coord(n,1)=dx*(col-0.5*(nxr+1));
        coord(n,2)=dx*(-row+0.5*(nyc+1)+nyr);
        coord(n,3)=0;
        ePhase(n,1)=0;
        n=n+1;
    end
end

%nested loops to position elements in left wing
for row=1:nyw
    for col=1:nxw
        coord(n,1)=dx*(col-0.5*(nxw+1));
        coord(n,2)=dx*(row-0.5*(nyc+1)-nyr-nyw);
        %coord(n,3)=F(coord(n, 1), -(coord(n, 2)+totWidth/2));
        coord(n,3)=0;
        ePhase(n,1)=Ph(coord(n, 1), -(coord(n, 2)+totWidth/2));
        %ePhase(n,1)=0;
        n=n+1;
    end
end

%nested loops to position elements in right wing
for row=1:nyw
    for col=1:nxw
        coord(n,1)=dx*(col-0.5*(nxw+1));
        coord(n,2)=dx*(+0.5*(nyc+1)+nyr+nyw-row);
        %coord(n,3)=F(coord(n, 1), (coord(n, 2)-totWidth/2));
        coord(n,3)=0;
        ePhase(n,1)=Ph(coord(n, 1), (coord(n, 2)-totWidth/2));
        %ePhase(n,1)=0;
        n=n+1;
    end
end

%element weighting with 24.3 dB gauss taper
a=zeros(N,1);
for b = 1:N
    a(b,1)=exp(-(coord(b,1)^2)/(2*xw^2))*exp(-(coord(b,2)^2)/(2*yw^2));
end

%calculate total power radiated [1] [2]
cc=zeros(N,1);
u=zeros(900,360);
```

```
v=zeros(900,360);
w=zeros(900,360);

for theta = 1:900
   for phi = 1:360
      u(theta,phi)=sind(theta/10)*cosd(phi);
      v(theta,phi)=sind(theta/10)*sind(phi);
      w(theta,phi)=cosd(theta/10);
   end
end

f=zeros(900,360);  %value of ration pattern electric field in theta and phi [1]

for theta = 1:900
   for phi = 1:360
      for b = 1:N

cc(b,1)=(k*u(theta,phi)*coord(b,1))+(k*v(theta,phi)*coord(b,2))+(k*w(theta,phi)*
coord(b,3));
          f(theta,phi)=(f(theta,phi)+abs(a(b,1))*exp(-
1i*k*ePhase(b,1))*exp(1i*cc(b,1)));       %phased array on
          %f(theta,phi)=(f(theta,phi)+(a(b,1))*exp(1i*cc(b,1)));
%phasing off
      end
   end
end

Ftot=zeros(900,360);
F1=zeros(900,360);

for theta=1:900
   for phi=1:360
      Ftot(theta,phi)=abs(f(theta,phi))^2;
      F1(theta,phi)=abs(f(theta,phi))^2*sind(theta/10);
   end
end

P0=(pi/900)*(pi/360)*sum(F1(:))/(2*pi);
P=10*log10(Ftot./P0);

%calculate power in 10 degree cone [2]
C=zeros(N,1);
U1=zeros(1000,360);
```

```
V1=zeros(1000,360);
W1=zeros(1000,360);

for theta = 1:1000
   for phi = 1:360
      U1(theta,phi)=sind(theta/100)*cosd(phi);
      V1(theta,phi)=sind(theta/100)*sind(phi);
      W1(theta,phi)=cosd(theta/100);
   end
end

f=zeros(1000,360);  %value of ration pattern electric field in theta and phi [2]

for theta = 1:1000
   for phi = 1:360
      for b = 1:N

C(b,1)=(k*U1(theta,phi)*coord(b,1))+(k*V1(theta,phi)*coord(b,2))+(k*W1(theta,
phi)*coord(b,3));
          f(theta,phi)=(f(theta,phi)+abs(a(b,1))*exp(-
1i*k*ePhase(b,1))*exp(1i*C(b,1)));       %phased array on
          %f(theta,phi)=(f(theta,phi)+(a(b,1))*exp(1i*cc(b,1)));
%phasing off
      end
   end
end

Fd=zeros(1000,360);

for theta=1:1000
   for phi=1:360
      Fd(theta,phi)=abs(f(theta,phi))^2;
      %F1(theta,phi)=abs(f(theta,phi))^2*sind(theta/10);
   end
end

Pb=10*log10(Fd./P0);       %total gain direcivity
P1=Pb-max(Pb(:));           %net directivity for finding angle

plotX=coord(:,1);
plotY=coord(:,2);
plotZ=coord(:,3);
```

```
%plots of beam from 0 to 90
axis=linspace(0,90,900);

figure(1)
plot(axis,P(:,45))
title('principal pattern cut at 45 deg')
xlabel('Angle \theta from perpendicular (degrees)')
ylabel('Gain (dBi)')
ylim([-50 40])

figure(2)
plot(axis,P(:,90))
title('principal pattern cut at 90 deg')
xlabel('Angle \theta from perpendicular (degrees)')
ylabel('Gain (dBi)')
ylim([-50 40])

figure(3)
plot(axis,P(:,180))
title('principal pattern cut at 0 deg')
xlabel('Angle \theta from perpendicular (degrees)')
ylabel('Gain (dBi)')
ylim([-50 40])

saveas(1,'45.jpg');
saveas(2,'90.jpg');
saveas(3,'0.jpg');

%plots of beam from 0 to 10
axis2=linspace(0,10,1000);

figure(4)
plot(axis2,Pb(:,45))
title('principal pattern cut at 45 deg')
xlabel('Angle \theta from perpendicular (degrees)')
ylabel('Gain (dBi)')
ylim([0 40])

figure(5)
plot(axis2,Pb(:,90))
title('principal pattern cut at 90 deg')
xlabel('Angle \theta from perpendicular (degrees)')
ylabel('Gain (dBi)')
```

```
ylim([0 40])

figure(6)
plot(axis2,Pb(:,180))
title('principal pattern cut at 0 deg')
xlabel('Angle \theta from perpendicular (degrees)')
ylabel('Gain (dBi)')
ylim([0 40])

saveas(4,'45 10.jpg');
saveas(5,'90 10.jpg');
saveas(6,'0 10.jpg');

%figure()
%surf(P)
%title('principal pattern cut')

%figure()
%scatter3(PX1, PY1, PZ1)

%figure()
%scatter3(plotX, plotY, plotZ)

Gain=max(Pb(:))      %max gain

deflectError=coord(:,3)-ePhase(:,1);

Width90=(sum(P1(:,90)>-3)+1)/50
Width0=(sum(P1(:,180)>-3)+1)/50
Width45=(sum(P1(:,45)>-3)+1)/50
maxError=max(max(deflectError), abs(min(deflectError)))/lambda*100
```

VITA

SCOTT AUSTIN GALLAWAY

Candidate for the Degree of

Master of Science

Thesis: EXAMINATION OF UAV WING STIFFNESS REQUIREMENTS FOR A STRUCTURALL INTEGRATED CONFORMAL ANTENNA ARRAY

Major Field: Mechanical and Aerospace Engineering

Biographical:

Education:

Completed the requirements for the Master of Science in Mechanical and Aerospace Engineering at Oklahoma State University, Stillwater, Oklahoma in July, 2017.

Completed the requirements for the Bachelor of Science in Mechanical Engineering at Oklahoma State University, Stillwater, Oklahoma in 2015.

Experience: Intern at Raytheon in 2014 and 2015

Professional Memberships: Engineers Without Borders, AIAA